Electronic Thesis and Dissertation Repository

2-16-2016 12:00 AM

Constant-Envelope Multi-Level Chirp Modulation: Properties, Receivers, and Performance

Mohammad A. Alsharef
The University of Western Ontario

Supervisor
Dr. Rao, Raveendra
The University of Western Ontario

Graduate Program in Electrical and Computer Engineering
A thesis submitted in partial fulfillment of the requirements for the degree in Doctor of Philosophy
© Mohammad A. Alsharef 2016

Follow this and additional works at: https://ir.lib.uwo.ca/etd

⚙ Part of the Systems and Communications Commons

Abstract

Constant envelope multi-level chirp modulations, with and without memory, are considered for data transmission. Specifically, three subclasses referred to as symbol-by-symbol multi-level chirp modulation, full-response phase-continuous multi-level chirp modulation and full-response multi-mode phase-continuous multi-level chirp modulation are considered. These modulated signals are described, illustrated, and examined for their properties. The ability of these signals to operate over AWGN is assessed using upper bounds on minimum Euclidean distance as a function of modulation parameters. Coherent and non-coherent detection of multi-level chirp signals in AWGN are considered and optimum and sub-optimum receiver structures are derived. The performance of these receivers have been assessed using upper and lower bounds as a function of SNR, modulation parameters, modulation levels, decision symbol locations, and observation length of receiver. Optimum multi-level chirp modulations have been determined using numerical minimization of symbol error rate. Closed-form expressions are derived for estimating the performance of multi-level chirp signals over several practical fading channels. Finally, spectral characteristics of digital chirp signals are presented and illustrated.

Acknowledgements

All praise be to Allah Almighty, the most merciful and most compassionate, for bestowing upon me His countless bounties and for providing me the opportunity to carry out my PhD degree. Without his guidance and blessings, nothing is possible.

I would like to express my sincerest gratitude and deep appreciation to my supervisor Dr.Raveendra K. Rao who has supported me throughout my PhD study at the University of Western Ontario. His extensive knowledge in the field of communications, encouragement, guidance, and constructive criticism have been valuable resources. Also, I would like to thank the examination committee members for their valuable remarks and considerable recommendations.

I am extremely grateful to my parents and my family for their support and encouragement over the years. The role of my parents in my upbringing and their prayers have played a major role in what I am today. I wish that I can compensate them for the past years.

I can never thank enough all my friends and my colleagues with whom I have the pleasure to work with in the same research lab for the unforgettable times we spent together. I have benefited from discussing diverse subjects related to the research and life in general.

Last but not least, I would like to thank Taif University for supporting me in completing my PhD study. Also, I thank the Ministry of Education in Saudi Arabia and the Saudi Cultural Bureau in Canada for their support.

Table of Contents

List of Tables

List of Figures

Acronyms

ACI	*Adjacent Channel Interference*
AWGN	*Additive White Gaussian Noise*
BER	*Bit Error Rate*
BOK	*Binary Orthogonal Keying*
BPSK	*Binary Phase Shift Keying*
CDMA	*Code Division Multiple Access*
CPC	*Continuous Phase Chirp*
CPFSK	*Continuous Phase Frequency Shift Keying*
CPM	*Continuous Phase Modulation*
CSS	*Chirp Spread Spectrum*
DCS	*Digital Communication Systems*
DS-BPSK	*Direct-Sequence Binary Phase Shift Keying*
EM	*Electromagnetic Interference*
FDMA	*Frequency Division Multiple Access*
FH	*Frequency Hopping*
FM	*Frequency Modulation*
FSK	*Frequency Shift Keying*
HF	*High Frequency*
ISM	*Industrial Scientific and Medical*
LFM	*Linear Frequency Modulation*
LPI	*Low Probability of Intercept*
MAN	*Metropolitan Area Network*
MCM	*Matched Chirp Modulation*
MCPCM	*M-level Continuous Phase Chirp Modulation*
MFSK	*M-ary Frequency Shift Keying*
MPSK	*M-ary Phase Shift Keying*
MSK	*Minimum Shift Keying*
OFDM	*Orthogonal Frequency Divivision Mlutplixing*

PAM	*Pulse Amplitude Modulation*
PAN	*Personal Area Network*
PDF	*Probability Density Function*
PSD	*Power Spectral Density*
QPSK	*Quadrature Phase Shift Keying*
RF	*Radio Frequency*
SAW	*Surface Wave Acoustic*
SER	*Symbol Error Rate*
SNR	*Signal to Noise Ratio*
TDMA	*Time Division Multiple Access*
WLAN	*Wireless Local Area Network*

Chapter 1
Introduction

1.1 Introduction to Communications

Communication has been one of the most important needs of humans throughout recorded history. It is essential in forming social unions, in educating the young, and in expressing a myriad of emotions and needs. Good communication is central to a civilized society. The host of communication disciplines in engineering have the central purpose of providing technological aids to human communication. The communication technology as one views it today became important with telegraphy, then telephony, then video, then computer communication and today the amazing mixture of all these in inexpensive, small portable devices. Communication enters daily lives in so many different ways. With telephones in hands, radios and televisions in living rooms, and with desktop, laptop, and tablet computers providing access to the Internet in offices and homes, one is able to communicate to every corner of the globe. Communication provides information to ships on high seas, aircraft in flight, and rockets and satellite in space. Indeed, the list of applications involving the use of communication in one way or another is almost endless.

1.2 Wireless Communications

In 1897, Guglielmo Marconi invented the first apparatus for transmitting radio waves over longer distance which was used to enable communication with ships in the English channel [1]. Since then, wireless communications has become one of the most rapidly growing industries in the world, and its products are now exerting an impact in our daily lives. Wireless communications today cover a very wide array of applications. The telecommunications industry is one of the largest industries worldwide

with more than $ 1 trillion in annual revenues for service and equipment. The largest and most noticeable part of telecommunications business is telephony. The principal wireless component of telephony is mobile telephony. The worldwide growth rate in cellular telephony is very aggressive, and reports suggest that the number of cellular telephony subscriptions worldwide has now surpassed the number of wired telephony subscriptions. However, cellular telephony is only one of a very wide array of wireless technologies that are being developed very rapidly at the present time. Among other technologies are wireless Internet and other Personal Area Network (PAN) systems, Wireless Local Area Network (WLAN) systems, wireless Metropolitan Area Network (MAN) systems, and a variety of satellite systems. These technologies are supported by a number of transmission and channel assignment technologies, including Time Division Multiple Access (TDMA), Code Division Multiple Access (CDMA) and other spread-spectrum systems, Orthogonal Frequency Division Multiplexing (OFDM) and other multi-carrier systems, and high-rate single-carrier systems. All these modern technologies use the basic principles that underlie the design and analysis of Digital Communication System (DCS) [2].

1.3 Digital Communication System

Modern society depends on electronic communication for most of its functioning. Among the many possible ways of communicating, the class of techniques refereed to as *digital communications* has become predominant in the 21st century, and indications are that this trend will continue. Digital communication is simply the practice of exchanging information by the use of finite sets of signals. Thus, most modern communication systems now contain digital interface between source and channel (such as cable, twisted pair wire, optical fibers or electromagnetic radiation through space). Digital interfaces are practical due to the availability of cheap, reliable, and miniaturized digital hardware. Also, the digital interface simplifies implementation and understanding, since source coding/decoding can be done independently of the channel, and similarly channel coding/decoding can be done independently of the

source. A generic model of a point-to-point digital communication system is shown in Fig.1.1.
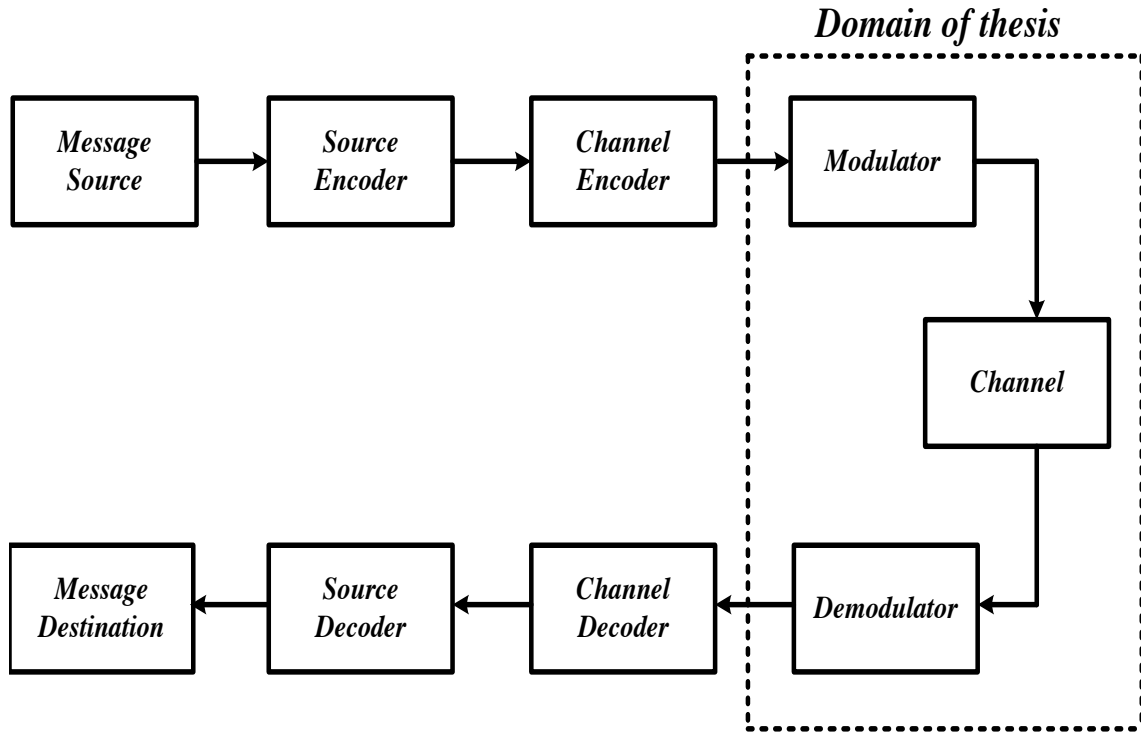
Figure 1.1: Model of point-to-point digital communication system

The message source generates messages which are to be transmitted to the receiver. In a digital communication system, the messages produced by the source are usually converted into a sequence of binary digits. The binary digits are almost universally used for digital communication and storage as well. The purpose of the source encoder is to provide an efficient representation of the source output that results in little or no redundancy [3]. The sequence of binary digits from the source encoder is fed to the channel encoder which introduces in a controlled manner some redundancy to combat the noise and interferences over the channel. The sequence of binary digits from the channel encoder is to be transmitted through the channel to the intended receiver. The channel may be either a pair of wires, a coaxial cable, a radio channel, a satellite channel, an optical fiber channel or some combination of these media [2],[3]. Such channels are basically waveform channels and hence, they cannot

be used to transmit directly the sequence of binary digits. A device that converts the digital information sequence into waveforms that are compatible with the characteristics of the channel is called the *digital modulator*. The output of the modulator is transmitted over the channel. At the receiving end of digital system, the *digital demodulator* processes the channel-corrupted transmitted waveforms and reduces them to represent an estimate of the transmitted digital sequence. The *channel decoder* uses this sequence in an attempt to reconstruct the original sequence from knowledge of the code used by the *channel encoder*, which is then fed to the *source decoder*. The source decoder attempts to reconstruct the original signal from the source. The focus of this thesis is *digital modulators* and its mate *digital demodulator* over some practical *channels*. Thus, in the next section, we present a simplified model of digital communication system that is appropriate for the development of works presented in this thesis.

1.4 Simplified Model of Digital Communication System

The partial block diagram, which consists of information source and digital modulators, of a typical digital communication system is shown in Fig. 1.2. The source output may be either an analog signal, such as an audio or video signal, or digital signal such as the output of a computer. In a DCS, the message produced by the source are assumed to be sequence of binary digits. This binary sequence is passed to an accumulator which accumulates K binary digits (and assigns unique amplitude level) before presenting it to the digital modulator. When $K = 1$, the digital modulator simply maps binary digits 0 to a waveform $S_1(t)$ and the binary digit 1 to a waveform $S_2(t)$, both over the bit interval of T_b sec. We call this binary modulation. Alternatively, the modulator may transmit K information bits at a time by using $M = 2^K$ distinct waveforms $S_i(t), i = 1, 2, \ldots, M$, one waveform for each of the 2^K possible $K-$bit sequence. We call this M-level or M-ary modulation ($M > 2$). If R is the bit rate of the input source, then a new $K-$bit sequence enters the modulator

every K/R seconds. Thus, when the channel bit rate R is fixed, the amount of time available to transmit one of the M waveforms corresponding to a $K-$bit sequence is K times the time period in a system that uses binary modulation.


```
┌──────────────┐       ┌──────────────┐  m_i  ┌──────────────┐  S_i(t)
│ Information   │──────▶│ Accumaulator │──────▶│   Digital    │──────┐
│   Source      │       │    K bits    │       │  Modulator   │      │
└──────────────┘       └──────────────┘       └──────────────┘      │
                                                                     ▼
                                                             ┌──────────────┐
                                                             │   Channel    │
                                                             └──────────────┘
  Output                                                            │
  Signal  ┌──────────────┐   ┌──────────────┐  m̂_i  ┌──────────────┐
  ◀───────│  Transducer  │◀──│ Message to   │◀──────│ Demodulator  │◀─┘
          └──────────────┘   │Binary Mapper │       └──────────────┘
                             └──────────────┘
```
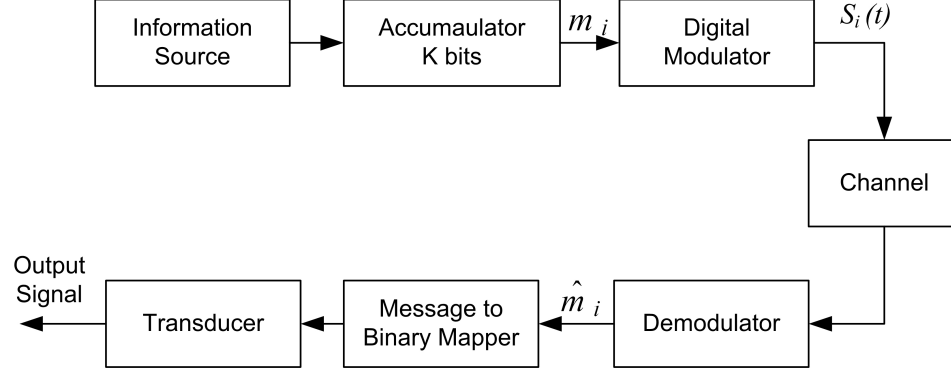
Figure 1.2: Partial Block Diagram of DCS

The communication channel is the medium that is used to send the signal from the transmitter to the receiver. Whatever the physical medium used for transmission of information, the essential feature is that the transmitted signal is corrupted in random manners by a variety of possible mechanisms. The simplest mathematical model for a communication channel is the additive noise channel. In this thesis, we model the additive noise channel to be white and Gaussian, with two-sided power spectral density of $\frac{N_0}{2}$ watts/Hz. Because this channel model applies to a broad class of physical communication channel and because of is mathematical tractability, this is the predominant channel model used in our communication system design and analysis.

At the receiver end of a digital communication system, the digital demodulator processes the channel-corrupted transmitted waveform and reduce the waveforms to a sequence of numbers that represent estimates of the data symbols which is subsequently converted into a sequence of binary digits that represent estimate of the source output at the transmitter.

While the prime issue of concern in the study of DCS is the efficient use of power and bandwidth, there exist situations where one sacrifices these efficiencies in order to meet other design objectives such as to provide secure communication in a hostile environment. A major advantage of such a system is its ability to reject interference, be it intentional or unintentional. The class of signals that cater to this requirement is referred to as spread-spectrum modulation. In recent years indoor wireless communication has gained increasing attention and its market share is expected to grow rapidly in the coming years due to its advantages over cable networks such as mobility of users, elimination of cabling and flexibility etc. Typical applications are cordless phone systems, WLANs for home and office applications and flexible mobile data transmission links between sensors, actuators, robots, and controller units in industrial environments. Due to the hostile electromagnetic (EM) environment, which includes severe EM emissions from other devices as well as distortions due to multi-path propagation, the robustness of the communication link is an extremely important feature in a wireless communication system. The spread-spectrum technology is well suited to provide robust data transmission in these applications.

In a spread-spectrum system, the transmitted signal is spread over a wide frequency band, often much wider than the minimum bandwidth required for conveying the information. An instance of spectrum spreading may be seen in conventional Frequency Modulation (FM), by employing frequency deviations greater than unity. The wide-band FM thus produced is often classified as a spread-spectrum system because the RF spectrum produced is much wider than that of the transmitted information. While in FM, the transmitted bandwidth is a function of both information bandwidth and the amount modulation, there are techniques in which spectrum spreading is accomplished using some signal or operation other than the information bearing signal that is transmitted. For example, in Direct Sequence (DS) and Frequency Hopping (FH) spread spectrum systems, the spreading and despreading functions are used in the transmitter and receiver, respectively [3]. In these spread spectrum systems, the synchronization of the despreading code is difficult and needs high computational effort. Linear Frequency Modulation (LFM) or chirp modulation is another type of spread spectrum signalling technique in which a carrier is swept

over a wideband during a given data pulse interval. Chirp modulation [4],[5] does not necessarily employ coding and produces a transmitted bandwidth much greater than the bandwidth of the information being transmitted. The growing interest in chirp modulation is mainly due to the advances in Surface Wave Acoustic (SAW) technology, which offers a rapid close-to-optimum method for both generation and correlation of wideband chirp pulses [6]. Chirp systems have found major applications in radar systems for reasons such as anti-eavesdropping, anti-interference and low-Doppler sensitivity. Among several applications of chirp signals in communication are radio telephony, cordless systems, air-ground communication via satellite repeaters [7], data communication in the High Frequency (HF) band and WLANs. In 2007, IEEE introduced Chirp Spread Spectrum (CSS) physical layer in the new wireless standard 802.15.4a [8]. Additionally this standard uses chirp modulation with no additional coding, whereas in 802.15.4 standard direct-sequence binary phase shift keying (DS-BPSK) and additional spreading code are used. This new standard targets applications such as industrial and safety control, sensor actuator networking, and medical and private communication devices. By applying CSS techniques to multidimensional multiple-access modulation, single-chip transceivers for wireless communication in the industrial, scientific, and medical (ISM) band have been developed and are commercially available [9].

1.5 Literature Survey and Motivation

Chirp signals were first used in World War II in radar technology and because it is easy to generate, they were used as a pulse compression techniques as well. In 1962, Winkler [10], who was motivated by the anti-interference, anti-eavesdropping, and low-Doppler sensitivity properties of chirp signals, considered chirp modulation for binary data transmission. In [10], two chirp signals were used, up-chirp (sinusoidal signal whose frequency increases linearly with time) and down-chirp (sinusoidal signal whose frequency decreases linearly with time), to map binary data for transmission of digital teletype, voice and telemetry signals. With the development of chirp communications, Berni and Gregg [11] investigated the performance of chirp modulation

in terms of its probability of bit error rate and spectrum usage and compared them with the performances of BPSK and binary FSK techniques. They concluded that BPSK is superior in performance compared to binary FSK and binary chirp modulation. Another author examined the capabilities of linear FM spread-spectrum signals for communication systems. Cook [12] has provided a systematic basis in order to choose appropriate modulation parameters by studying different factors such as frequency-modulation indicies, time-bandwidth product and cross-talk criteria. Also, he has established criteria for performance bounds and suggested a further comparison with other conventional spread-spectrum techniques based on these criteria. Gott and Newsome [13] proposed wide-band chirp signals for data transmission in the HF band and evaluated the performance of these signals experimentally. They concluded that by using orthogonal signals and matched filter detection, both narrow-band and wide-band systems offer equivalent performance for the same bit energy. To combine the anti-interference property that chirp signals have and the bandwidth efficiency that differential phase-shift keying have, Gott and Karia [14] subsequently applied the concept of differential encoding technique for binary data transmission using chirp signals. By using hardware devises, they have evaluated the performance of the proposed system in white noise, in single carrier interference and under the effect of Doppler frequency shift. They have concluded that the proposed system has a better performance than conventional chirp system in white noise and single carrier interference. In [15], Dayton has extended the concept of chirp modulation for data transmission using satellites in the HF band. In [16], Kowatsch et. al. investigated the anti-jam performance of a combined PSK and chirp signal system. They have concluded that such a system can assure Low Probability of Intercept (LPI) and hence better anti-jam performance. In [17], Kowatsch and Lafferl presented a spread spectrum transmission system that uses a combination of chirp modulation and pseudo-random PSK. In [18], Elkhamy and Shaaban introduced a new class of chirp modulation referred to as Matched Chirp Modulation (MCM), which is an improved version of the conventional chirp modulation. They have analyzed the performance of MCM using optimum non-coherent and partially coherent receivers. It is shown that MCM offers good performance over dispersive communication channels.

Combining the chirp signalling technique with some kind of pseudo-random coding, it is possible to achieve a substantial improvement in anti-jam performance. Such a system is presented and analyzed in [19] by Elhakeem and Targi. In [20]. Wang, Fei, and Li have proposed a structure for the chirp Binary Orthogonal Keying (BOK) system and have obtained an expression for the probability of bit error. It is shown that chirp BOK performs better than traditional BOK modulation in Additive White Gaussian Noise (AWGN) channel. In all the above chirp systems binary data transmission and receivers that are required to make independent bit-by-bit decisions are considered. In [21], Hirt and Pasupathy consider binary chirp signals by introducing phase continuity at bit transitions. They demonstrated that coherent binary phase continuous chirp (CPC) modulation can offer, at most, 1.66 dB improvement over BPSK. They have extended this work to non-coherent situation in [22]. In [23], Aulin and Sundberg have investigated the performance and spectrum of M-ary CPM over one symbol interval, the so-called full response systems. They have derived an expression for the probability of error in terms of the Euclidean distance. Also, they have extended this work to partial response signalling in [24]. In [25], Raveendra considers binary phase continuous chirp modulation with time-varying modulation parameters referred to as dual-mode binary chirp modulation and has shown that it can outperform binary CPC modulation. More recently, in [26] , Bhumi and Raveendra have considered digital asymmetric phase continuous chirp signals for data transmission and have shown that it can outperform dual-mode chirp modulation considered in [21]. In [27], Wilson and Gaus have presented a new procedure to calculate the power spectrum of digital continuous-phase signals with multi-h phase codes. They have generalized the method so that it can handle various frequency pulse shapes, multi-level signalling and different sets of modulation indicies. It is well known that any binary continuous phase modulated (CPM) signal can be decomposed exactly into sum of a few PAM signals. Mengali and Morelli in [28], have extended this idea to M-ary CPM waveforms. They have found that the decomposition has so many terms especially with a long memory signalling schemes. As a result, they have proposed an approximation with less number of terms. In recent years there have been a number of publications [25], [29, 30, 31, 32, 33, 34] that clearly exhibit the choice of chirp

modulation in a variety of digital communication systems. The error performance of chirp modulation over frequency-selective and non-selective fading channels such as Rayleigh fading and Nakagami-m fading have been investigated in [35] and closed-form error probabilities expressions were developed. The performance analysis with closed-form bit error probability expressions for Chirp modulation in the maximum ratio combining (MRC) diversity system has been investigated in [36]. Moreover, various kinds of nonlinear chirp signals such as quadratic, exponential, trigonometric and hyperbolic, have been applied in multiuser chirp spread spectrum system in [37] and in [38].

In digital communication, it is well known that M-level signalling schemes can be used for reducing the bandwidth requirements of baseband Pulse Amplitude Modulation (PAM) data transmission systems [3]. In some cases, M-level signalling is a natural choice when the message signal is inherently M-level like the English alphabet. In a typical M-level signalling technique, the output of a binary source is combined into groups of k bits which will result in 2^k different bit patterns. Each block of k bits is a symbol that is mapped to a distinct signal that occupies $T_s = kT_b$ seconds. Therefore, by using M-level signalling, there is bandwidth saving of $1/k$ or in other words we can transmit data at a rate that is k times faster than the corresponding binary case. In practice, we seldom find a channel that has the exact bandwidth required for transmitting the output of source using binary signalling schemes. M-level signalling may be used to utilize the additional bandwidth to provide increased immunity to channel noise. However, this saving in bandwidth comes at the expense of increased power requirements and at the expense of error performance. The transmitted power must be increased by a factor of M^2/k compared to the binary case to achieve same performance.

The research was motivated by applying the concept of M-level signalling to the chirp signals. Also, because Continuous Phase Modulation (CPM) is an attractive modulation scheme due to its excellent power and bandwidth characteristics, a new class of signal called M-level Continuous Phase Chirp Modulation (M-CPCM) is proposed in this thesis. A comprehensive study of this class of signals in terms of symbol error rate (SER) performance over various wireless communication chan-

nels, bandwidth efficiency, complexity and other geometric properties have not been considered yet and will be accomplished in this thesis.

1.6 Thesis Objectives

The objectives of this thesis are mentioned below:

- Memoryless multi-level chirp modulation

  General description of this modulation system is provided and its properties are given and illustrated. Optimum algorithms for coherent and non-coherent detection of these signals in AWGN are derived and structures of optimum receivers are identified. Bounds on the symbol error rate performance of the optimum receivers are illustrated as a function of Signal to Noise Ratio, and modulation parameters h, peak-to-peak frequency deviation divided by the symbol rate, and w, frequency sweep width divided by the symbol rate. Optimum memoryless multi-level chirp systems are determined.

- Multi-level Continuous Phase Chirp Modulation (M-CPCM)

  General description of M-CPCM signals are given and their properties are illustrated. Coherent and non-coherent detection of M-CPCM signals in AWGN are considered. Structures of optimum receivers are derived and their performance analysis are presented. Optimum coherent and non-coherent M-CPCM systems have been determined and illustrated.

- Minimum Euclidean distance properties for M-CPCM signals as a function of the modulation parameters (q, w) and observation intervals for the full response signaling

  M-CPCM with full response signaling is proposed and studied. The geometric properties of this class of signals are analyzed using the criterion of minimum Euclidean distance in the signal space and hence its ability to operate over AWGN channel. Bounds on the achievable Euclidean distance are derived.

- Multi-mode Multi-level Continuous Phase Chirp (M-CPCM)

  A new signaling technique called multi-mode M-CPCM is proposed. These signals are described and their ability to perform over the coherent Gaussian channel is investigated.

- Performance of multi-level chirp over fading channels

  Closed-form expressions for symbol error rate performance bounds of the M-level chirp modulation over Rayleigh, Nakagami-m and Generalized-K (K_G) fading channel, are derived. These bounds are illustrated as a function of energy per bit to noise ratio, Eb/No, channel fading parameters, observation length n of the receiver and modulation parameters (q, w).

- Power spectra of M-CPCM

  A general method is presented for calculation of the power spectra of M-CPCM signals. The method can handle arbitrary M-level data and works for arbitrary set of modulation parameters (q, w). Also, the method presented can be used to calculate the power spectrum of arbitrary phase-continuous signals in general. Numerical results are presented to illustrate power spectra of M-CPCM as a function of modulation parameters. The technique can be used to study power/bandwidth trade offs available with M-CPCM.

1.7   Thesis Organization

The thesis is organized as follows: In Chapter 2, the concept of utilizing chirp signals for digital modulation is explained. The M-level chirp signals are described using squared minimum Euclidean distance (d^2_{min}) criteria. Modulation parameters that affect Euclidean distance are described and optimum parameters sets (q, w) that maximizes the distance are derived. Coherent and non-coherent optimum detection of these signals in AWGN is considered.

In Chapter 3, M-CPCM signals are proposed for data transmission and the problem of calculating the minimum squared normalized Euclidean distance (d^2_{min})

for M-CPCM with different observation interval n is considered. Bounds on the minimum Euclidean distance are derived which are used to evaluate the probability of error of the maximum-likelihood detection. In addition, optimum values of the modulation parameters (q, w) that maximizes (d^2_{min}) are obtained.

In Chapter 4, the problem of detection of M-CPCM signals in additive, white, Gaussian noise is addressed. The structures of optimum coherent and non-coherent receivers are derived. Closed-form expressions for symbol error rates of these receivers are derived and illustrated as a function of modulation parameters. A comparison of error rate performance of M-level chirp modulations with other conventional M-level modulations is also provided.

In Chapter 5, the concept of varying the modulation parameters is introduced in M-CPCM. These multi-mode signals are described and illustrated. The detection and performance of multi-mode M-CPCM signals in AWGN is considered. Optimum dual-model M-CPCM systems have been determined. A comparison of error rate performance of these signals with the corresponding single mode is also provided.

Chapter 6 is devoted to the performance analysis of multi-level chirp modulation over fading channels. In particular, closed-form expressions for error rates bounds for M-level chirp modulation over Rayleigh, Nakagami-m and Generalized-k (K_G) fading channels are derived. These bounds are illustrated as a function of energy per bit to noise ratio, E_b/No, channel fading parameters, and modulation parameters (q, w).

In Chapter 7, power spectra of M-CPCM signals are calculated and compared with other modulation schemes. Numerical results for power spectra as a function of modulation parameters (q, w) are presented.

In Chapter 8, the contributions of this thesis and the conclusions from the results obtained are summarized. Also, areas for further research in the light of the needs of modern reliable communication systems are outlined.

Chapter 2

Memoryless Constant-Envelope Multi-Level Chirp Modulation: Coherent and Non-Coherent Detection

2.1 Introduction

In this Chapter, memoryless constant-envelope multi-level chirp modulated signals are proposed for data transmission. These signals are described, illustrated, and examined for their properties. The ability of these signals to operate over AWGN channel is assessed by using minimum Euclidean distance criteria. Next, coherent and non-coherent detection of multi-level chirp modulated signals in AWGN are addressed with optimum detection algorithms, and hence optimum receiver structures are obtained. The performances of these receivers are analyzed and closed-form expressions for symbol error probabilities are derived. Optimum coherent and non-coherent multi-level chirp systems have been determined by minimizing the symbol error rate expressions as a function of signal-to-noise ratio (E_b/N_0), M, modulation level and the set of chirp modulation parameters (q, w). A comparison of performance of multi-level chirp modulation with conventional multi-level modulations such as MPSK and MFSK is also given.

2.2   Constant Envelope Multi-Level Chirp Modulated Signals

The general expression for constant envelope multi-level chirp modulated signal is given by [39]:

$$S_i(t) = \sqrt{\frac{2E_s}{T_s}} \ \cos(w_c t + \phi_i(t) + \theta), \qquad 0 \le t \le T_s, \ i = 1, 2, \dots, M \qquad (2.1)$$

where E_s is the symbol energy, T_s is the symbol duration, w_c is the angular carrier frequency, $\phi_i(t)$ is the information carrying phase, and θ is the starting phase (at $t = 0$).

The information carrying phase $\phi_i(t)$, $i = 1, 2, \dots, M$, is given by:

$$\phi_i(t) = d_i \ g(t) \qquad (2.2)$$

where

$$d_i = \begin{cases} +i, & \text{if } i \text{ is odd} \\ -(i-1), & \text{if } i \text{ is even} \end{cases} \qquad (2.3)$$

represents one of the M input symbols or levels $\pm 1, \pm 3, \dots, \pm(M-1)$ applied to the modulator. The phase function $g(t)$ is given by:

$$g(t) = \begin{cases} 0, & t \le 0, \ t > T_s \\ 2\pi \int\limits_0^t f_d(\tau) d\tau, & 0 \le t \le T_s \\ \pi q = \pi(h - w), & t = T_s \end{cases} \qquad (2.4)$$

where πq denotes the ending phase at $t = T_s$ sec, and $f_d(t)$ is the instantaneous frequency function as given by:

$$f_d(t) = \begin{cases} 0, & t \le 0, \ t > T_s \\ \left(\frac{h}{2T_s}\right) - \left(\frac{w}{T_s^2}\right)t, & 0 \le t \le T_s \end{cases} \qquad (2.5)$$

Using (2.5) in (2.4), (2.2) can be written as:

$$\phi_i(t) = \begin{cases} 0, & t \leq 0, \quad t > T_s \\ d_i\pi \left\{ h\left(\frac{t}{T_s}\right) - w\left(\frac{t}{T_s}\right)^2 \right\}, & 0 \leq t \leq T_s \\ d_i\pi q = d_i\pi(h - w), & t = T_s \end{cases} \tag{2.6}$$

In (2.6), h and w are dimensionless parameters: h represents the peak-to-peak frequency deviation divided by the symbol rate $\frac{1}{T_s}$, and w represents the frequency sweep width divided by the symbol rate $\frac{1}{T_s}$. Since $h = (q + w)$, (q, w) are chosen to be the set of independent signal modulation parameters. It is noted that in an M-level (or M-ary) chirp modulation system, there exist M linear frequency sweeps each uniquely corresponding to the input data $\pm 1, \pm 3, \ldots, \pm(M - 1)$. For example, in a 2-level (binary) system, the linear frequency sweep of the chirp signal assumes a positive or a negative slope corresponding to one of the two information symbols -1 or +1, respectively. A schematic block diagram of the M-level chirp modulation system is shown in Fig. 2.1.
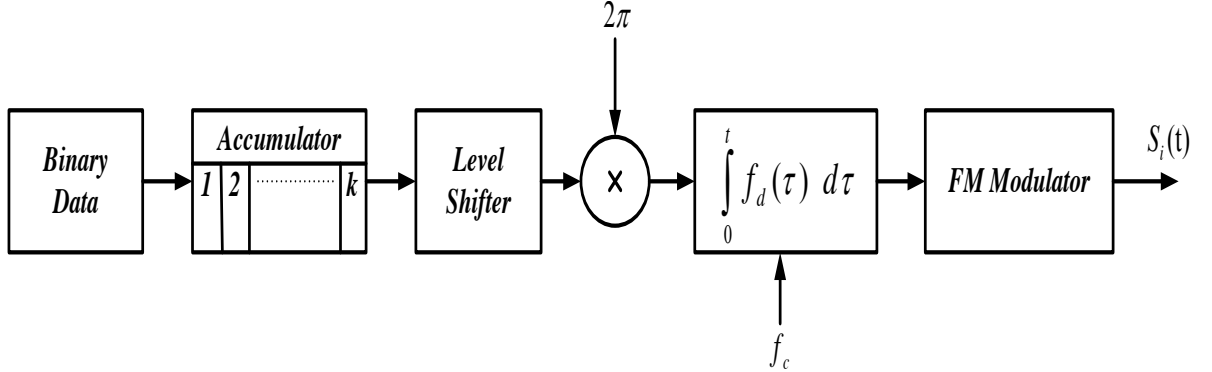
Figure 2.1: Schematic block diagram of M-level $(M = 2^k)$ chirp modulator

It is noted from (2.6) that the phase function is quadratic and hence the frequency function is linear. In Fig. 2.2, both frequency and phase functions are plotted for binary chirp signals.
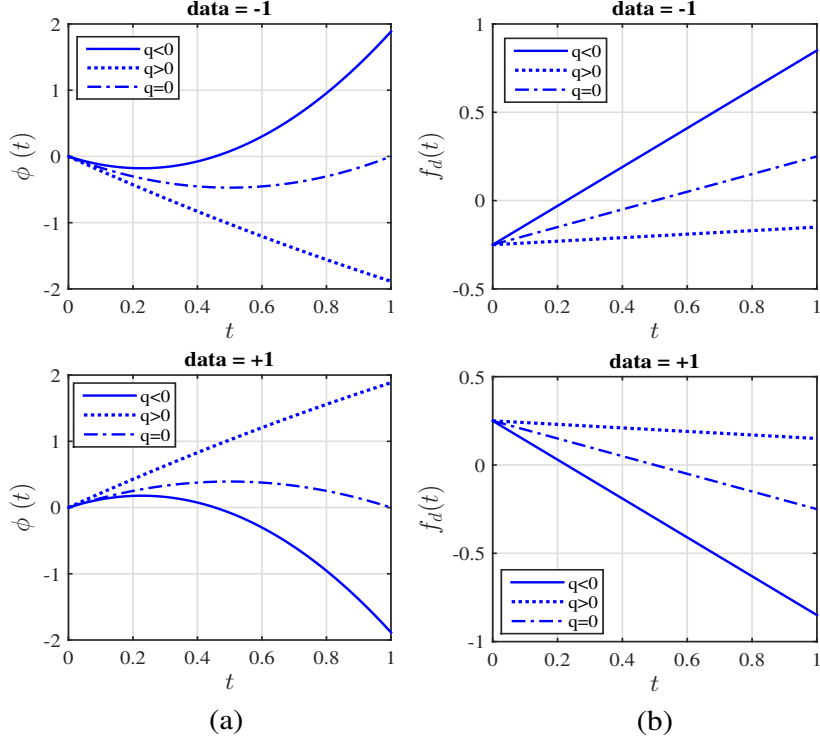
Figure 2.2: Phase (a) and frequency (b) as a function of time for arbitrary binary chirp signal

2.2.1   2-level (2-ary) or Binary Chirp Modulation

In binary chirp modulation, the input to the modulator takes values ± 1. The modulated binary chirp signals are plotted in Fig. 2.3, for arbitrary (q, w). The up-chirp signal represents binary data '-1' which has increasing frequency with respect to time and similarly the down-chirp signal represents binary data '$+1$' with decreasing frequency. These signals are given by [39]:

$$
\left.
\begin{aligned}
+1 &\longrightarrow S_1(t) = \sqrt{\frac{2E_b}{T_b}} \; \cos\left[w_c t + \pi \left\{ h\left(\tfrac{t}{T_b}\right) - w\left(\tfrac{t}{T_b}\right)^2 \right\} \right] \\[2mm]
-1 &\longrightarrow S_2(t) = \sqrt{\frac{2E_b}{T_b}} \; \cos\left[w_c t - \pi \left\{ h\left(\tfrac{t}{T_b}\right) - w\left(\tfrac{t}{T_b}\right)^2 \right\} \right]
\end{aligned}
\right\} \quad 0 \le t \le T_b \qquad (2.7)
$$

where $E_s = E_b$ and $T_s = T_b$; E_b and T_b represent the bit energy and duration,

respectively.
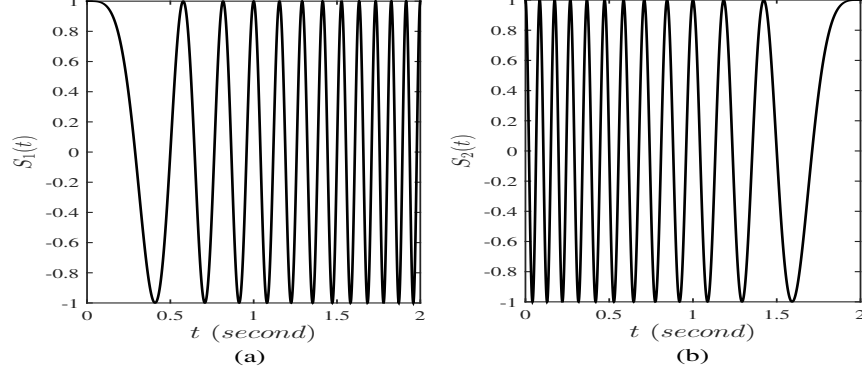
Figure 2.3: Up-chirp (a) and down-chirp (b) Signals

2.2.2 4-level (4-ary) or Quaternary Chirp Modulated Signals

In 4-level chirp modulation, the input to the modulator takes values $\pm 1, \pm 3$. Fig. 2.4 shows 4-level chirp modulated signals. The four possible modulated signals can be written as [39]:

$$\left.\begin{array}{l} +1 \longrightarrow S_1(t) = \sqrt{\dfrac{2E_s}{T_s}} \ \cos\left[2\pi f_c t + 1\pi\left\{h\left(\dfrac{t}{T_s}\right) - w\left(\dfrac{t}{T_s}\right)^2\right\}\right] \\[3mm] -1 \longrightarrow S_2(t) = \sqrt{\dfrac{2E_s}{T_s}} \ \cos\left[2\pi f_c t - 1\pi\left\{h\left(\dfrac{t}{T_s}\right) - w\left(\dfrac{t}{T_s}\right)^2\right\}\right] \\[3mm] +3 \longrightarrow S_3(t) = \sqrt{\dfrac{2E_s}{T_s}} \ \cos\left[2\pi f_c t + 3\pi\left\{h\left(\dfrac{t}{T_s}\right) - w\left(\dfrac{t}{T_s}\right)^2\right\}\right] \\[3mm] -3 \longrightarrow S_4(t) = \sqrt{\dfrac{2E_s}{T_s}} \ \cos\left[2\pi f_c t - 3\pi\left\{h\left(\dfrac{t}{T_s}\right) - w\left(\dfrac{t}{T_s}\right)^2\right\}\right] \end{array}\right\} \ 0 \le t \le (T_s = 2T_b)$$

(2.8)

where $E_s = 2E_b$ and $T_s = 2T_b$.
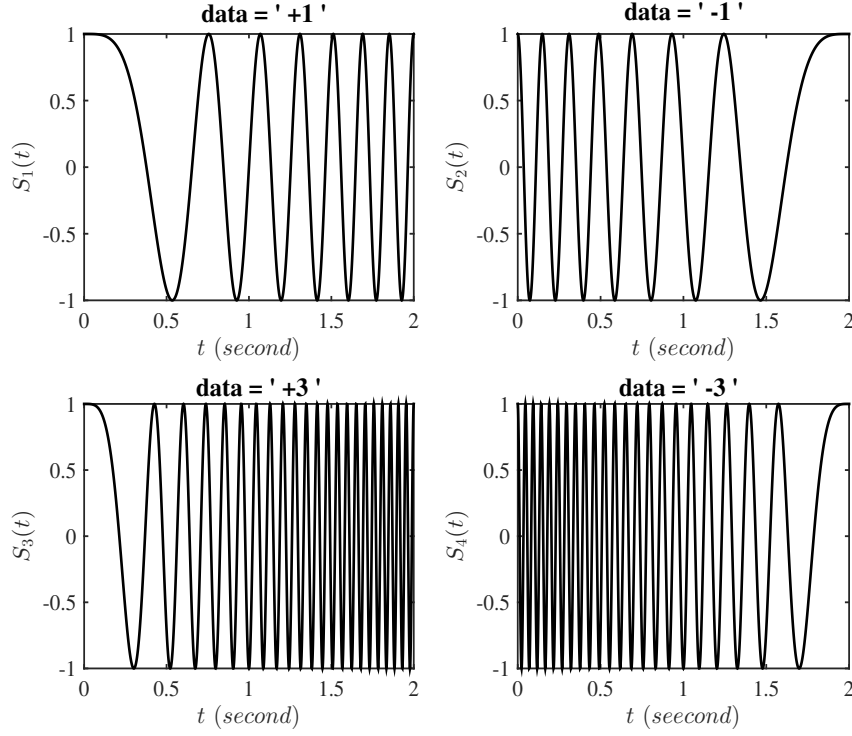
Figure 2.4: 4-level chirp modulated signals as a function of time

2.3 Minimum Euclidean Distance Properties

The Euclidean distance between modulated waveforms in signal-space is a key concept [40] in understanding the ultimate utility of arbitrary signaling technique in any digital communication system. With reference to the set of multi-level chirp modulated waveforms given in (2.1), the squared Euclidean distance between signals $S_i(t)$ and $S_j(t)$ is given by:

$$D^2(S_i, S_j) = \int_0^{T_s} \left[S_i(t) - S_j(t)\right]^2 \ dt \qquad (2.9)$$

which can be simplified and is given by:

$$D^2(S_i, S_j) = 2E_s(1 - \rho(S_i, S_j)) \qquad (2.10)$$

where d_i is the symbol associated with $S_i(t)$ and d_j is the symbol associated with $S_j(t)$, and:

$$\rho(S_i, S_j) = \frac{1}{E_s} \int_0^{T_s} S_i(t) \, S_j(t) \, dt \tag{2.11}$$

represents the normalized correlation between $S_i(t)$ and $S_j(t)$. For sufficiently large SNR, the performance of the optimum maximum likelihood receiver [40] is dominated by the minimum Euclidean distance [3] and is given by:

$$D^2_{min} = \min_{\substack{all\ i,j \\ i \neq j}} \{D^2(S_i, S_j)\} \tag{2.12}$$

and the performance of the optimum receiver is given by:

$$P_e \simeq Q\left[\sqrt{\frac{D^2_{min}}{2N_0}}\right] \tag{2.13}$$

By using energy normalization $d^2 = \frac{D^2}{2E_b}$, it becomes easy to compare different M-level modulation schemes on an equal $\frac{E_b}{N_0}$ basis. It is noted that $d^2_{min} = 2$ for BPSK and QPSK modulations. Thus, an estimate of SNR gain relative to BPSK is given by:

$$G = 10 \log_{10}\left(\frac{d^2}{2}\right) \tag{2.14}$$

For M-level chirp modulation, a closed-form expression for $D^2(S_i, S_j)$ can be obtained (derived in Appendix A) and is given by:

$$D^2(S_i, S_j) = 2E_s(1 - \rho(S_i, S_j)) \tag{2.15}$$

where

$$\rho(S_i, S_j) = \frac{1}{\sqrt{2\gamma w}} \left[\cos(\Omega) \, \mathbb{C} + \sin(\Omega) \, \mathbb{S}\right] \tag{2.16}$$

and

$$\mathbb{C} = \mathbf{C}(u_h) - \mathbf{C}(u_l), \quad \mathbb{S} = \mathbf{S}(u_h) - \mathbf{S}(u_l)$$

$$\Omega = \frac{\pi \gamma h^2}{4w}, \quad \gamma = |d_i - d_j|$$

$$u_h = \sqrt{\frac{\gamma}{2} \frac{(w-q)}{\sqrt{w}}}, \quad u_l = \sqrt{\frac{\gamma}{2} \frac{(w+q)}{\sqrt{w}}}$$

The value d_i $(\pm 1, \pm 3, ..., \pm(M-1))$ is the data associated with the signal $S_i(t)$ and d_j $(\pm 1, \pm 3, ..., \pm(M-1))$ is the data associated with the signal $S_j(t)$. The function $\mathbf{C}(.)$ and $\mathbf{S}(.)$ are the Fresnel cosine and sine integrals [41] which are given by:

$$\mathbf{C}(u) = \int_0^u \cos(\frac{\pi x^2}{2}) dx \tag{2.17}$$

$$\mathbf{S}(u) = \int_0^u \sin(\frac{\pi x^2}{2}) dx \tag{2.18}$$

In order to estimate the limiting SNR gain G given by (2.14) for arbitrary M-level chirp modulation, $d_{min}^2 (= D_{min}^2 / 2E_b)$ needs to be computed using (2.12), (2.15), and (2.16). Table 2.1 shows sets (q, w) that maximize the minimum distance, d_{min}^2, for $M = 2$, 4, 8, and 16 chirp modulations. For M-level chirp, PSK, and FSK modulations d_{min}^2 are shown in Table 2.2.

Table 2.1: (q, w) maximizing d_{min}^2 for M-level chirp modulated signals

M	(q, w)	$\max\{d_{min}^2\}$	G (dB)
2	(0.37, 1.50)	1.635	-0.875
4	(0.20, 0.71)	3.263	2.126
8	(0.20, 0.71)	4.895	3.887
16	(0.20, 0.71)	6.526	5.136

Table 2.2: d_{min}^2 for M-level chirp modulated signals, M-PSK, and M-FSK modulations

M	M-ary Chirp	M-PSK	M-FSK
2	1.635	2.000	1.000
4	3.263	2.000	2.000
8	4.895	0.878	3.000
16	6.526	0.304	4.000

In arriving at the optimum (q, w) sets in Table 2.1, the range of modulation parameter space is bounded by $(0, 0) \leq (q, w) \leq (3, 5)$. In Fig. 2.5 to 2.7 contour and surface plots of d_{min}^2 as a function of modulation parameters q and w are shown. It is noted from Fig. 2.5 that the optimum or the best 2-level chirp modulation is achieved for the set $(q = 0.37, w = 1.5)$. For this optimum 2-level chirp modulation $d_{min}^2 = 1.635$ (Table 2.1) and thus the corresponding SNR gain relative to BPSK is -0.875 dB. It is worthwhile to note that there exist multiple (q, w) sets that result in the same d_{min}^2 thereby suggesting that it is possible to design 2-level chirp systems with varying interference rejection capabilities and yet maintain the same bit error rate performance. For example, in Fig. 2.5, 2-level $(0.37, 1.50)$ and $(0.30, 1.70)$ chirp systems offer the same d_{min}^2 of 1.635. These two systems, therefore have the same bit error rate performance. However, their bandwidth are different and hence different interference rejection capabilities. The surface plots in Figs. 2.6 and 2.7 show the variation of d_{min}^2 as a function of q and w. These plots also confirm that $(q, w) = (0.37, 1.50)$ and $(q, w) = (0.30, 1.70)$ achieve the best distance for 2-level chirp modulation. Table 2.1 also lists the achievable SNR gains relative to BPSK for M=4, 8, and 16-level chirp modulations.
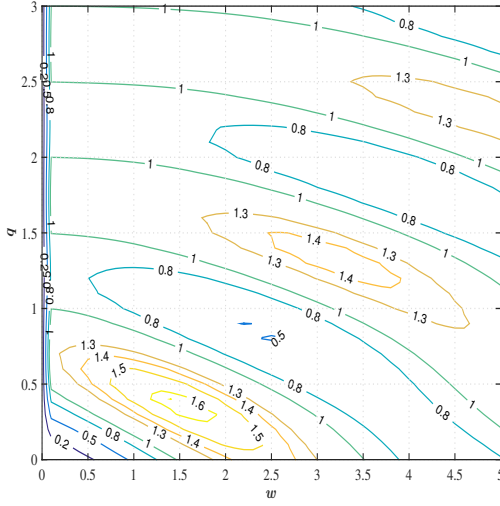
Figure 2.5: Contour plot of d_{min}^2 for 2-level chirp signals
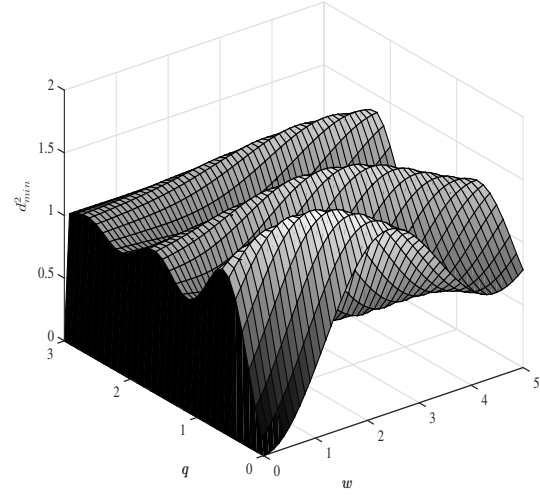
Figure 2.6: Surface plot of d_{min}^2 for 2-level chirp signals
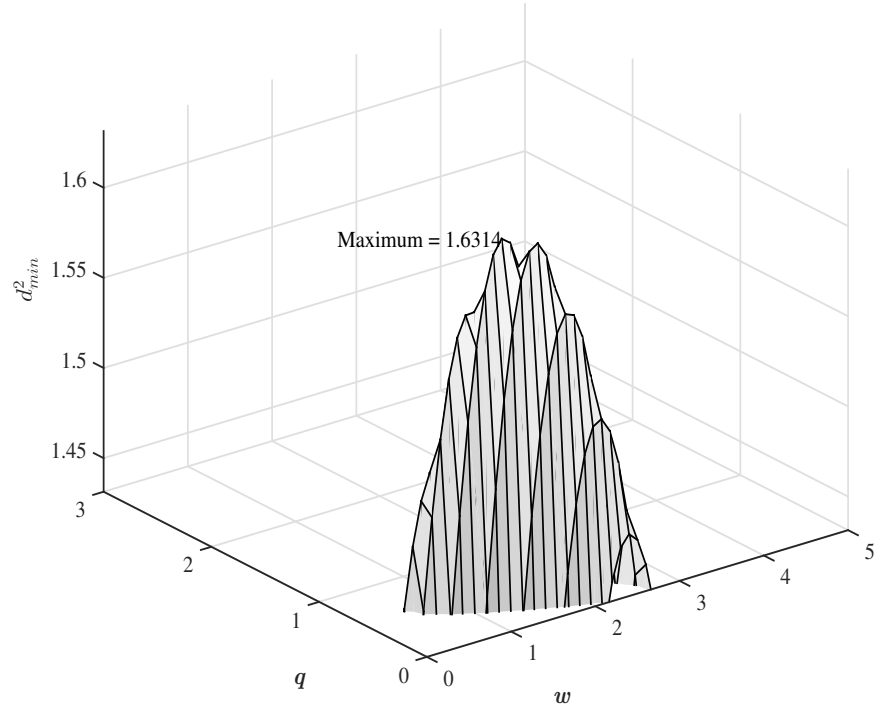
Figure 2.7: Surface plot of d_{min}^2 for 2-level chirp signals

Observation similar to those presented for 2-level chirp modulation can be made for $M = 4, 8$, and 16-level modulations. Figs. 2.8 and 2.9 show contour and surface plots

for d^2_{min} for the 4-level chirp signals. In Fig. 2.8, again it is observed that 4-level chirp systems with same symbol error rate can be designed with different interference rejection capabilities. It is noted that maximum $d^2_{min} = 3.26$ is achieved for two sets of modulation parameters $(q, w) = (0.40, 1.40)$ and $(q, w) = (0.30, 1.70)$. Fig. 2.10 shows multiple peaks of $\max\{d^2_{min}\}$ at different sets of modulation parameters.
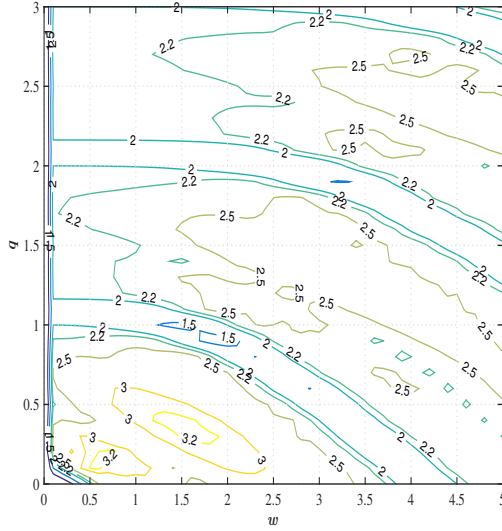
Figure 2.8: Contour plot of d^2_{min} for 4-level chirp signals
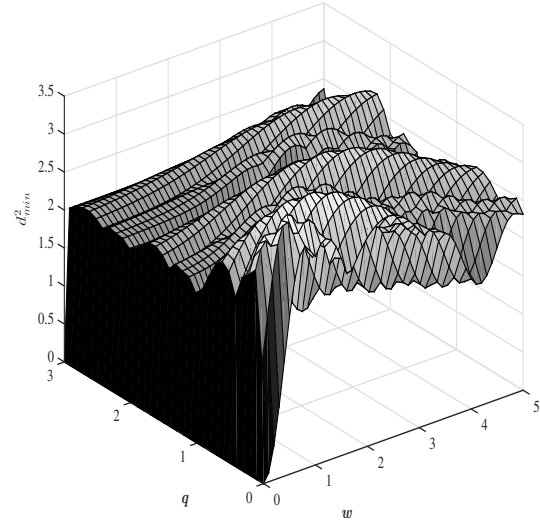
Figure 2.9: Surface plot of d^2_{min} for 4-level chirp signals
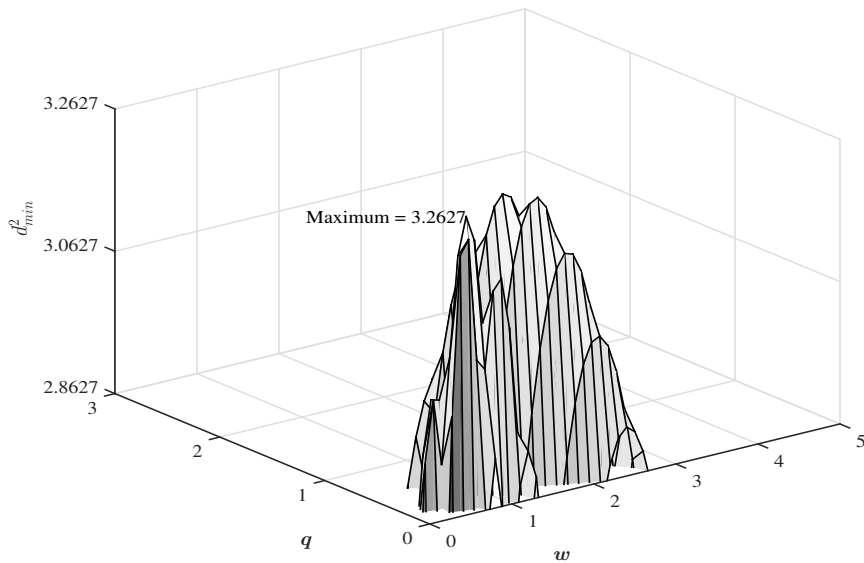
Figure 2.10: Surface plot of d^2_{min} for 4-level chirp signals

For the 8-level chirp signals, Figs. 2.11 and 2.12, show the contour and surface plots for d_{min}^2. It is observed that $\max\{d_{min}^2\} = 4.89$ can be achieved for multiple sets of modulation parameters (q, w). Fig. 2.13 illustrates the maximum peaks of d_{min}^2 which can occur at $(q, w) = (0.4, 1.4)$ and $(q, w) = (0.3, 1.7)$.
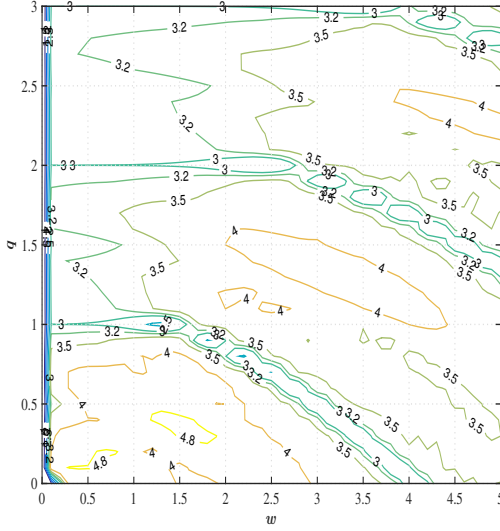
Figure 2.11: Contour plot of d_{min}^2 for 8-level chirp signals
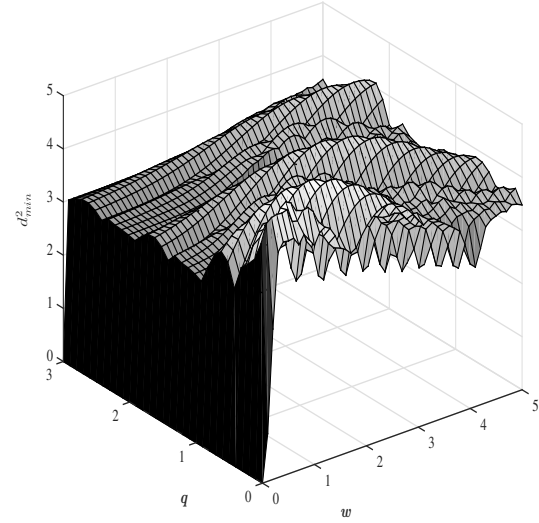
Figure 2.12: Surface plot of d_{min}^2 for 8-level chirp signals
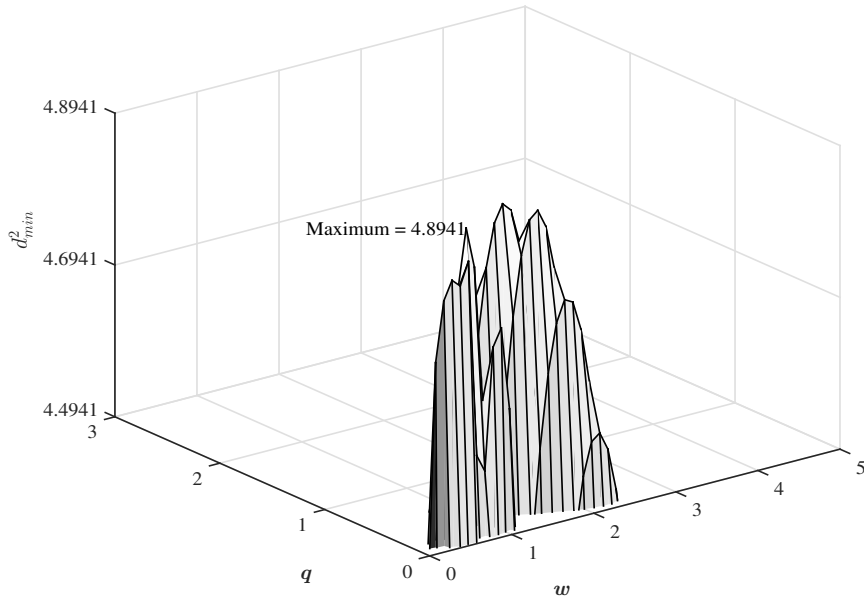
Figure 2.13: Surface plot of d_{min}^2 for 8-level chirp signals

Figs. 2.14-2.16 show the contour and surface plots for 16-level chirp signals. $\max\{d^2_{min}\} = 6.53$ occurs at different sets of modulation parameters $(q, w) = (0.4, 1.4)$ and $(0.3, 1.7)$.
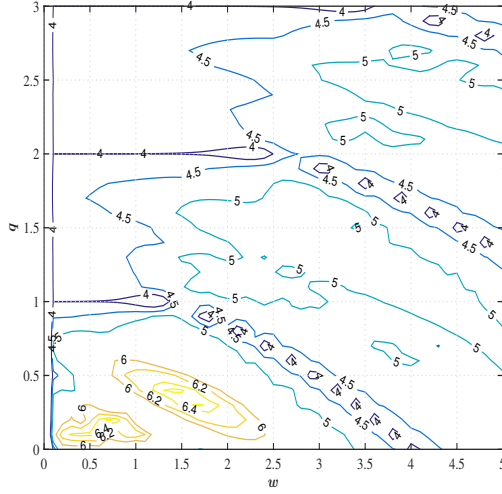
Figure 2.14: Contour plot of d^2_{min} for 16-level chirp signals
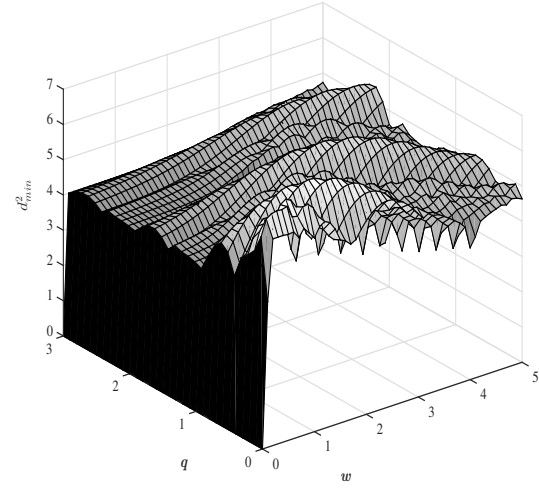
Figure 2.15: Surface plot of d^2_{min} for 16-level chirp signals
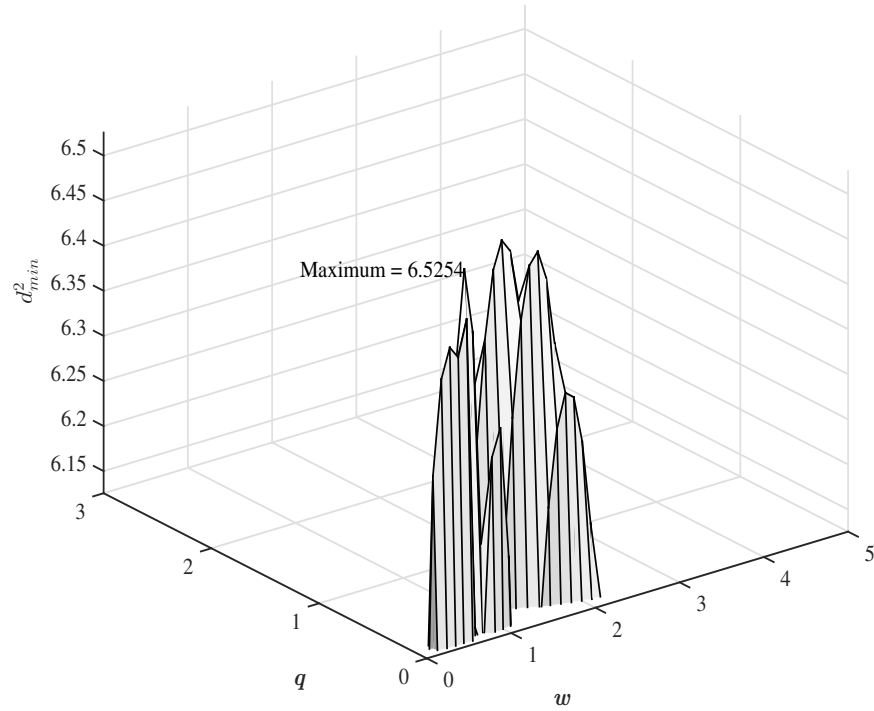
Figure 2.16: Surface plot of d^2_{min} for 16-level chirp signals

In general, it is observed that M-level chirp systems provide very good flexibility in terms of system design as a function of modulation parameters q and w. It is noted that $\max\{d_{min}^2\}$ is an indication of the ultimate ability of a given signaling technique in AWGN. Also, this distance provides an upper bound on the achievable performance of the conceptual maximum likelihood receiver [42]. In the next Section, detection of M-level chirp modulated signals in AWGN is addressed to obtain the structure of the optimum receiver. Both coherent and non-coherent detection situations are considered.

2.4 Coherent Detection and Performance of Multi-level (M-ary) Chirp Signals

2.4.1 Coherent Detection

The detection of M-level chirp modulated signals can be stated as an M-hypotheses testing problem [40] as given by:

$$\left. \begin{array}{l} H_1 : r(t) = S_1(t) + n(t) \\ H_2 : r(t) = S_2(t) + n(t) \\ \quad\vdots \\ H_M : r(t) = S_M(t) + n(t) \end{array} \right\} \quad 0 \le t \le T_s \quad (2.19)$$

where $S_i(t), i = 1, 2, \ldots, M$ are the M chirp modulated signals given by (2.1), $r(t)$ is the received waveform, and $n(t)$ is the AWGN with two-sided spectral density of $\frac{N_0}{2}$ watts/Hz. For coherent detection, θ in (2.1) is set equal to zero. The detection problem is to observe the received waveform $r(t)$ in (2.19), $0 \le t \le T_s$, and to produce an optimum decision as to which of the M equally likely chirp signals was transmitted. It is noted that the M outputs of the chirp modulator are equally likely and hence their *a priori* probabilities are given by:

$$P(S_1) = P(S_2) = \cdots = P(S_M) = \frac{1}{M} \quad (2.20)$$

and their symbol energies are the same and is given by:

$$E_s = \int\limits_0^{T_s} S_i^2(t) \ dt, \qquad i = 1, 2, \ldots, M \tag{2.21}$$

The solution to the M-hypothesis testing problem stated in (2.19) is the Bayesian receiver that performs the maximum Likelihood Ratio Test (LRT) [40]. Such a test determines the M likelihood functions given by:

$$\Lambda(R|H_i) = p_{r|H_i}(R|H_i), \qquad i = 1, 2, \ldots, M \tag{2.22}$$

where

$$R = S_i + \underline{N} \tag{2.23}$$

and

$$\begin{aligned} R &= [r_1, \ldots, r_N]^T \\ S_i &= [s_{i1}, \ldots, s_{iN}]^T \\ \underline{N} &= [n_1, \ldots, n_N]^T \end{aligned} \tag{2.24}$$

with

$$\left. \begin{aligned} r_j &\triangleq r(t_j) \\ s_{ij} &\triangleq S_i(t_j) \\ n_j &\triangleq n(t_j) \end{aligned} \right\} \quad j = 1, 2, \ldots, N \tag{2.25}$$

Assuming the noise samples are i.i.d, (2.23) can be written as:

$$p_{r|H_i}(R|H_i) = \prod_{j=1}^N p_n(r_j - s_{ij}) \tag{2.26}$$

$$\Lambda(R|H_i) = p_{r|H_i}(R|H_i) = \prod_{j=1}^N \frac{1}{\sqrt{\pi N_0}} e^{-\frac{(r_j - s_{ij})^2}{N_0}}, \qquad i = 1, 2, \ldots, M \tag{2.27}$$

which can be written as:

$$\Lambda(R|H_i) = \left(\frac{1}{\pi N_0}\right)^{N/2} \exp\left\{\frac{1}{N_0}\left[2\sum_{j=1}^{N} r_j r_{ij} - \sum_{j=1}^{N} r_j^2 - \sum_{j=1}^{N} r_{ij}^2\right]\right\}, \qquad i = 1, 2, \ldots, M$$

(2.28)

canceling the common terms and taking limit in the mean (l.i.m) as $N \to \infty$, [40] (2.28) can be written as:

$$\Lambda(R|H_i) = \exp\left[\frac{2}{N_0}\int_0^{T_s} r(t)\, S_i(t)\, dt\right]$$

(2.29)

where $\int_0^{T_s} r(t)\, S_i(t)\, dt$ is the correlation of the received waveform $r(t)$ with the known signal $S_i(t)$, over $0 \le t \le T_s$. Also, it is noted that:

$$\underset{N\to\infty}{l.i.m} \sum_{j=1}^{N} r_j^2 = \int_0^{T_s} r^2(t)\, dt$$

(2.30)

and

$$\underset{N\to\infty}{l.i.m} \sum_{j=1}^{N} s_{ij}^2 = \int_0^{T_s} S_i^2(t)\, dt, \qquad i = 1, 2, \ldots, M$$

(2.31)

The optimum receiver just needs to determine the M likelihood functions $\Lambda(R|H_i), i = 1, 2, \ldots, M$, and choose the maximum of these for obtaining a decision on the data transmitted. By taking natural logarithm on both sides of (2.29), we get log likelihood functions given by:

$$\acute{l}_i = \ln\left[\acute{\Lambda}(R|H_i)\right] = \frac{2}{N_0}\int_0^{T_s} r(t)\, S_i(t)\, dt, \quad i = 1, 2, \ldots, M$$

(2.32)

Multiplying both sides by $\frac{N_0}{2}$, the M likelihood functions in (2.32) can be written

as:

$$l_i = \int_0^{T_s} r(t)\; S_i(t)\; dt, \quad i = 1, 2, \ldots, M \tag{2.33}$$

The optimum coherent receiver will determine M log likelihood functions l_i, $i = 1, 2, \ldots, M$, and produces an estimate of the transmitted data $\hat{d}$ based on the largest of these values. Thus, the decision rule is:

$$l_k = \max\{l_1, l_2, \ldots, l_M\} \tag{2.34}$$

The receiver decides the transmitted data as:

$$\hat{d} = \begin{cases} +k, & k \quad \text{odd} \\ -(k-1), & k \quad \text{even} \end{cases} \tag{2.35}$$

The structure of the receiver that implements the decision rule of (2.34) is shown in Fig. 2.17.
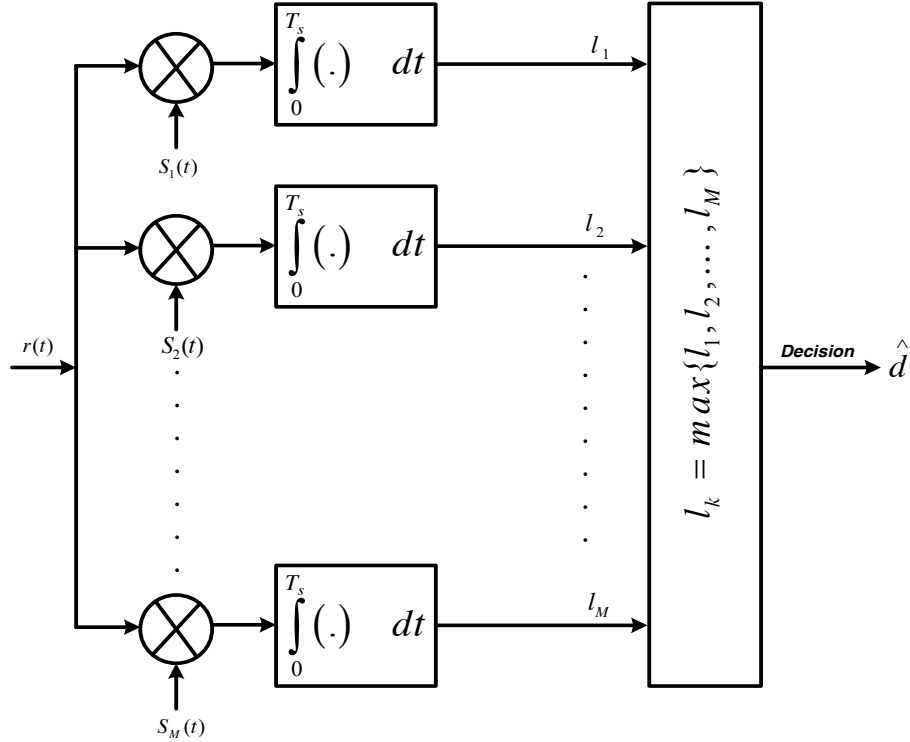
Figure 2.17: Optimum coherent receiver for M-level chirp modulation

2.4.2 Error Rate Performance

With reference to Fig. 2.17, it is noted that the decision variable $l_i, i = 1, 2, \ldots, M,$ are Gaussian random variables. Let hypothesis H_j be true. Then, the received signal is given by:

$$r(t) = S_j(t) + n(t), \quad 0 \leq t \leq T_s \tag{2.36}$$

The conditional probability of the receiver making a symbol error is given by:

$$P\left(\epsilon/H_j\right) = P_r\left[l_1 > l_j \ or \ l_2 > l_j \ldots \ or \ l_M > l_j | H_j\right] \tag{2.37}$$

Using the identity $P(x_1 + x_2 + \ldots x_n) \leq \sum\limits_{j=1}^{n} p(x_j)$, and fitting a union bound [40], and averaging over all H_j, the probability of symbol error can be bounded and is given by:

$$P_M(\epsilon) \leq \sum_{j=1}^{M} \sum_{\substack{i=1 \\ i \neq j}}^{M} P(H_j) P_r\left[l_i > l_j | H_j\right] \tag{2.38}$$

Assuming all hypotheses are equally likely, the average symbol probability of error can be simplified and is given by:

$$P_M(\epsilon) \leq \frac{1}{M} \sum_{j=1}^{M} \sum_{\substack{i=1 \\ i \neq j}}^{M} P_r\left[l_i > l_j | H_j\right] \tag{2.39}$$

where
$$P_r\left[l_i > l_j | H_j\right] = \frac{1}{2}\left\{1 - \mathrm{erf}\left[\sqrt{\frac{E_b \log_2(M)}{2N_0}\left(1 - \rho(i,j)\right)}\right]\right\} \tag{2.40}$$

and

$$\mathrm{erf}(x) \triangleq \frac{2}{\sqrt{\pi}} \int_0^x e^{-t^2} \, dt \tag{2.41}$$

The quantity $\rho(i, j)$ is the normalized correlation between $S_i(t)$ and $S_j(t)$ and is defined in (2.16).

2.4.3 Numerical Results

The performance of the optimum coherent M-level chirp receiver (Fig. 2.17) can be evaluated using the expression for symbol error probability given by (2.39). The symbol error probability is a function of: i) M, number of modulation levels; ii) $\frac{E_b}{N_0}$, Signal-to-Noise-Ratio (SNR), and iii) (q, w), the set of modulation parameters. The set (q, w) which should be chosen for a given M and $\frac{E_b}{N_0}$ is the one that minimizes the probability of symbol error given by (2.39). This has been done numerically and optimum sets (q_{opt}, w_{opt}) have been determined for $M = 2, 4, 8$, and 16, at $\frac{E_b}{N_0} = 6, 8$, and 10 dB. It is observed that (q_{opt}, w_{opt}) obtained are the same at all three SNRs for each $M = 2, 4, 8$, and 16. These are tabulated in Table 2.3. For 2-level chirp modulation, the set $(0.36, 1.52)$ minimizes the probability of bit error, $P_2(\epsilon)$, at an SNR of 6 dB, yielding $\min\{P_2(\epsilon)\} = 5.37 \times 10^{-3}$. Similarly, sets $(0.40, 2.40)$, $(0.95, 0.25)$, and $(0.95, 0.50)$ minimize $P_4(\epsilon)$, $P_8(\epsilon)$, and $P_{16}(\epsilon)$ for 4-, 8-, and 16-level chirp modulations, respectively. In order to understand the effect of (q, w) on symbol error probability, $P_M(\epsilon)$, relative to $\min\{P_M(\epsilon)\}$ are shown in Figs 2.18-2.21 for M=2,4,8, and 16. The contours in these figures show $\log_{10}\left(P_M(\epsilon)/\min\{P_M(\epsilon)\}\right)$, where $P_M(\epsilon)$ is the symbol error probability for a given set of modulation parameters (q, w) and $\min\{P_M(\epsilon)\}$ is the symbol error probability for the optimum set of modulation parameters (q_{opt}, w_{opt}) given in Table 2.3. For example, in Fig. 2.18, the contour 1.1071 indicates that there exist a sub-range of q and w for which symbol error probability is $10^{1.1071}$ times that of the symbol error probability for the optimum set $(0.36, 1.52)$. The larger the value of the contour, the poorer is the performance relative to the optimum chirp modulation. It is observed from these contour plots that as the number of modulation levels increases, symbol error probability becomes less sensitive to (q, w).

Figure 2.18: $\log_{10}\left(P_2(\epsilon)/\min\{P_2(\epsilon)\}\right)$ contour plot for coherent 2-level chirp receiver at 6 dB SNR
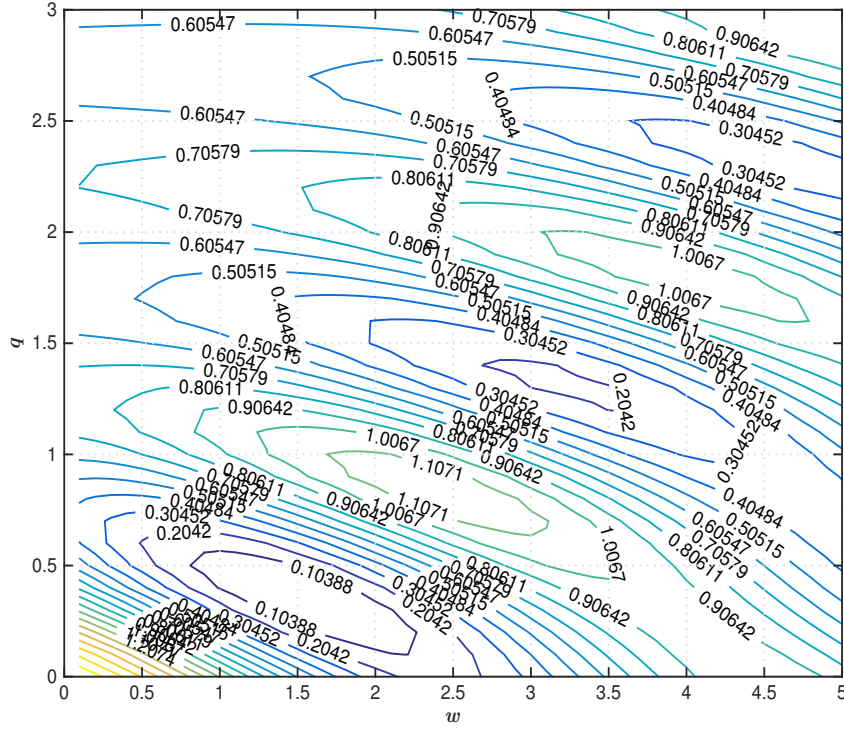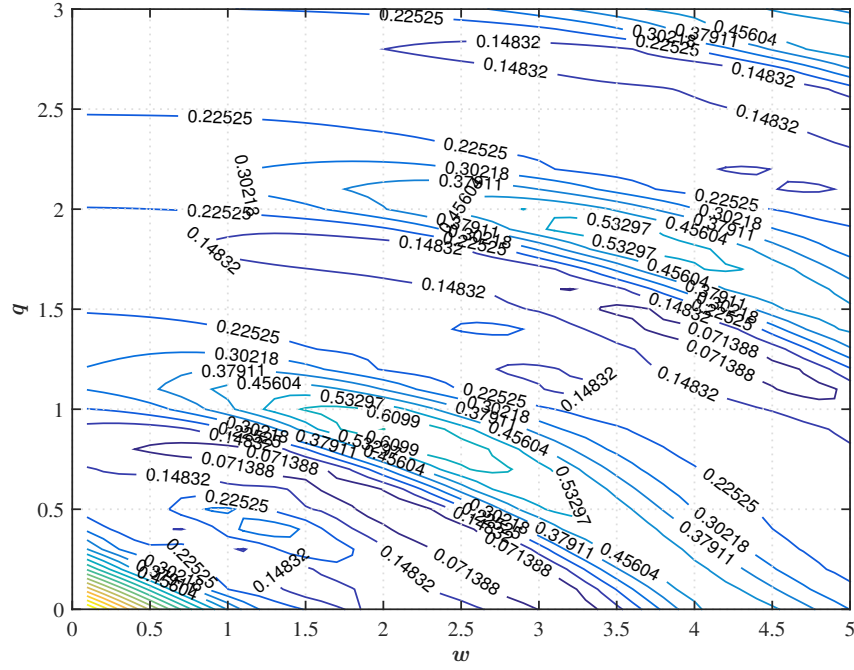
Figure 2.19: $\log_{10}\left(P_4(\epsilon)/\min\{P_4(\epsilon)\}\right)$ contour plot for coherent 4-level chirp receiver at 6 dB SNR
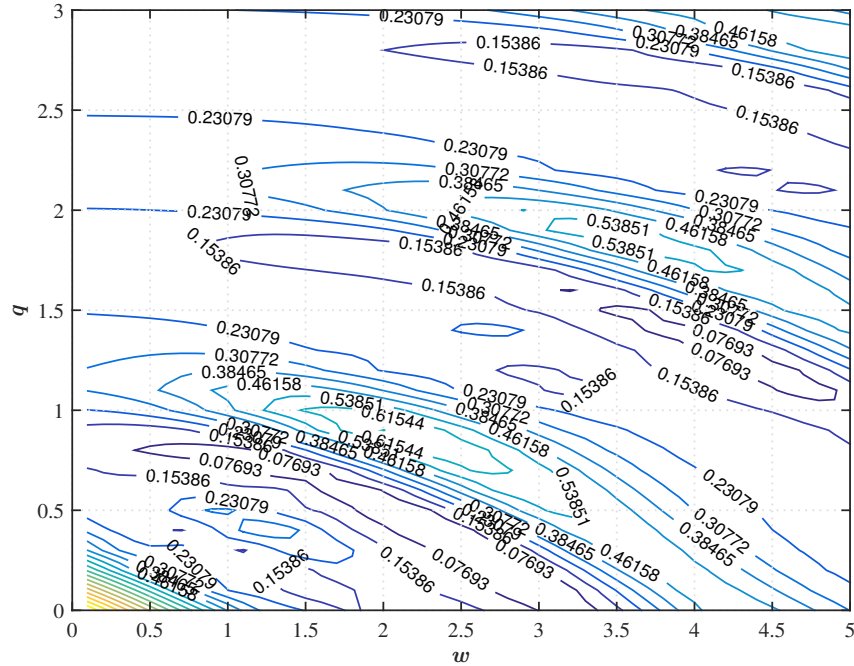
Figure 2.20: $\log_{10}\left(P_8(\epsilon)/\min\{P_8(\epsilon)\}\right)$ contour plot for coherent 8-level chirp receiver at 6 dB SNR
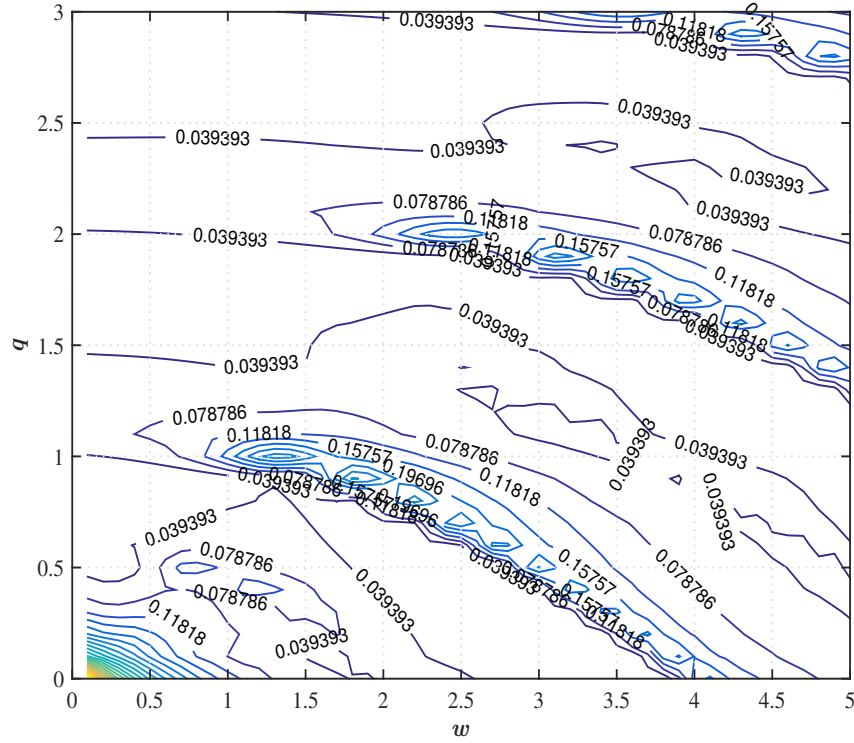
Figure 2.21: $\log_{10}\left(P_{16}(\epsilon)/\min\{P_{16}(\epsilon)\}\right)$ contour plot for coherent 16-level chirp receiver at 6 dB SNR

Table 2.3: Optimum modulation parameters (q_{opt}, w_{opt}) for $M =$ 2,4,8 and 16-chirp systems

Modulation Size (M)	(q, w)
2	(0.36,1.52)
4	(0.40,2.40)
8	(0.95,0.25)
16	(0.95, 0.50)

Fig. 2.22 shows the error rate performance of the optimum binary chirp system ($q = 0.36$ and $w = 1.52$). In the same figure, performances of BPSK and binary orthogonal FSK are shown. Table 2.4 summarizes bit error rate performance of optimum 2-level chirp, BPSK, and 2-level coherent orthogonal FSK systems as a function of SNR (=6,8, and 10 dB).
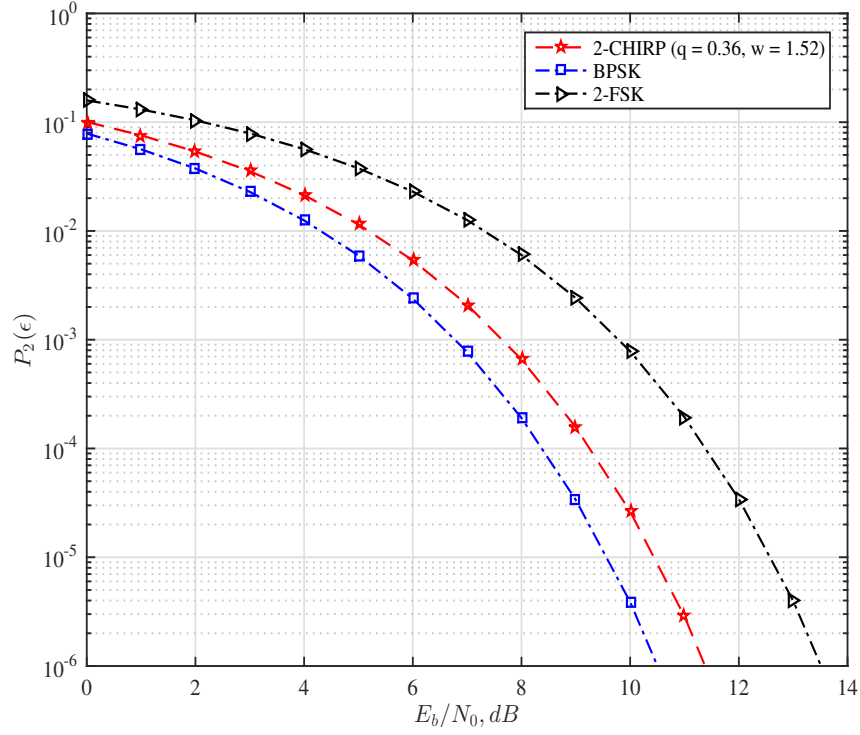
Figure 2.22: Error probability performance of optimum coherent binary chirp system $(q = 0.36, w = 1.52)$

Table 2.4: Bit Error Rate Comparison of Optimum 2-level chirp, BPSK and binary FSK

SNR (dB)	$P_2(\epsilon)$		
	2-chirp	**BPSK**	**2-FSK**
6	5.37×10^{-3}	2.39×10^{-3}	2.30×10^{-2}
8	6.59×10^{-4}	1.91×10^{-4}	6.00×10^{-3}
10	2.63×10^{-5}	3.87×10^{-6}	7.83×10^{-4}

In order to examine the behavior of binary chirp modulation as a function of modulation parameters w and q, in Fig. 2.23 and Fig. 2.24 error probability performances are shown as a function of w and q, respectively. It is observed that for

a fixed value of q the bit error rate performance is not very sensitive to variation in the value of w; however, for a fixed value of w, error probability performance is more sensitive to variation in the value of q.

Figure 2.23: Error probability performance of coherent binary chirp system as a function of w, for a fixed value of $q = 0.36$

In Fig.2.25, the symbol error rate performances of optimum 4-level chirp, QPSK and 4-FSK modulations are shown. It is observed that the optimum 4-level chirp system is superior to 4-FSK by around 1 dB and to QPSK by nearly 0.5 dB. Table 2.5 summarizes the behavior of $P_4(\epsilon)$ values at 6, 8 and 10 dB for these modulations.

Figure 2.24: Error probability performance of coherent binary chirp system as a function of q, for a fixed value of $w = 1.52$

Figure 2.25: Error probability performance of coherent 4-level optimum chirp system ($q = 0.4, w = 2.4$)

Table 2.5: Symbol Error Rate Performance of Optimum 4-level chirp, QPSK and 4-FSK

SNR (dB)	$P_4(\epsilon)$		
	4-chirp	**QPSK**	**4-FSK**
6	2.79×10^{-3}	4.78×10^{-3}	7.17×10^{-3}
8	1.37×10^{-4}	3.82×10^{-4}	5.73×10^{-4}
10	1.32×10^{-6}	7.74×10^{-6}	1.16×10^{-5}

Fig.2.26 shows the performance of optimum 8-level chirp modulation. In the same figure, performances of 8-PSK and orthogonal 8-FSK are shown. Table 2.6 summarizes the $P_8(\epsilon)$ values for 6, 8 and 10 dB for these modulations. It is observed that 8-level chirp system has nearly same performance as that of 8-FSK and outperform 8-PSK by nearly 5 dB.

Table 2.6: Symbol Error Rate Performance of Optimum 8-level chirp, 8-PSK and 8-FSK

SNR (dB)	$P_8(\epsilon)$		
	8-chirp	**8-PSK**	**8-FSK**
6	1.39×10^{-3}	6.14×10^{-2}	1.92×10^{-3}
8	2.87×10^{-5}	1.85×10^{-2}	4.75×10^{-5}
10	6.93×10^{-8}	3.03×10^{-3}	1.51×10^{-7}

In Fig.2.27, the error rate performances of optimum 16-level chirp, 16-PSK and 16-FSK modulation are shown. Table 2.7 summarizes $P_8(\epsilon)$ values for 6, 8 and 10
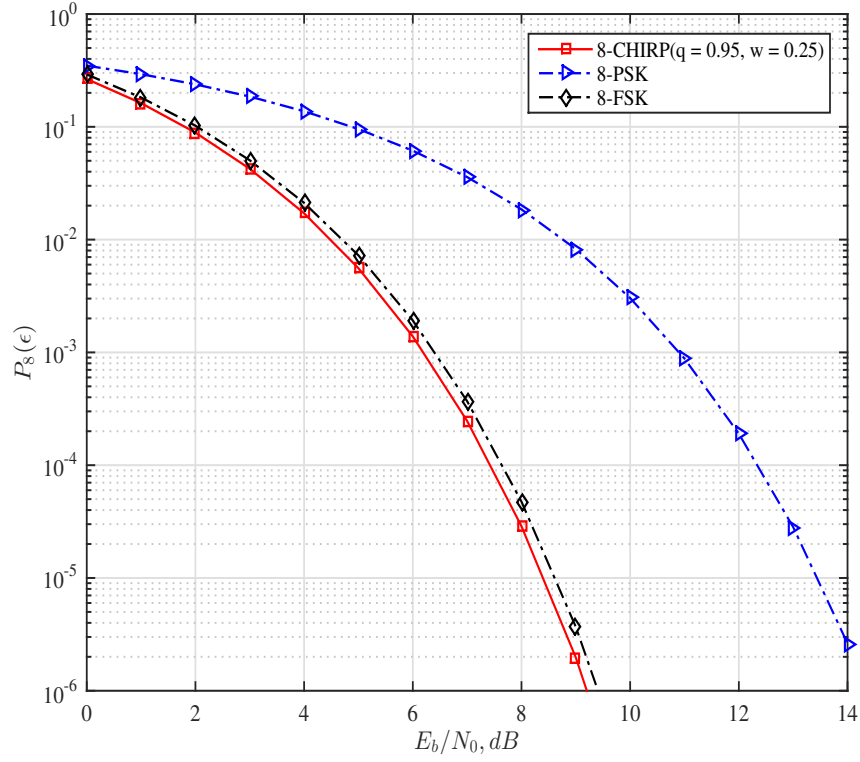
Figure 2.26: Error probability performance of coherent 8-level optimum chirp system ($q = 0.95, w = 0.25$)

dB for these modulations. It is observed that the optimum 16-ary chirp system is superior to 16-PSK for SNR> 7 dB and has a performance almost same as 16-FSK.

Table 2.7: Symbol Error Rate Performance of Optimum 16-level chirp, 16-PSK and 16-FSK

SNR (dB)	$P_{16}(\epsilon)$		
	16-chirp	16-PSK	16-FSK
6	3.75×10^{-4}	2.71×10^{-1}	4.95×10^{-4}
8	2.56×10^{-6}	1.66×10^{-1}	3.80×10^{-6}
10	1.12×10^{-9}	8.10×10^{-2}	1.91×10^{-9}
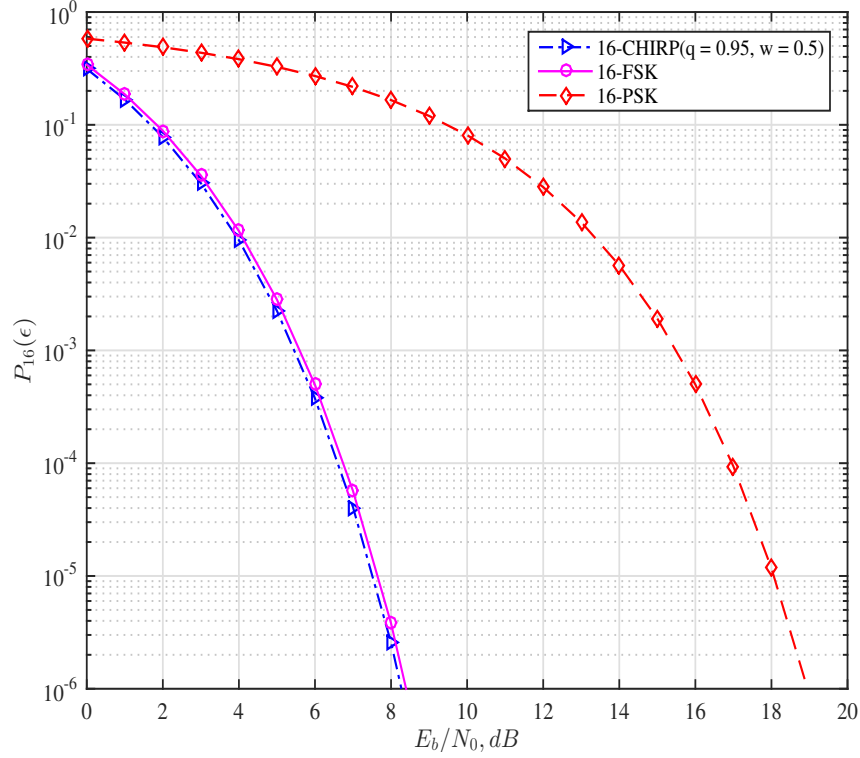
Figure 2.27: Error probability performance of coherent 16-level optimum chirp system $(q = 0.95, w = 0.5)$

2.5 Non-Coherent Detection and Performance of Multi-level (M-ary) Chirp Signals

2.5.1 Non-Coherent Detection

The received M-level chirp modulated signals in AWGN can be stated as:

$$H_i : r(t) = S_i(t, \theta) + n(t), \qquad 0 \le t \le T_s, \qquad i = 1, \dots, M \qquad (2.42)$$

The detection problem is similar to the problem stated for the coherent case in (2.19) except that the starting phase θ in (2.42) is considered to be an independent uniformly

distributed random variable with probability density given by:

$$p_\theta(\theta) = \begin{cases} \dfrac{1}{2\pi}, & 0 < \theta \leq 2\pi \\ \\ 0, & \text{elsewhere} \end{cases} \tag{2.43}$$

The solution to the hypothesis testing problem in (2.42) is the maximum likelihood ratio test (LRT) [40]. Following the development presented for the coherent detection case in Section 2.4, the optimum non-coherent receiver for multi-level chirp modulation computes the M likelihood function given by:

$$
\begin{aligned}
l_1 &= \int_\theta \exp\left[\frac{2}{N_0} \int_0^{T_s} r(t)\, S_1(t,\theta)\, dt \right] p_\theta(\theta)\ d\theta \\
&\quad\quad \vdots \\
&\quad\quad \vdots \\
l_M &= \int_\theta \exp\left[\frac{2}{N_0} \int_0^{T_s} r(t)\, S_M(t,\theta)\, dt \right] p_\theta(\theta)\ d\theta
\end{aligned}
\tag{2.44}
$$

Using (2.43) in (2.44), the M likelihood functions can be written as:

$$l_i = I_0\left(\frac{2}{N_0} Z_i \right), \quad i = 1, 2, \ldots, M \tag{2.45}$$

where

$$Z_i^2 = \left(\int_0^{T_s} r(t)\, S_i(t,0)\, dt \right)^2 + \left(\int_0^{T_s} r(t)\, S_i(t, \frac{\pi}{2})\, dt \right)^2 \tag{2.46}$$

and I_0 is the zeroth-order Bessel function [3]. Since $I_0(.)$ is a monotonically increasing function, the optimum receiver simplify computes the max $\{Z_1, \ldots, Z_M\}$ to arrive at an estimate of the data transmitted. The receiver that dictates this decision rule is shown in Fig. 2.28.
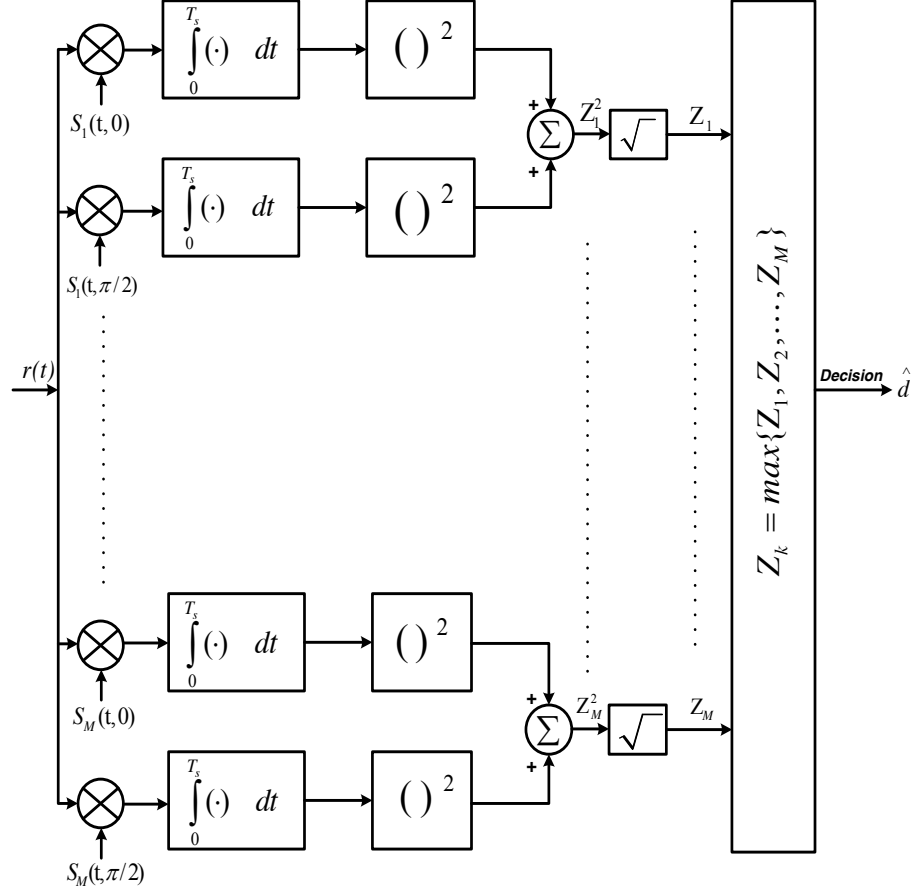
Figure 2.28: Optimum non-coherent receiver for M-level chirp signals

Thus, the decision rule can be stated as:

$$Z_k = \max\{Z_1, Z_2, \ldots, Z_M\} \tag{2.47}$$

The receiver decides the transmitted data as:

$$\hat{d} = \begin{cases} +k, & k \text{ odd} \\ -(k-1), & k \text{ even} \end{cases} \tag{2.48}$$

2.5.2 Error Rate Analysis

The symbol error probability performance of the optimum non-coherent receiver shown in Fig. 2.28 can be derived by noting that $Z_i s$ are Rician random variables [3].

Assuming hypothesis H_j is true, the probability of making a symbol error is given by:

$$P\left(\epsilon/H_j\right) = Pr\left[Z_1 > Z_j \text{ or } Z_2 > Z_j \ldots \text{ or } Z_M > Z_j | H_j\right] \qquad (2.49)$$

Employing the union bounding technique used for the case of coherent receiver in Section 2.4, the conditional probability of symbol error is given by:

$$P(\epsilon|H_j) \leq \sum_{\substack{i=1 \\ i \neq j}}^{M} Pr\left[Z_i > Z_j | H_j\right] \qquad (2.50)$$

Averaging over all equally likely hypotheses, the probability of symbol error is given by:

$$P_M(\epsilon) \leq \frac{1}{M} \sum_{j=1}^{M} \sum_{\substack{i=1 \\ i \neq j}}^{M} Pr\left[Z_i > Z_j | H_j\right] \qquad (2.51)$$

where $Pr\left[Z_i > Z_j | H_j\right]$ is the probability of Rician random variable Z_i exceeding another Rician random variable Z_j [40] and is given by:

$$Pr\left[Z_i > Z_j | H_j\right] = \frac{1}{2}\left[1 - Q(\sqrt{b}, \sqrt{a}) + Q(\sqrt{a}, \sqrt{b}))\right] \qquad (2.52)$$

where

$$\left\{\begin{matrix} a \\ \\ b \end{matrix}\right\} = \frac{E_s}{2N_0}\left(1 \mp \sqrt{1 - |\rho_c(i,j)|^2}\right) \qquad (2.53)$$

and $Q(x,y)$ is the Marcum Q function defined as:

$$Q(x,y) = \int_y^\infty \exp\left[-\left(\frac{x^2 + u^2}{2}\right)\right] I_0(xu) \, u \, du \qquad (2.54)$$

The quantity $\rho_c(i, j)$ denotes the complex correlation which is given by:

$$\rho_c(i, j) = \frac{1}{2E_s} \int_0^{T_s} S_i^c(t) \; S_j^{c*}(t) \; dt \tag{2.55}$$

where

$$S_k^c(t) = S_k(t, 0) + j \; S_k(t, \pi/2), \;\; k = 1, 2, ..., M$$

and $*$ denotes complex conjugation. Appendix B provides derivation for the closed form expression for equation (2.55) which is given by:

$$\rho_c(i, j) = \left[\frac{\cos(\Omega)}{\sqrt{2\gamma w}} \; \mathbb{C}_r + \frac{\sin(\Omega)}{\sqrt{2\gamma w}} \; \mathbb{S}_r \right]$$

$$+ j \left[\frac{\cos(\Omega)}{\sqrt{2\gamma w}} \; \mathbb{C}_i + \frac{\sin(\Omega)}{\sqrt{2\gamma w}} \; \mathbb{S}_i \right] \tag{2.56}$$

where

$$\mathbb{C}_r = \mathbf{C}(u_h) - \mathbf{C}(u_l), \;\; \mathbb{S}_r = \mathbf{S}(u_h) - \mathbf{S}(u_l)$$

$$\mathbb{C}_i = \mathbf{S}(u_h) - \mathbf{S}(u_l), \;\; \mathbb{S}_i = -\mathbf{C}(u_h) + \mathbf{C}(u_l)$$

$$\Omega = \frac{\pi\gamma h^2}{4w}, \;\; \gamma = |d_i - d_j|$$

$$u_h = \sqrt{\frac{\gamma}{2}} \frac{(w - q)}{\sqrt{w}}, \;\; u_l = \sqrt{\frac{\gamma}{2}} \frac{(w + q)}{\sqrt{w}}$$

The value $d_i \; (\pm 1, \pm 3, ..., \pm(M - 1))$ is the data associated with the signal $S_i^c(t)$ and $d_j \; (\pm 1, \pm 3, ..., \pm(M - 1))$ is the data associated with the signal $S_j^j(t)$. The function $\mathbf{C}(.)$ and $\mathbf{S}(.)$ are the Fresnel cosine and sine integral which were defined in (2.17) and (2.18).

2.5.3 Numerical Results

The symbol error rate performance of the optimum non-coherent receiver for multi-level chirp modulation can be determined using equations (2.51). The symbol error rate is a function of i) M, ii) $\frac{E_b}{N_0}$ and (iii) (q, w). An insight into the behavior of symbol error rate of non-coherent chirp modulation can be obtained using contour plots shown in Fig. (2.29), Fig. (2.30), and Fig. (2.31), for $M = 2$, $M = 4$, and $M = 8$ chirp systems. From these figures it is observed that there exist nearly orthogonal chirp systems for $M = 2, 4$, and 8 modulation levels. Again multiple sets of (q, w) exists, for each of these M, for which nearly orthogonal chirp modulation can be found. Lower the value of the contour closer it is to the orthogonal signaling.
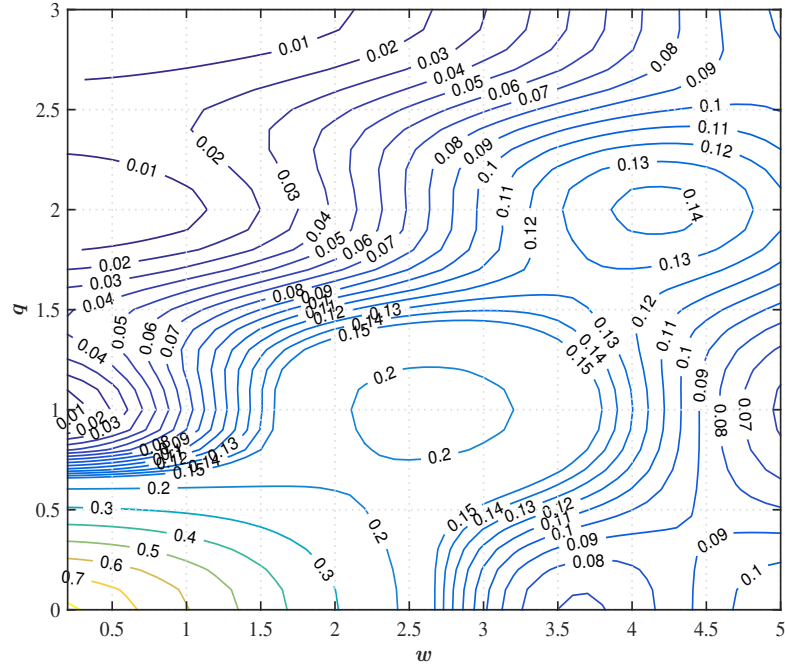
Figure 2.29: $\log_{10}\left(P_2(\epsilon)/\min\{P_2(\epsilon)\}\right)$ contour plot for non-coherent 2-level chirp receiver at 6 dB SNR

Figure 2.30: $\log_{10}\left(P_4(\epsilon)/\min\{P_4(\epsilon)\}\right)$ contour plot for non-coherent 4-level chirp receiver at 6 dB SNR

Figure 2.31: $\log_{10}\left(P_8(\epsilon)/\min\{P_8(\epsilon)\}\right)$ contour plot for non-coherent 8-level chirp receiver at 6 dB SNR
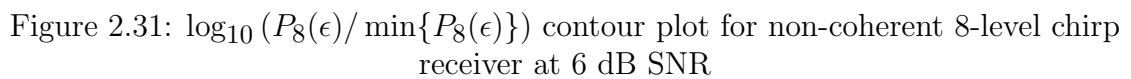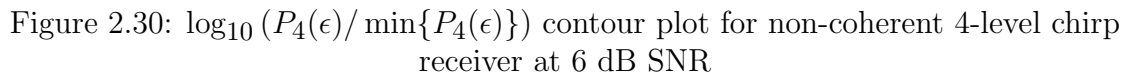
For the case of $M = 2$ (binary) orthogonal chirp modulation has been found for ($q = 2.00, w = 0.05$). The bit error rate performance of 2-level non-coherent chirp system for $(2.00, 0.05)$ is shown in Fig. 2.32. In the same figure 2-DPSK performance is also shown for comparison. Non-coherent orthogonal FSK and optimum non-coherent 2-chirp with ($q = 2.00, w = 0.05$) have the same performance and these systems are poorer by 3 dB when compared to binary DPSK (differentially coherent system). In order to understand the sensitivity of q and w on bit error rate, in Fig. 2.33 and 2.34 performances are plotted with q and w fixed and correspondingly w and q are varied. It is noted that in 2-level non-coherent chirp system with q fixed at 2.00, orthogonality is lost rapidly as w increases. On the other hand, for w fixed at 0.05, the orthogonality of the system remains nearly the same with variation in q. Table (2.8) summarizes $P_2(\epsilon)$ values at 6, 8, and 10 dB for 2-level optimum non-coherent chirp, non-coherent 2-FSK and 2-DPSK modulations.
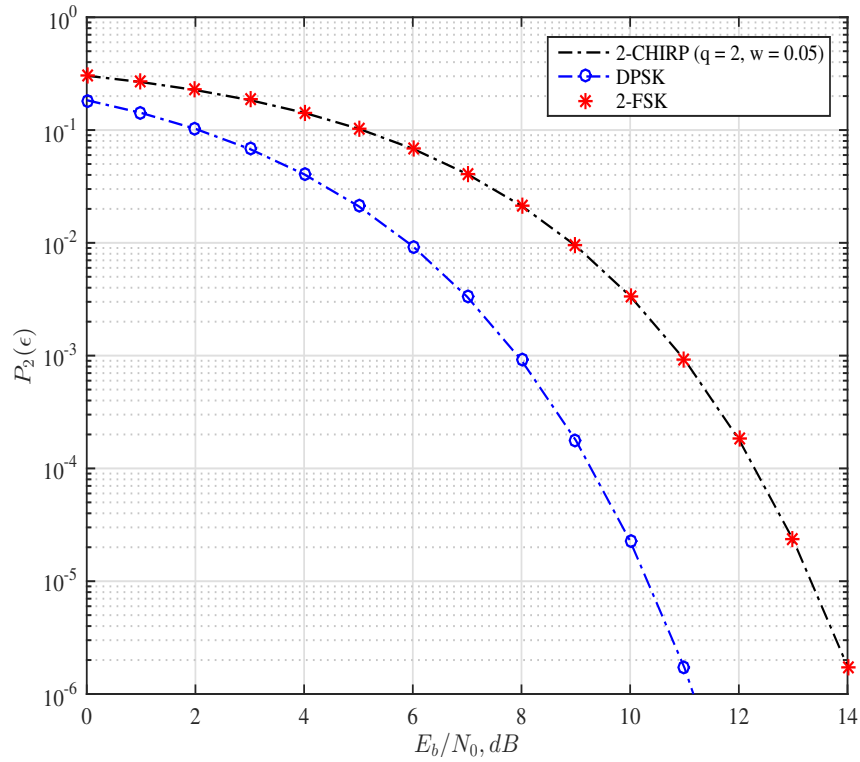
Figure 2.32: Error probability performance of optimum ($q = 2.00, w = 0.05$) non-coherent binary chirp system
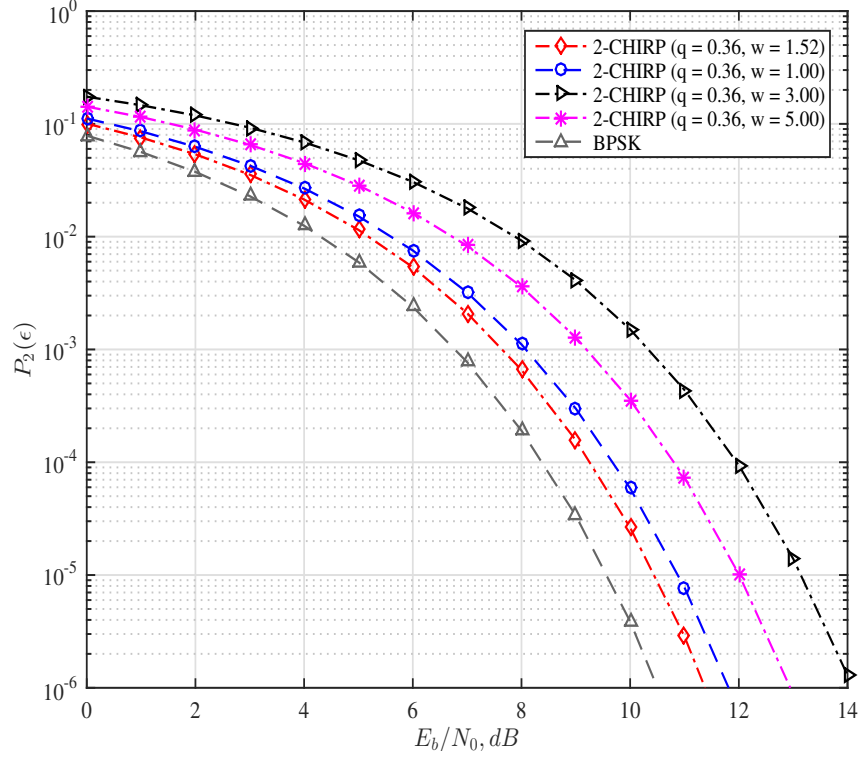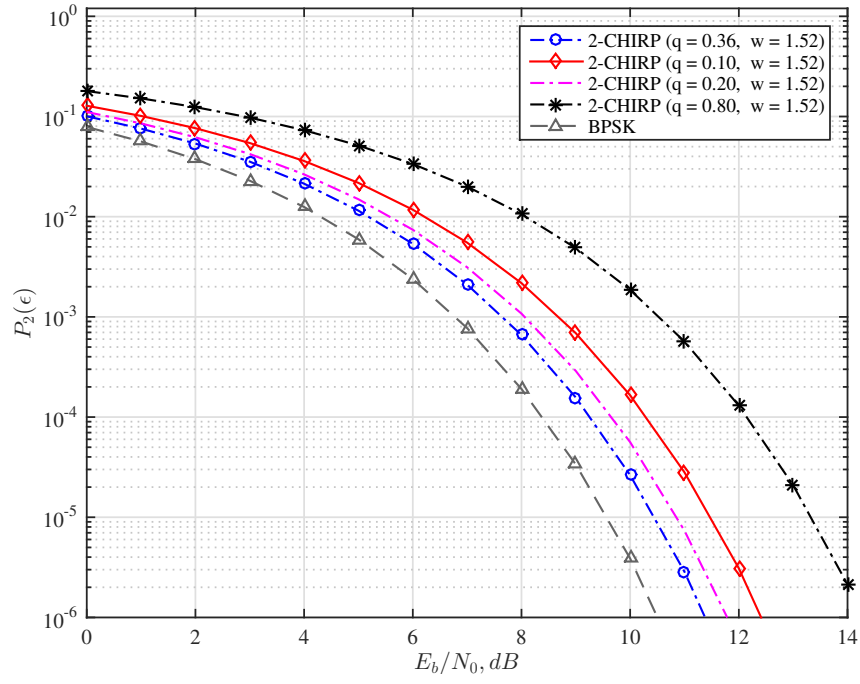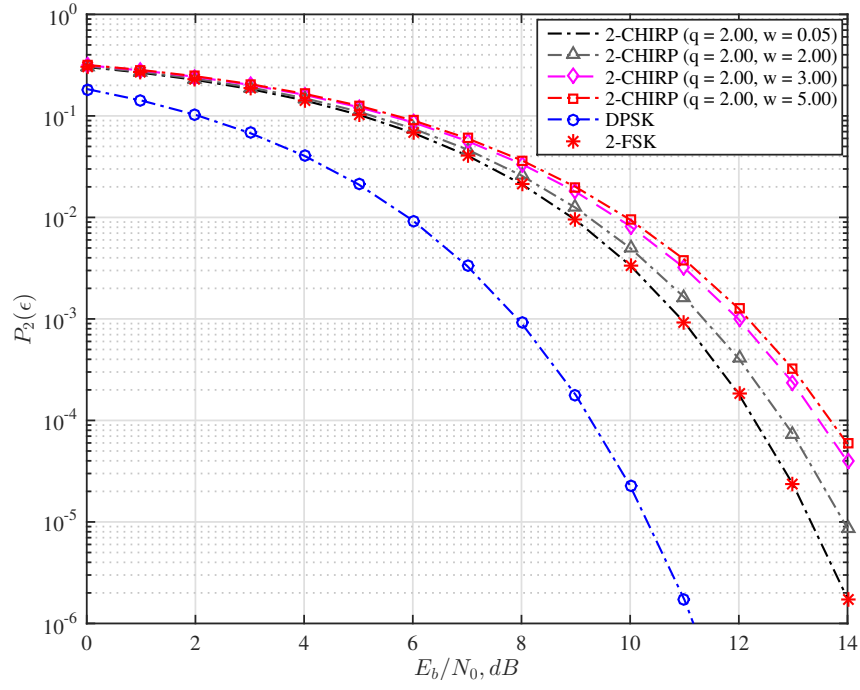
Figure 2.33: Error probability performance of non-coherent binary chirp system as a function of w, for a fixed value of $q = 2.00$
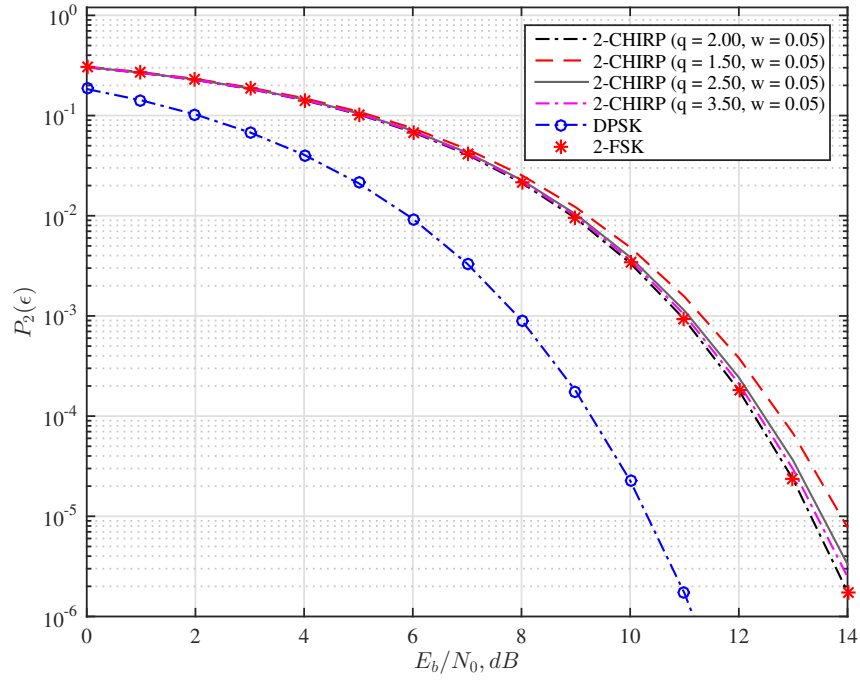
Figure 2.34: Error probability performance of non-coherent binary chirp system as a function of q, for a fixed value of $w = 0.05$
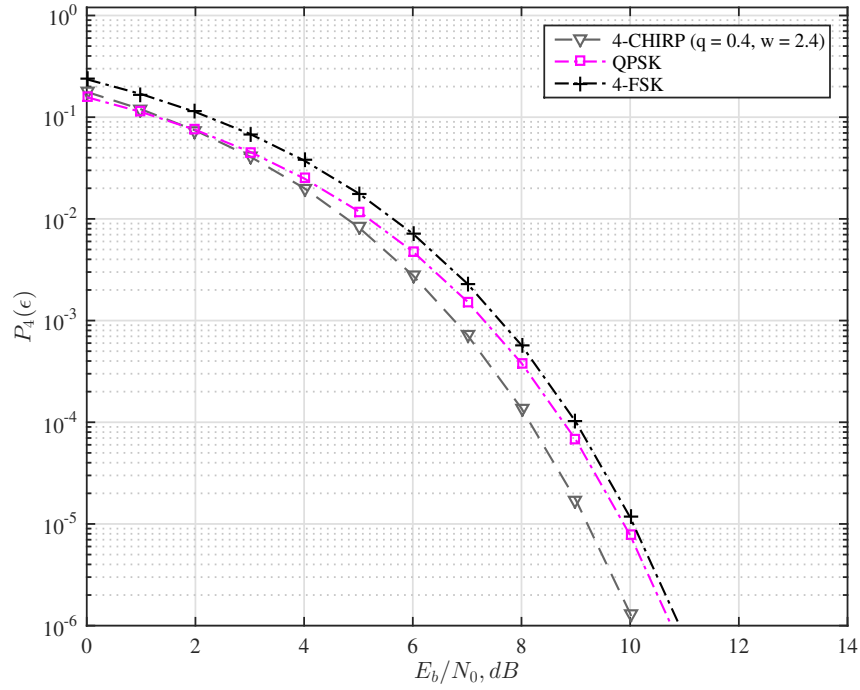
Table 2.8: Symbol Error Rate Performance of Optimum Non-coherent 2-level chirp, 2-DPSK and 2-FSK

SNR (dB)	$P_2(\epsilon)$		
	2-chirp	**2-DPSK**	**2-FSK**
6	6.83×10^{-2}	9.33×10^{-3}	6.83×10^{-2}
8	2.13×10^{-2}	9.09×10^{-4}	2.13×10^{-2}
10	3.37×10^{-3}	2.27×10^{-5}	3.37×10^{-3}

In Fig. 2.35, the symbol error rates performances of optimum 4-level non-coherent chirp along with the performance of 4-level DPSK and 4-level non-coherent FSK are shown. Table (2.9) summarizes $P_4(\epsilon)$ values at 6, 8, and 10 dB. It is observed that the performance of optimum 4-level non-coherent chirp system ($q = 2.00$ and $w = 0.10$) and 4-level non-coherent orthogonal FSK are the same and 4-DPSK is inferior by 2.5 dB to these modulations. It is noted that 4-level non-coherent chirp system with $q = 2.00$ and $w = 0.10$ happens to be orthogonal signaling technique.
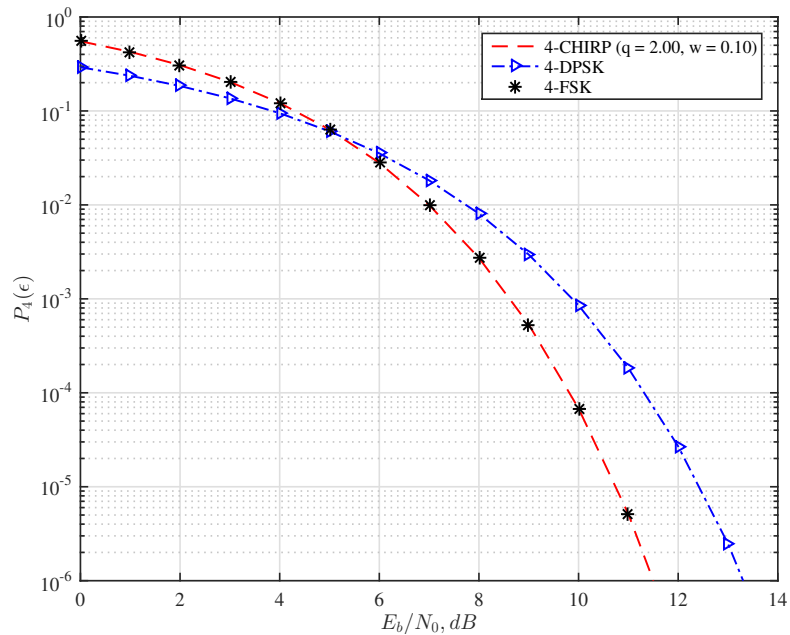
Figure 2.35: Error probability performance of ($q = 2.00, w = 0.10$) non-coherent 4-ary chirp system

Table 2.9: Symbol Error Rate Performance of Optimum Non-coherent 4-level chirp, 4-DPSK and 4-FSK

SNR (dB)	$P_4(\epsilon)$		
	4-chirp	4-DPSK	4-FSK
6	2.80×10^{-2}	3.54×10^{-2}	2.80×10^{-2}
8	2.73×10^{-3}	8.08×10^{-3}	2.73×10^{-3}
10	6.81×10^{-5}	8.54×10^{-4}	6.81×10^{-5}

In the case of 8-level non-coherent chirp system, orthogonality has been found for the set of modulation parameters $(q = 3.00, w = 0.10)$. Symbol error rate performance of this chirp system along with performance of 8-level orthogonal non-coherent FSK and 8-DPSK are shown in Fig. 2.36. In Table (2.10), $P_8(\epsilon)$ for these systems at 6, 8, and 10 dB are shown. Optimum 8-level chirp system is superior to 8-DPSK by nearly 6 dB.
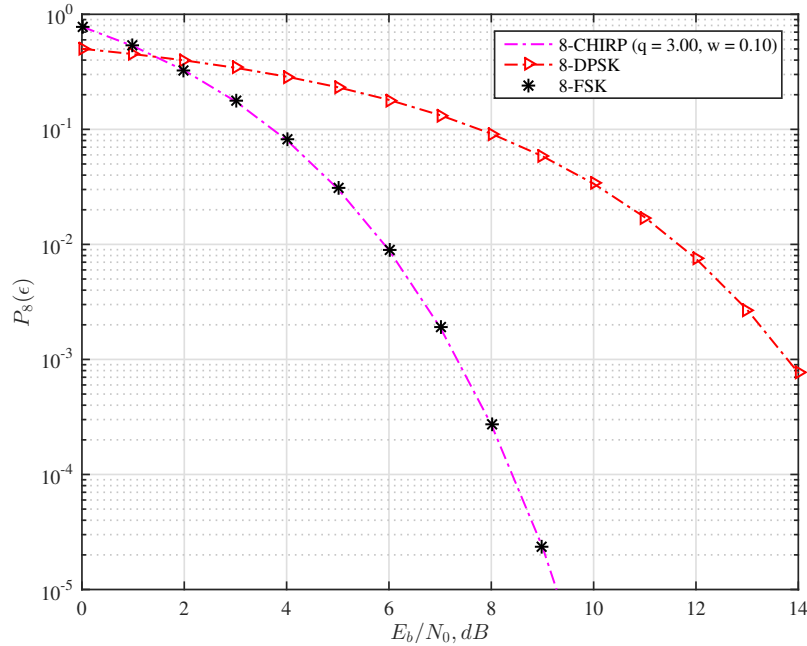
Figure 2.36: Error probability performance of $(q = 3.00, w = 0.10)$ non-coherent 8-ary chirp system

Table 2.10: Symbol Error Rate Performance of Optimum Non-coherent 8-level chirp, 8-DPSK and 8-FSK

SNR (dB)	$P_8(\epsilon)$		
	8-chirp	**8-DPSK**	**8-FSK**
6	8.93×10^{-3}	1.83×10^{-1}	8.93×10^{-3}
8	2.72×10^{-4}	9.17×10^{-2}	2.72×10^{-4}
10	1.07×10^{-6}	3.37×10^{-2}	1.07×10^{-6}

2.6   Conclusions

In this Chapter constant-envelope multi-level (M-ary) chirp modulation has been proposed for data transmission. Such technique is also referred to as memoryless modulation and symbol-by-symbol modulation, as the modulated signal during any arbitrary symbol interval carries no information about the past or future symbols and hence symbol-by-symbol detection is the optimum technique.

The proposed multi-level chirp modulated signals are mathematically described as a function of modulation parameters (q, w). The ability of these signals to operate over AWGN is assessed using the concept of minimum Euclidean distance in signal-space. For example, it is shown that 2-, 4-, 8-, and 16-level chirp modulations exist that can offer gains up to -0.875, 2.126, 3.887, and 5.136 dB, respectively, relative to BPSK.

Coherent and non-Coherent detection of multi-level chirp signals in AWGN were considered and structure of optimum receivers have been derived. Closed-form expressions for symbol error rates for these receivers have been derived. Through minimization of these expressions optimum multi-level coherent and non-coherent chirp systems have been determined. It is shown that there exist optimum coherent 2-level (binary) chirp modulation that is superior in performance to coherent 2-level (binary) orthogonal FSK by nearly 2 dB and inferior in performance to BPSK by only 0.8 dB.

4-level and 8-level coherent chirp systems have been found whose performance are better and nearly the same compared to coherent 4-FSK and 8-FSK, respectively. In the non-coherent case, it is shown that M (2, 4, and 8)-level non-coherent chirp systems exist that offer same performance as that of M (2, 4, and 8)-level non-coherent orthogonal FSK system.

Chapter 3

Constant Envelope Multi-Level Chirp Modulation with Memory: Signals and Distance Properties

3.1 Introduction

In Chapter 2, memoryless multi-level chirp modulation was considered. In such a modulation, the ending phase of the transmitted signal during any arbitrary symbol interval is not the same as the starting phase of the signal in the next symbol interval. Hence, discontinuity exists at symbol transitions. For this reason, such a modulation is referred to as memoryless, symbol-by-symbol, or discontinuous-phase chirp modulation. When the phase at symbol transition is constrained to be continuous, one obtains a class of chirp modulations with memory. These signals are collectively referred to as M-level ($M-$ary) Continuous Phase Chirp Modulation ($M-$CPCM). The memory introduced by constraining the phase to be continuous at bit transitions provides smooth spectral behavior of the transmitted signal and also permits multiple-symbol detection providing enhanced symbol error rate performance. The intent in this Chapter is to propose constant envelope phase-continuous multi-level chirp modulation. These modulated signals are mathematically described and their signal-space properties are examined thoroughly.

Signal space approach is a key element in receiver design and performance analysis. Because it is easier to represent signals in space as vectors, and the Euclidean distance properties can then be used to determine essential system parameters such as detection and spectral efficiency. Minimum Euclidean distance analysis is significant in determining the ultimate error rate performance over AWGN channel. Moreover,

probability of error performance becomes a function of minimum Euclidean distance at high SNR [3].

In this Chapter, a closed form expression for Euclidean distance for M-CPCM is derived as functions of modulation parameters q and w and observation interval n. Upper bounds on the minimum distance are then derived to estimate the limiting value on the SNR Gain G_n and to know for which value of observation interval n the distance can reach its bound. Next, the numerical results for this class of signals are sketched as 3-D surfaces to better understand M-CPCM signals. A comparison of the minimum distance properties of M-CPCM with other conventional modulation schemes is also presented.

3.2 M-level Continuous Phase Chirp Modulation (M-CPCM) Signals

The general expression for M-CPCM signal is given by [39]:

$$S(t,d) = \sqrt{\frac{2E_s}{T_s}} \, \cos(w_c t + \phi(t,d) + \theta), \quad 0 \leq t < \infty \tag{3.1}$$

where E_s is the symbol energy during the symbol duration T_s seconds, w_c is the angular carrier frequency, $\phi(t,d)$ is the information carrying phase, and θ is the starting phase (at $t = 0$). The information carrying phase for M-CPCM signal is given by:

$$\phi(t,d) = d_i g(t - (i-1)T_s) + \pi q \sum_{k=1}^{i-1} d_k, \quad (i-1)T_s \leq t \leq iT_s \tag{3.2}$$

and

$$d = d_1, d_2, d_3, \ldots$$

is an infinitely long sequence of uncorrelated M-ary data symbols, each taking one of the values:

$$d_i = \pm 1, \pm 3, \pm 5, \ldots, \pm(M-1); \quad i = 1, 2, \ldots \tag{3.3}$$

with a probability

$$P(d_i) = \frac{1}{M}; \quad i = 1, 2, \ldots \tag{3.4}$$

In (3.2), the phase function $g(t)$ is given by:

$$g(t) = \begin{cases} 0, & t \leq 0, \ t > T_s \\ 2\pi \int_0^t f(\tau)d\tau, & 0 \leq t \leq T_s \\ \pi q = \pi(h - w), & t = T_s \end{cases} \tag{3.5}$$

and $f(t)$ is the instantaneous frequency as a function of time. For chirp signaling:

$$f(t) = \begin{cases} 0, & t \leq 0, \ t > T_s \\ \left(\frac{h}{2T_s}\right) - \left(\frac{w}{T_s^2}\right)t, & 0 \leq t \leq T_s \end{cases} \tag{3.6}$$

using (3.6) in (3.5), (3.5) can be written as:

$$g(t) = \begin{cases} 0, & t \leq 0, \ t > T_s \\ \pi \left\{ h\left(\frac{t}{T_s}\right) - w\left(\frac{t}{T_s}\right)^2 \right\}, & 0 \leq t \leq T_s \\ \pi q = \pi(h - w), & t = T_s \end{cases} \tag{3.7}$$

where h and w are dimensionless parameters, h represents the peak-to-peak frequency deviation divided by the symbol rate $\frac{1}{T_s}$, and w represents the frequency sweep width divided by the symbol rate $\frac{1}{T_s}$. Since $h = (q + w)$, we choose (w, q) to be independent signal modulation parameters.

It is instructive to sketch the phase trajectories generated by (3.2) for all possible values of the data sequence. For example, in the case of 2-CPCM with symbols $d_i = \pm 1$ and for four bit time intervals, the set of phase trajectories beginning at time $t = 0$ is shown in Fig. 3.1 (for $(q, w) = (0.5, 2.2)$). The phase trajectories for 4-CPCM is shown in Fig. 3.2. These phase diagrams are called phase trees. It is noted that the phase tree for M-CPCM is a continuous function of time. For simplicity, θ has been set equal to zero for coherent transmission.
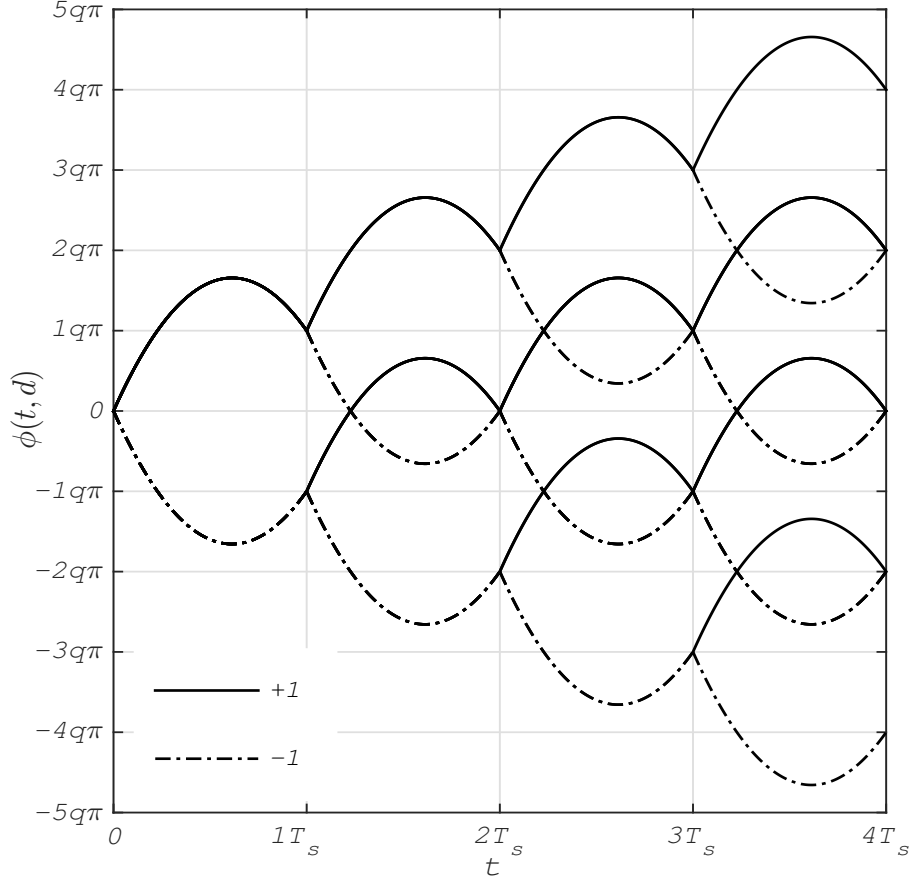
Figure 3.1: Phase tree for 2-CPCM signal

From (3.2), it is observed that the phase of the signal during the ith symbol interval is not only a function of the data during the ith symbol interval, but also it is a function of the past symbols $d_1, d_2, \ldots, d_{i-1}$ that have entered the modulator. The first-term in (3.2) is the phase due to the ith symbol and the second-term is referred
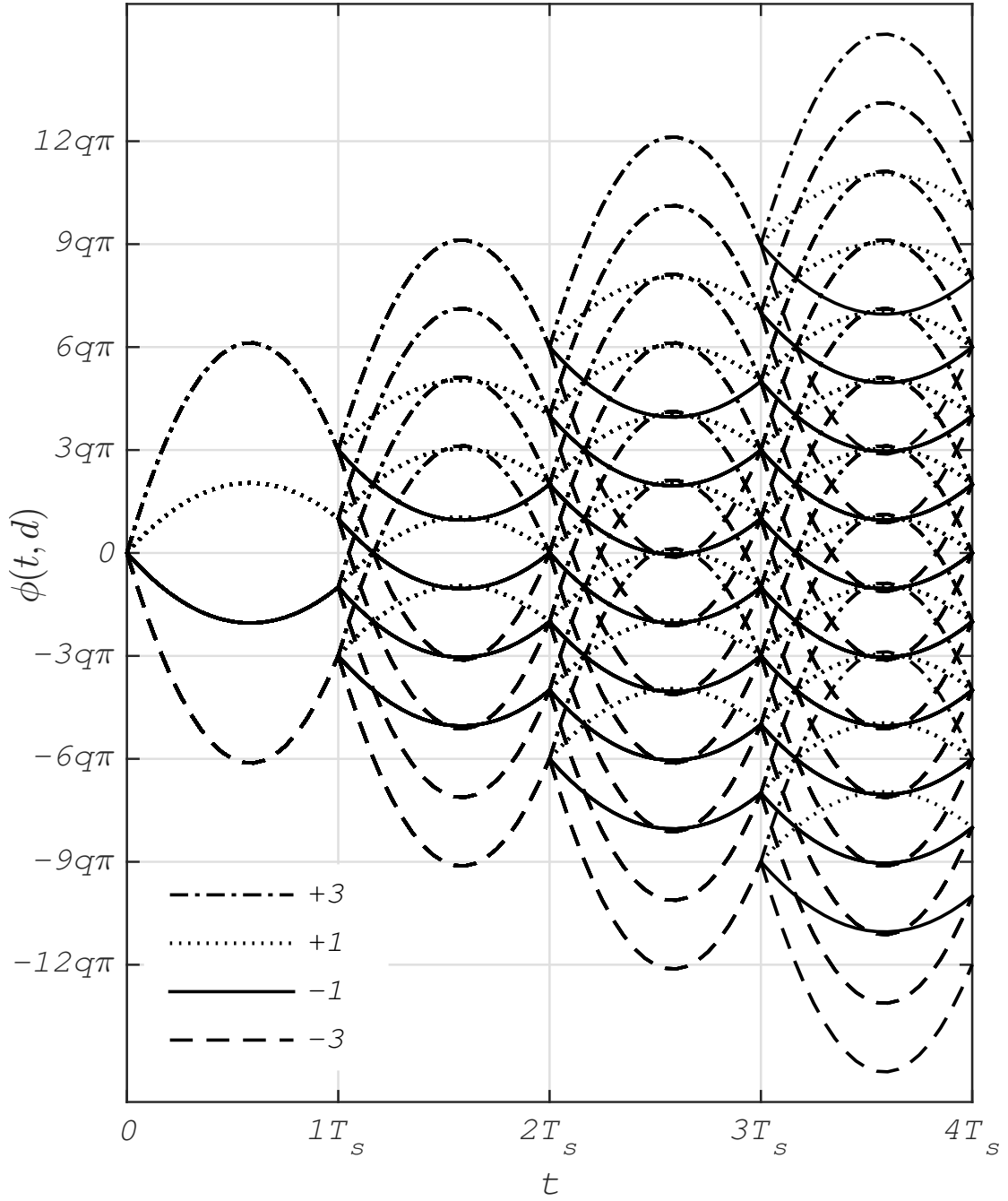
Figure 3.2: Phase tree for 4-CPCM signal

to as the accumulated phase due to the past symbols. Since phase is always modulo 2π and further by appropriately choosing the value of modulation parameter q, it is possible to model the M-CPCM signal to be a finite-state trellis [3]. For example,

for 2-CPCM with $q = \frac{1}{2}$ the phase tree in Fig. 3.1 becomes a 4-state trellis diagram shown in Fig. 3.3.
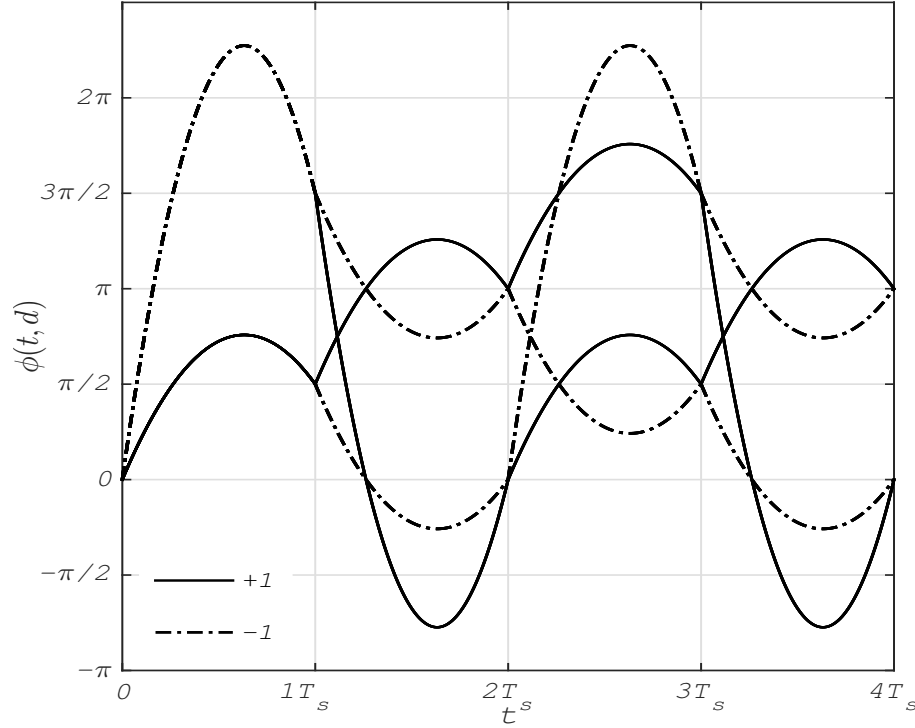
Figure 3.3: Phase trellis for 2-CPCM signal with $q = \frac{1}{2}$ and arbitrary w

3.3   Minimum Euclidean Distance Properties

The M-CPCM signal is assumed to be transmitted over an AWGN channel with two-sided PSD of $\frac{N_0}{2}$ watts/Hz. Thus, the received signal available for observation can be written as:

$$r(t) = S(t, d) + n(t) , \quad 0 \leq t < \infty \tag{3.8}$$

where $n(t)$ is a Gaussian random process and $S(t, d)$ is the received M-CPCM signal. A receiver which minimizes the probability of erroneous decision is required to observe $r(t)$ over $0 \leq t < +\infty$ and to choose the infinitely long sequence $d = (d_1, d_2, \dots)$ which minimizes the error probability. Such a receiver is referred to as MLSE receiver

and is impractical for theoretical investigation. Instead, a sub-optimum receiver that observes the received signal over n symbol intervals and makes a decision about a specific data symbol can be studied. Thus, we consider a receiver that observes

$$r(t) = S(t,d) + n(t) , \quad 0 \le t \le nT_s \tag{3.9}$$

where $d = (d_1, d_2, \ldots, d_n)$ and produces an estimate $\hat{d}_1$ of d_1. The optimum detector is the one that observes $r(t)$ in (3.9) and maximizes the log likelihood functions given by:

$$l_i = \int_0^{nT} r(t) S(t,d) \ dt, \quad i = 1, 2, \ldots, M \tag{3.10}$$

As $n \to \infty$, MLSE receiver is obtained. It is noted that there are M^n sequences of data, $(d_1, d_2, \ldots, d_n)$, are possible, but the detector is only interested in finding an estimate $\hat{d}_1$ of d_1. Thus, M^n sequences can be formed into M groups:

$$\begin{cases} d_1 = -(M-1), d_2, \ldots, d_n \\ \qquad\qquad \vdots \\ d_1 = -1, d_2, \ldots, d_n \\ d_1 = +1, d_2, \ldots, d_n \\ \qquad\qquad \vdots \\ d_1 = +(M-1), d_2, \ldots, d_n \end{cases} \tag{3.11}$$

where d_k, $k = 2, 3, \ldots, n$, takes values $\pm 1, \pm 3, \ldots, \pm(M-1)$. It is noted that the receiver need not find the specific sequence $d_2, \ldots, d_n$ which maximizes (3.10) to choose $\hat{d}_1$ as an estimate of d_1. This aspect will be explained in Chapter 4 where receiver structure for detection of M-CPCM signals in AWGN is derived. For large SNR, the probability of erroneous decision can be upper bounded using union bound

[40] and is given by:

$$P_e \leq \frac{1}{M^{n-1}} \sum_{\substack{j=1 \\ v \neq u}}^{M^{n-1}} \sum_{k=1}^{M^{n-1}} Q\left[\frac{D_n(vj, uk)}{\sqrt{2N_0}}\right] \tag{3.12}$$

where

$$Q(x) \triangleq \frac{1}{\sqrt{2\pi}} \int_x^\infty e^{-\frac{t^2}{2}} dt \tag{3.13}$$

The quantity $D_n(vj, uk)$ represents the Euclidean distance between the signals $S(t, d_1 = v, A_j)$ and $S(t, d_1 = u, A_k)$ and is given by:

$$D_n(vj, uk) = \left[\int_0^{nT_s} \left|S(t, d_1 = v, A_j) - S(t, d_1 = u, A_k)\right|^2 dt\right]^{\frac{1}{2}} \tag{3.14}$$

The distance between waveforms is a key concept [40] in understanding the ultimate utility of any arbitrary signaling scheme in digital communications. The squared Euclidean distance is given by:

$$D_n^2(vj, uk) = \int_0^{nT_s} \left|S(t, d_1 = v, A_j) - S(t, d_1 = u, A_k)\right|^2 dt \tag{3.15}$$

$$= \sum_{l=1}^n \int_{(l-1)T_s}^{lT_s} [S(t, d_1 = v, A_j) - S(t, d_1 = u, A_k)]^2 \ dt$$

$$= \sum_{l=1}^n \int_{(l-1)T_s}^{lT_s} [S^2(t, d_1 = v, A_j) - 2S(t, d_1 = v, A_j)S(t, d_1 = u, A_k) + S^2(t, d_1 = u, A_k)] \ dt. \tag{3.16}$$

Using (3.1) and neglecting the high frequency term, (3.16) can be written as:

$$D_n^2(vj, uk) = 2E_s(n - \sum_{l=1}^{n} \frac{1}{T_s} \int_0^{T_s} \cos\{\Delta\phi_l(t, vj, uk)\} \ dt) \tag{3.17}$$

where

$$\Delta\phi_l(t, vj, uk) = \gamma_l \ g(t) + \pi q \sum_{i=1}^{l-1} \gamma_i.$$

$\Delta\phi_l(t, vj, uk)$ represents the phase difference between the signals $S(t, d_1 = v, A_j)$ and $S(t, d_1 = u, A_k)$ during the lth symbol interval with the difference term $\gamma_l = d_l^j - d_l^k$ which is given by:

$$
\begin{cases}
\gamma_1 = v - u = 2, 4, 6, ..., 2(M-1), \\[2mm]
\gamma_l = d_l^j - d_l^k = 0, \pm 2, \pm 4, ..., \pm 2(M-1), \quad l = 2, 3, ..., n
\end{cases}
\tag{3.18}
$$

In the above equations $S(t, d_1, A_j)$ denotes the transmitted M-CPCM signal given by (3.1) over $0 \leq t \leq nT_s$, with the first symbol as d_1 and A_j represents a particular data sequence, i.e, $n - 1$ tuple $(d_2, d_3, \ldots, d_n)$. A closed-form expression for squared Euclidean distance given in (3.17) has been obtained and is given by:

$$D_n^2(vj, uk) = 2E_s\{n - \sum_{l=1}^{n} \frac{1}{\sqrt{2|\gamma_l|w}} [\cos(\Omega_l)(C(x_l) + C(y_l))$$

$$+ \sin(\Omega_l)(S(x_l) + S(y_l))]\} \tag{3.19}$$

where

$$\Omega_l = \frac{\pi}{2} \frac{(w+q)^2}{2w} |\gamma_l| + 2q \, \text{sgn}(\gamma_l) \sum_{r=1}^{l-1} \gamma_r$$

$$x_l = \sqrt{\frac{|\gamma_l|}{2w}} (w - q)$$

$$y_l = \sqrt{\frac{|\gamma_l|}{2w}}(w + q)$$

$$\text{sgn}(x) = \begin{cases} +1, & x \geq 0 \\ -1, & x < 0 \end{cases}$$

$$\gamma_l = d_l^j - d_l^k$$

$$\gamma_1 = v - u$$

$$E_s = E_b \log_2(M).$$

$C(x)$ and $S(x)$ are defined in (2.17) and (2.18), respectively. It is noted that $D_n^2(vj, uk)$ is a function of $\gamma_1, \gamma_2, \ldots, \gamma_n$ which is the difference sequence. Thus, it is sufficient to consider the difference sequence instead of the pair of sequences $d_1^j, d_2^j, \ldots, d_n^j$ and $d_1^k, d_2^k, \ldots, d_n^k$. The error probability given by (3.12), for high SNR can be approximated by:

$$P_e \cong \Gamma_0 \, Q\left[\frac{D_{n,\min}}{\sqrt{2N_0}}\right] \tag{3.20}$$

where Γ_0 is some positive constant independent of $\frac{E_b}{N_0}$. The quantity $D_{n,\min}$ is the minimum of $D_n(vj, uk)$ with respect to all pair of sequences $d_1^j, d_2^j, \ldots, d_n^j$ and $d_1^k, d_2^k, \ldots, d_n^k$, $j, k = 1, 2, \ldots, M^{n-1}$, with the restriction of $v \neq u$. That is:

$$D_{n,\min}^2 = \min_{\substack{v,u,j,k \\ v \neq u}} \{D_n^2(vj, uk)\} \tag{3.21}$$

Using energy normalization, the normalized squared Euclidean distance can be expressed as:

$$d^2 = \frac{D_n^2}{2E_b} \tag{3.22}$$

By using this normalization, one can compare different M-level or (M-ary) modulations on an equal $\frac{E_b}{N_0}$ basis. As a reference point, it is noted that $d_{min}^2 = 2$ for MSK,

BPSK, and QPSK. An estimate of the SNR gain relative to BPSK is then obtained using:

$$G_n = 10 \log_{10} \left[\frac{d_n^2}{2} \right] \tag{3.23}$$

3.4 Bounds on The Minimum Euclidean Distance

An important tool in the analysis of the distance properties associated with the M-CPCM signals is its phase tree. To calculate the maximum squared Euclidean distance associated with this signalling set, with signals in that set defined over n symbol intervals, all pairs of phases trajectories in the phase tree over n symbol intervals must be considered. The phase trajectories over the first symbol interval, however, must not coincide. The squared Euclidean distance is then determined using (3.19) for all these pairs. Using the fact that the Euclidean distance is a non-decreasing function of observation length n, an upper bound for any n, may be obtained by considering just a few representative pairs of infinitely long sequences. Good candidates for all these sequences are pairs that merge as soon as possible. Fig. 3.4 shows the merging point for 2-CPCM system that occurs at $t = 2T_s$. Turning to the 4-CPCM case, Fig. 3.5, the merging points are denoted by A, B, C, D and E. It is noted that there are more than one merging point and two different trajectories can have the same merging point. It is seen that such an infinitely long sequence is:

$$\tilde{\gamma} = +x_0, -x_0, 0, 0, \ldots \quad ; \quad x_0 = 2, 4, 6, \ldots., 2(M-1) \tag{3.24}$$

Using (3.24), an upper bound on the minimum Euclidean squared distance for M-CPCM for all n is given by:

$$d_{B,M}^2(q,w) = \log_2(M) \min_{1 \leq p \leq M-1} \{ 2 - \frac{\cos(p\pi q)}{\sqrt{pw}} [\cos(\frac{\pi p(q^2 + w^2)}{2w})(C(x) + C(y)) +$$

$$\sin(\frac{\pi p(q^2 + w^2)}{2w})(S(x) + S(y))] \} \tag{3.25}$$
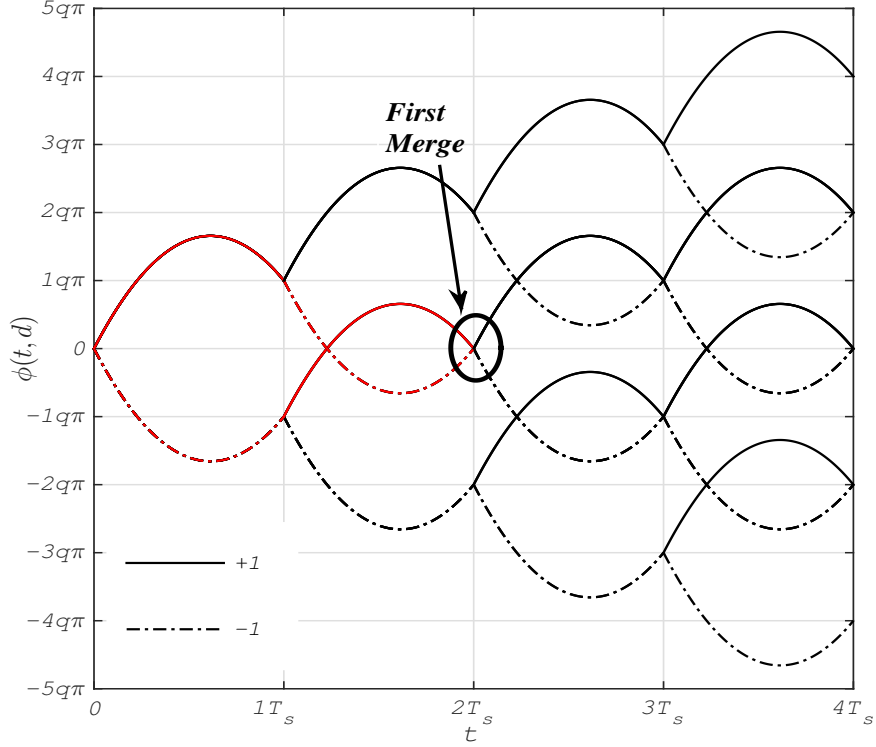
Figure 3.4: Phase tree for 2-CPCM signal with merging point

where

$$x = \sqrt{\frac{p}{w}}(w - q)$$

$$y = \sqrt{\frac{p}{w}}(w + q)$$

and the quantities $C(\cdot)$ and $S(\cdot)$ are the Fresnel cosine and sine integral that are defined in (2.17) and (2.18), respectively. It is noted that:

$$d_{B,M}^2(q, w) = d_{B,M}^2(-q, w) = d_{B,M}^2(|q|, w) \tag{3.26}$$

3.5 Numerical Results and Discussion

Since the upper bound of (3.25) is a function of the set of signal modulation parameters (q, w), $d_{B,M}^2$ was computed over the range of modulation parameters $0 < q \leq 2$
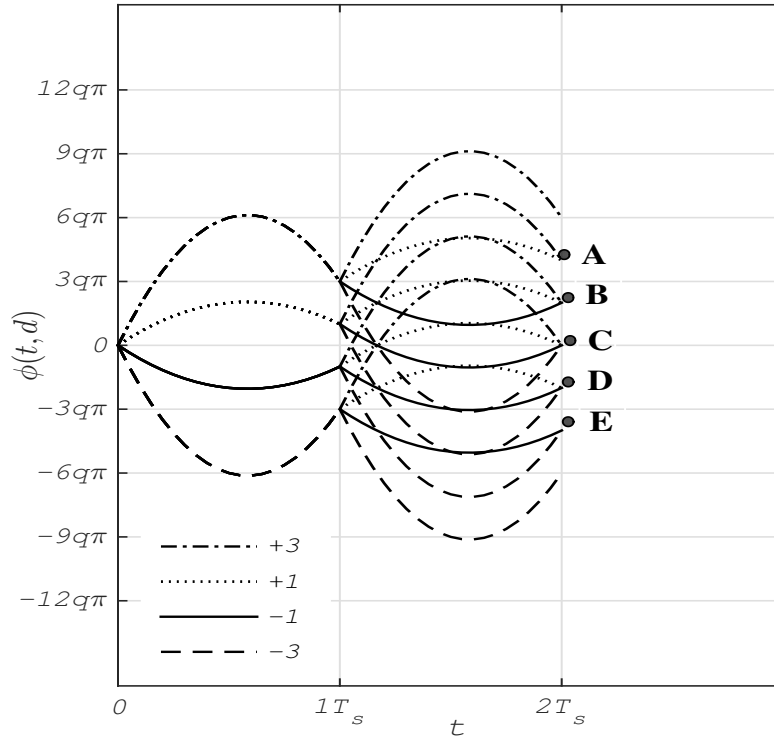
Figure 3.5: Phase tree for 4-CPCM signal with merging points

and $0 < w \leq 10$. The results of this computation are shown in Table 3.1, where (q, w) that maximized the upper bound $d_{B,M}^2(q, w)$ are shown for 2-, 4-, and 8-CPCM.

Table 3.1: (q, w) maximizing $d_{B,M}^2$ for M-CPCM

M	(q, w)	max $\{d_{B,M}^2\}$	G_n (dB)
2	(0.0, 2.4)	2.93	1.66
4	(0.0, 9.6)	4.51	3.53
8	(1.9, 6.9)	6.00	4.77

The maximum in Table 3.1 gives an estimate of the limiting gain achievable with M-CPCM. For example, 4-CPCM offers an advantage of 3.53 dB, at best, relative to BPSK. However, it should be noted that the actual value of d_n^2 given by (3.22)

will be smaller than the global maximum. That is, for $q \neq 0$, a value of d_n^2 close to the maximum value may be found out. Also, it is observed that there exist multiple sets of (q, w) that achieve the upper bound distance shown in Table 3.1. In Figs. 3.6 - 3.8 are shown 3-D surface plots of $d_{B,M}^2$ for 2-, 4-, and 8-CPCM as a function of modulation parameters q and w.
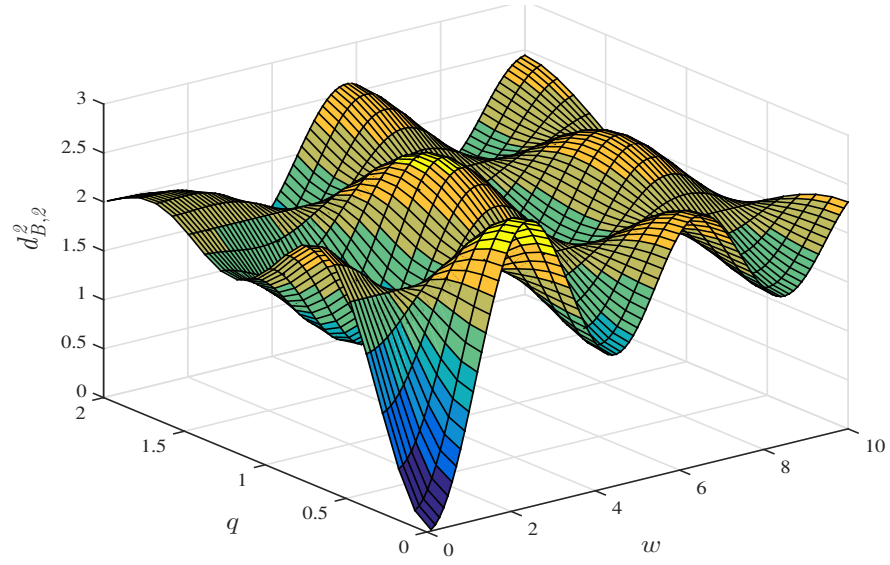
Figure 3.6: Surface plot of $d_{B,2}^2$ as a function of q and w for 2-CPCM
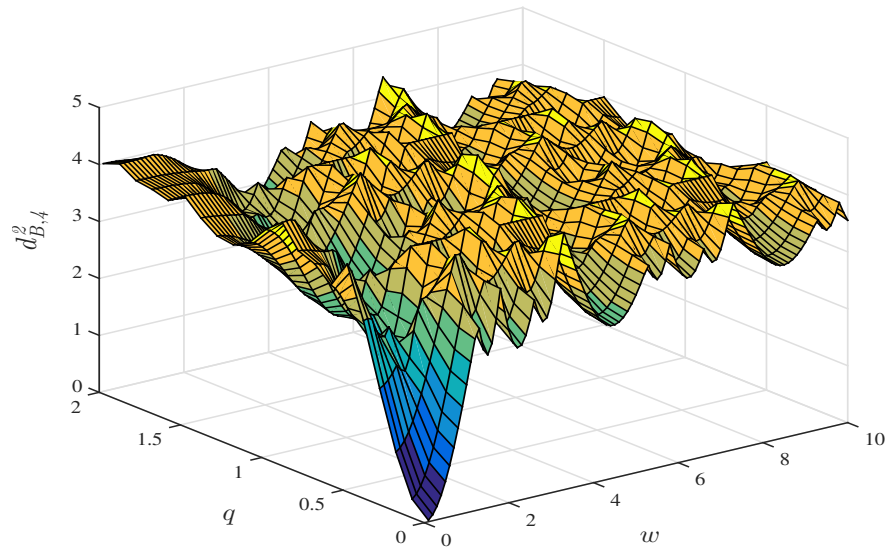
Figure 3.7: Surface plot of $d_{B,4}^2$ as a function of q and w for 4-CPCM
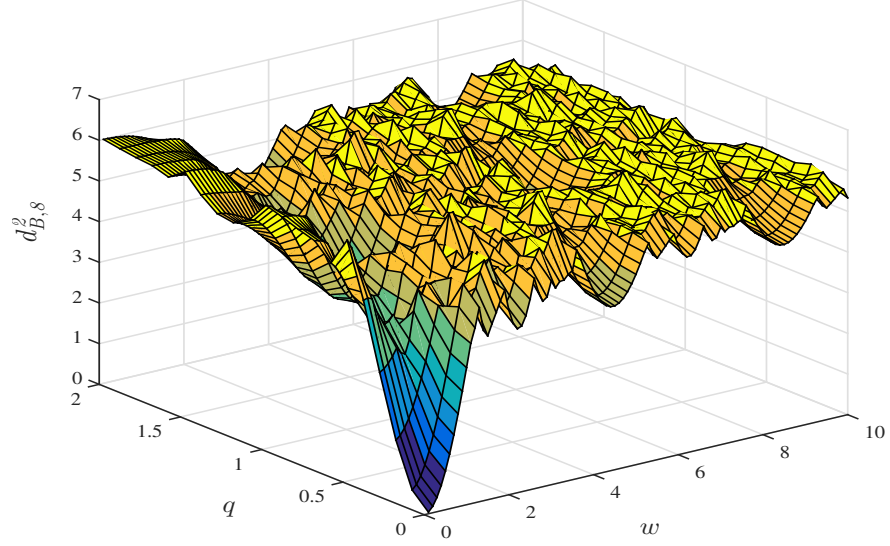
Figure 3.8: Surface plot of $d_{B,8}^2$ as a function of q and w for 8-CPCM

M-level (M-ary) Continuous Phase Frequency Shift Keying (M-CPFSK) is a well-studied modulation technique in the literature [23], [24], [42]. This signalling technique can serve as a good comparison to the M-CPCM signalling proposed in this thesis. It is noted that with $w = 0$ in (3.1)-(3.7), M-CPCM becomes M-CPFSK and h becomes the well-known *modulation index* of an FM signal. Thus, for comparison, in Fig. 3.9 are shown $d_{B,M}^2$ for 2-, 4-, and 8-CPFSK signaling. Table 3.2 shows the values of h that maximizes $d_{B,M}^2$ for M-CPFSK [23].

Table 3.2: h maximizing $d_{B,M}^2$ for M-CPFSK

M	h	max $\{d_{B,M}^2\}$	G_n (dB)
2	0.72	2.43	0.84
4	0.91	4.23	3.25
8	0.96	6.13	4.86
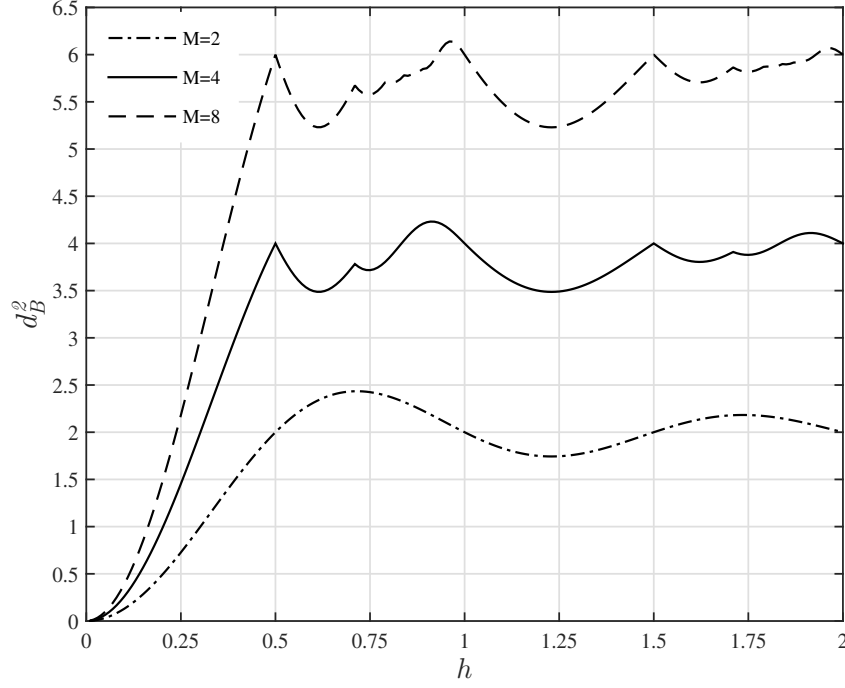
Figure 3.9: d_B^2 for M-CPFSK for (M=2, 4, 8)

While $d_{B,M}^2$ given in (3.25) provides an estimate of the ultimate gain inherent in M-CPCM, the actual minimum squared Euclidean distance $D_{n,min}^2$ in (3.19) is a function of the number of observation intervals n of the optimum receiver and the set of modulation parameters (q, w). For a given n, one is required to find the optimum or the best (q, w) that maximizes $D_{n,min}^2$. For simplicity, we denote $D_n^2 = \max\{D_{n,min}^2\}$. In Tables 3.3 - 3.5, optimum (q, w) that maximize d_n^2 $(= \frac{D_n^2}{2E_b})$ and G_n (dB) are shown for $n = 2, 3, 4$, and for $M = 2, 4$, and 8. The maximization has been carried out in the modulation parameter space $(0, 0) < (q, w) \leq (2, 10)$. In these Tables, for the sake of comparison, results for M-CPFSK are also shown. It is observed from Table 3.3 that the 2-CPCM system with $(q = 0.20, w = 2.40)$ and an observation length of the optimum receiver of $n = 4$ provides an SNR gain of 1.4 dB relative to BPSK which implies that nearly 84 % of the SNR gain inherent in 2-CPCM is realized with only $n = 4$. The best 2-CPCM has a limiting SNR gain of 1.66 dB (Table 3.1). Optimum 2-CPCM system with $n = 4$ outperforms corresponding optimum 2-CPFSK system by nearly 0.6 dB; relative to BPSK. Similarly, from Tables 3.4 and 3.5, it is observed that optimum 4-CPCM and 8-CPCM systems, for $n = 4$, offer SNR

gains, relative to BPSK, of 3.29 and 3.29 dB, respectively. Equivalently, optimum 4-CPCM and 8-CPCM systems, for $n = 4$, realize nearly 93 % and 70 % of SNR gains inherent in corresponding 4-CPCM and 8-CPCM systems, respectively. This observation indicates that an observation interval longer than 4 symbols can be used to obtain further advantages in SNR, relative to BPSK.

Table 3.3: Optimum modulation parameters maximizing d_n^2 and G_n for 2-CPCM and 2-CPFSK

n	2-CPCM			2-CPFSK		
	(q, w)	$\max\{d_n^2\}$	G_n (dB)	h	$\max\{d_n^2\}$	G_n (dB)
2	(0.30, 1.9)	2.404	0.79	0.76	2.03	0.065
3	(0.20, 2.4)	2.761	1.4	0.72	2.43	0.846
4	(0.20, 2.4)	2.761	1.4	0.72	2.43	0.846

Table 3.4: Optimum modulation parameters maximizing d_n^2 and G_n for 4-CPCM and 4-CPFSK

n	4-CPCM			4-CPFSK		
	(q, w)	$\max\{d_n^2\}$	G_n (dB)	h	$\max\{d_n^2\}$	G_n (dB)
2	(0.40, 6.6)	3.690	2.66	3.75	3.89	2.89
3	(0.40, 2.6)	4.27	3.29	3.8	3.97	2.97
4	(0.40, 2.6)	4.27	3.29	0.85	4.08	3.09

Table 3.5: Optimum modulation parameters maximizing d_n^2 and G_n for 8-CPCM and 8-CPFSK

n	8-CPCM			8-CPFSK		
	(q, w)	$\max\{d_n^2\}$	G_n (dB)	h	$\max\{d_n^2\}$	G_n (dB)
2	(1.10, 4.20)	4.67	3.68	0.90	3.88	2.88
3	(1.10, 3.60)	5.22	4.16	0.45	4.46	3.48
4	(1.10, 3.70)	5.22	4.16	0.45	5.03	4.00
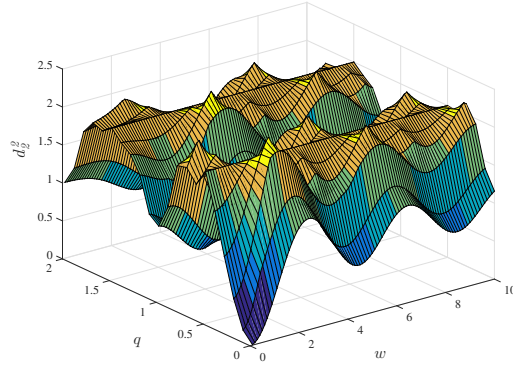
(a) max $\{d_2^2\}$=2.404; (0.30, 1.9)

(b) max $\{d_2^2\}$=2.761; (0.20, 2.4)
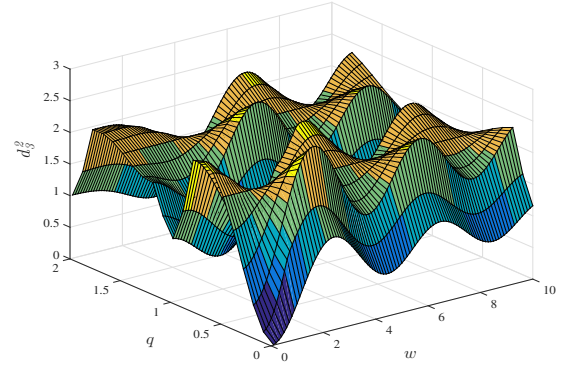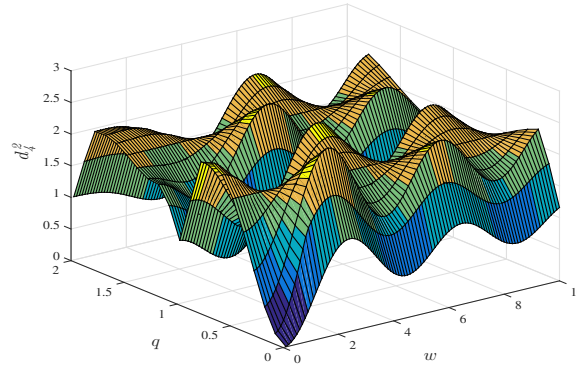
(c) max $\{d_2^2\}$=2.761; (0.20, 2.4)

Figure 3.10: Surface plots of d_n^2 as a function of q and w for (a) $n = 2$, (b) $n = 3$, and (c) $n = 4$ for 2-CPCM

In Fig. 3.10, 3-D surface plots for 2-CPCM system are shown for $n = 2, 3$, and 4. These figures provides an understanding of how modulation parameters q and w affect the distance properties of the signalling technique. Similar surface plots for 4-CPCM and 8-CPCM are shown in Figs. 3.11 and 3.12, respectively. The $\max\{d_n^2\}$ in these figures correspond to the values presented in Tables 3.3, 3.4, and 3.5, for 2-, 4-, 8-CPCM, respectively, for $n = 2, 3$, and 4.

(a) max $\{d_2^2\}$=3.69; (0.40, 6.6)

(b) max $\{d_3^2\}$=4.27; (0.40, 2.60)

(c) max $\{d_4^2\}$=4.27; (0.40, 2.6)
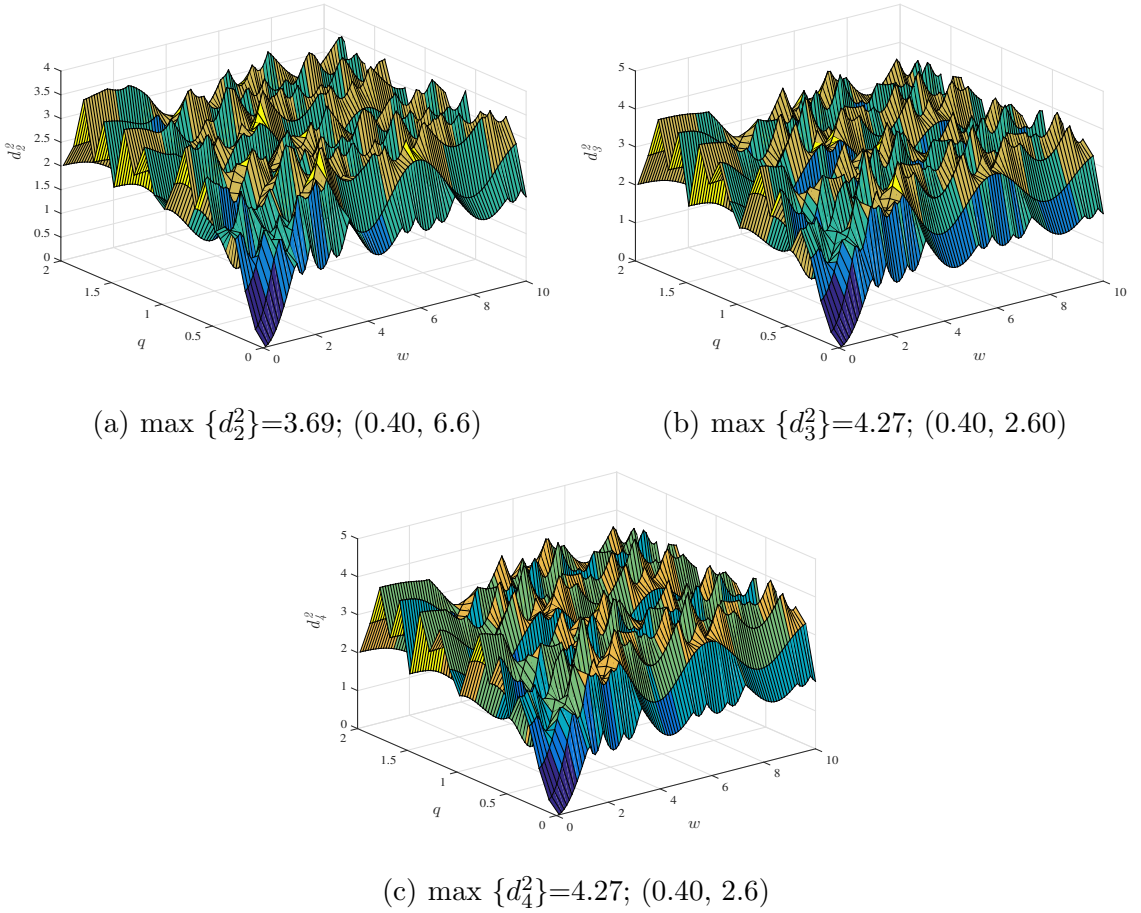
Figure 3.11: Surface plots of d_n^2 as a function of q and w for (a) $n = 2$, (b) $n = 3$, and (c) $n = 4$ for 4-CPCM

(a) max $\{d_2^2\}$=4.67; (1.1, 4.2)

(b) max $\{d_3^2\}$=5.22; (1.1, 3.6)

(c) max $\{d_4^2\}$=5.22; (1.1, 3.7)
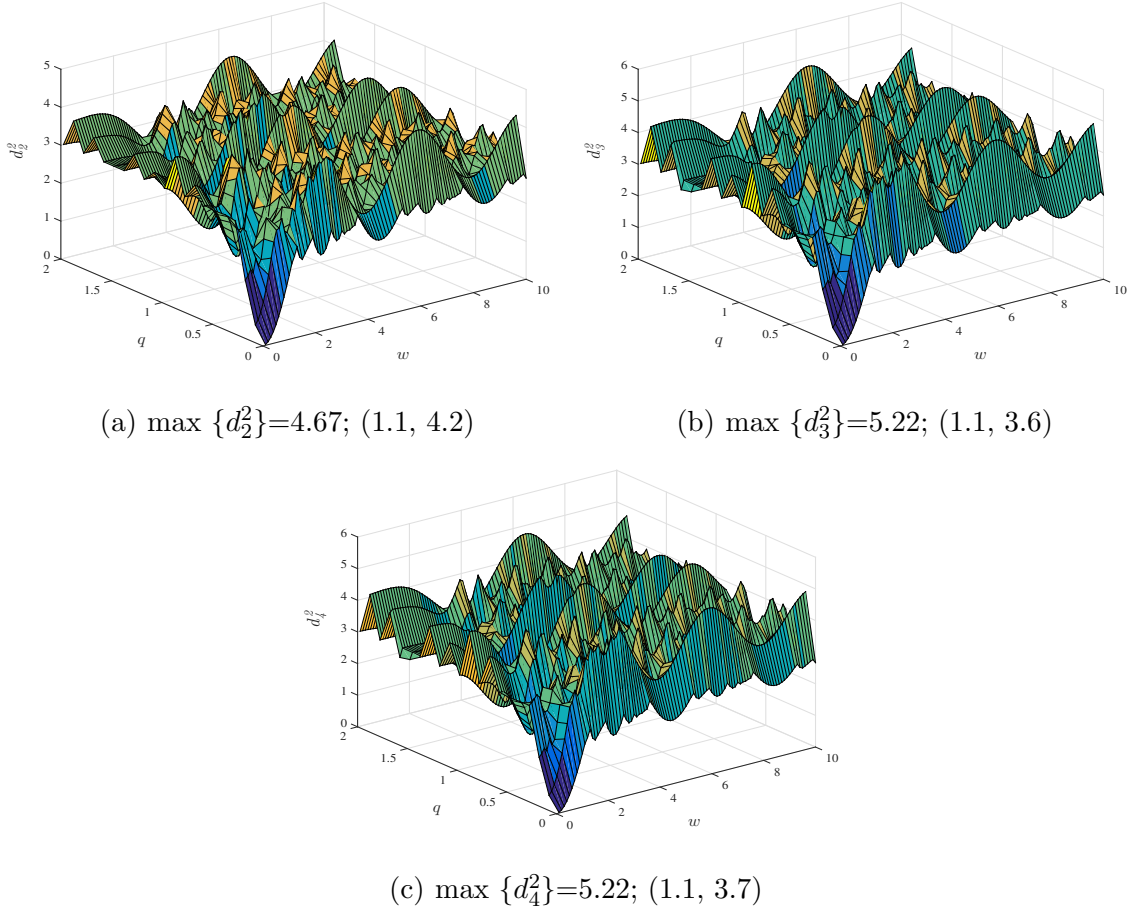
Figure 3.12: Surface plots of d_n^2 as a function of q and w for (a) $n=2$, (b) $n=3$, and (c) $n=4$ for 8-CPCM

In order to understand the sensitivity of one modulation parameter (say q) with the other varying (say w), in Figs. 3.13 and 3.14, d_2^2 are plotted as a function of w and q, with q and w fixed, respectively. For 2-CPCM the optimum modulation parameters are $q=0.30$ and $w=1.9$, for two observation intervals (i.e. $n=2$). These parameters result in max$\{d_2^2\}$=2.404 (Table 3.3). It is observed that d_2^2 is very sensitive to variations in w when q is fixed. This implies that system parameters need to be chosen carefully for optimum error rate performance. Similar observations are in order for the case when w is varied with q fixed. A general observation regarding M-CPCM is that there always exist multiple sets of (q, w) that yield the same error rate performance.
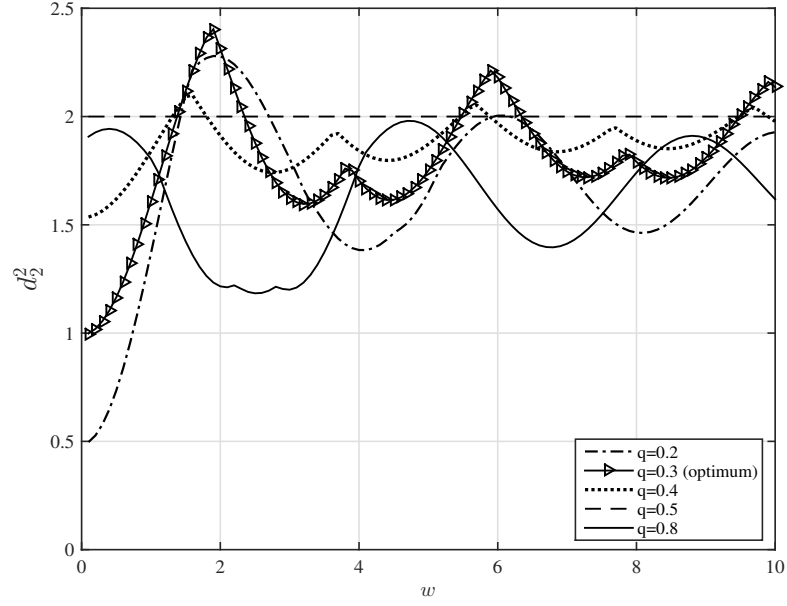
Figure 3.13: Squared Euclidean distance d_2^2 as a function of w for 2-CPCM with $(q = 0.2, \mathbf{0.3}, 0.4, 0.5, 0.8)$
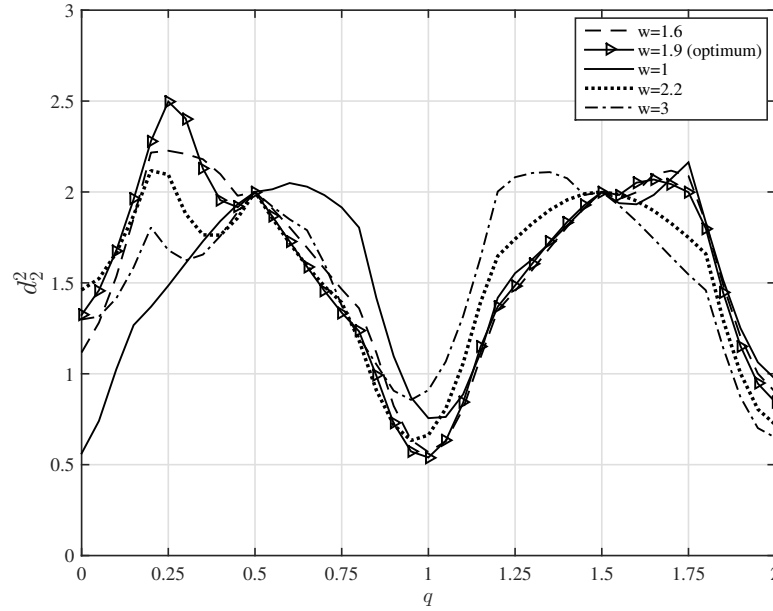
Figure 3.14: Squared Euclidean distance d_2^2 as a function of q for 2-CPCM with $(w = 1.6, \mathbf{1.9}, 1, 2.2, 3)$

In Fig. 3.15, contour plots of $G_n(q, w)$ (SNR gain relative to BPSK) for 2-CPCM system for $n = 2, 3$, and 4 are shown. For example, in Fig. 3.15(a), the contour with

a value equal to 0.79 indicates sets of (q, w) that achieve the best performance in a 2-CPCM system with an observation length $n = 2$. Contour with a value equal to 0 denotes 2-CPCM systems with performance equal to that of BPSK. The negative value contours represent 2-CPCM systems that have performance poorer than BPSK.

(a) $n=2$

(b) $n=3$

(c) $n=4$
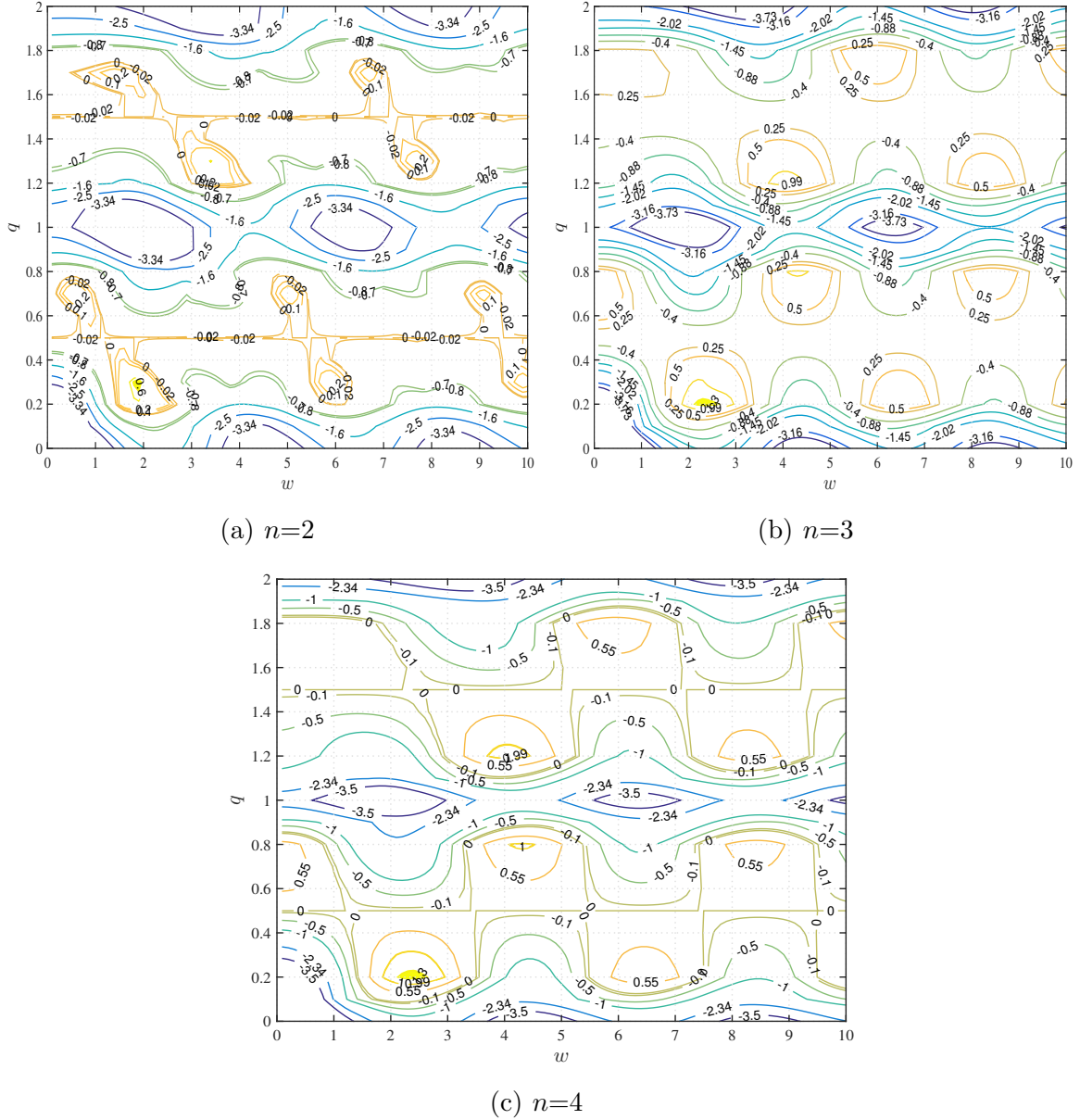
Figure 3.15: Contour plots of $G_n(q, w)$ for 2-CPCM signals for (a) $n = 2$, (b) $n = 3$, and (c) $n = 4$

3.6　Conclusions

In this Chapter, a class of signals refereed to as M-CPCM is introduced for digital data transmission. This class of signals represent multi-level chirp modulation with memory. A general description of M-CPCM is given and the independent modulation parameters that characterize such a system are identified and described. Using the notion of minimum Euclidean distance in signal-space, the limiting SNR gains inherent is 2-, 4-, and 8-CPCM systems have been established. It is shown that 2-, 4-, and 8-CPCM systems have at least 1.66, 3.53, and 4.77 dB advantage relative to BPSK. Also, an analysis of how to realize these SNR gains as a function of the number of observation intervals, n, of the receiver is presented. It is shown that with just $n = 4$, 84 %, 93 %, and 70 % of the inherent gains available with 2-, 4-, and 8-CPCM systems can be realized by appropriately choosing the modulation parameters q and w. Several 3D and contour plots of Euclidean distance as a function of q, w, and n are provided that can be used in the design of M-CPCM systems for data transmission.

Chapter 4

Detection and Performance of M-CPCM in AWGN Channel

4.1 Introduction

In Chapter 3, multi-level chirp modulation with memory called M-CPCM is introduced and its geometric properties is examined in depth. The class of M-CPCM signals have inherent memory by virtue of phase-continuity at symbol transitions and can be exploited to gain advantage in terms of symbol error rate performance. In this Chapter the problem of detection of M-CPCM signals over AWGN channel is addressed. Both coherent and non-coherent detection situations are considered and structures of optimum receivers are derived. Symbol error probability bounds on the performance of these receivers are then derived and optimum M-CPCM systems are determined. A comparison of the performance of M-CPCM with other comparable multi-level modulations such as M-CPFSK is also provided. Comments are offered on the complexities of coherent and non-coherent receiver structures from the viewpoint of implementation.

4.2 Coherent Detection of M-CPCM

The transmitted M-CPCM signal during the ith symbol interval can be written as (Chapter 3):

$$S(t, d) = \sqrt{\frac{2E_s}{T_s}} \ \cos(w_c t + d_i g(t - (i - 1)T_s) +$$

$$\pi q \sum_{k=1}^{i-1} d_k + \theta), \quad (i - 1)T_s \leq t \leq iT_s \qquad (4.1)$$

where

$$g(t) = \begin{cases} 0, & t \leq 0, \quad t > T_s \\[2mm] \pi \left\{ h\left(\frac{t}{T_s}\right) - w\left(\frac{t}{T_s}\right)^2 \right\}, & 0 \leq t \leq T_s \\[2mm] \pi q = \pi(h - w), & t = T_s \end{cases} \tag{4.2}$$

and $d = (d_1, d_2, \ldots, d_n)$ denotes the first n symbols transmitted. The transmitted M-CPCM signal over $0 \leq t \leq nT_s$ is modeled as $S(t, d_\delta, A, \theta)$ where d_δ represents the decision symbol and $A = (d_1, d_2, \ldots, d_{\delta-1}, d_{\delta+1}, \ldots, d_n)$ represents the sequence of remaining $(n-1)$ data symbols. Since d_i, $i = 1, 2, \ldots, n$, can take values $\pm 1, \pm 3, \ldots, \pm(M-1)$, A represents $(n-1)$-tuple $(d_1, d_2, \ldots, d_{\delta-1}, d_{\delta+1}, \ldots, d_n)$. The starting phase at $t = 0$ is denoted by θ. With this model for the M-CPCM signal over n symbol intervals, next the detection problem is addressed in 4.2.1.

4.2.1   Optimum Coherent Receiver

For coherent transmission θ can be set equal to zero in (4.1). The detection strategy is to observe the received waveform over n symbol intervals in the presence of AWGN with two-sided power spectral density of $\frac{N_0}{2}$ watts/Hz and to arrive at an optimum decision about a specific data symbol transmitted, say d_δ, $\delta = 1, 2, \ldots, n$, during this interval. Thus, the detection problem is to observe the received waveform:

$$r(t) = S(t, d_\delta, A) + n(t) , \quad 0 \leq t \leq nT_s \tag{4.3}$$

and produce an estimate $\hat{d}_\delta$ of d_δ. In (4.3), $A = (d_1, d_2, \ldots, d_{\delta-1}, d_{\delta+1}, \ldots, d_n)$ represents one of the $m = M^{n-1}$ possible sequence of data symbols. The detection problem in (4.3) is the well-known composite hypothesis testing problem [40] and the solution is the likelihood ratio test. Following the developments in Chapter 2, for the

M-CPCM signals at hand, the likelihood functions are given by:

$$l_1 = \int_A \exp\left[\frac{2}{N_0} \int_0^{nT_s} r(t)\ S(t, d_\delta = +1, A)\ dt\right] p(A)\ dA$$

$$l_2 = \int_A \exp\left[\frac{2}{N_0} \int_0^{nT_s} r(t)\ S(t, d_\delta = -1, A)\ dt\right] p(A)\ dA$$

$$\vdots$$

$$\vdots \tag{4.4}$$

$$l_{M-1} = \int_A \exp\left[\frac{2}{N_0} \int_0^{nT_s} r(t)\ S(t, d_\delta = +(M-1), A)\ dt\right] p(A)\ dA$$

$$l_M = \int_A \exp\left[\frac{2}{N_0} \int_0^{nT_s} r(t)\ S(t, d_\delta = -(M-1), A)\ dt\right] p(A)\ dA$$

where the probability density of the composite parameter A is given by:

$$p(A) = p(d_1)p(d_2)\ldots p(d_{\delta-1})p(d_{\delta+1})\ldots p(d_n) \tag{4.5}$$

and the densities:

$$p(d_i) = \frac{1}{M}\left[\delta(d_i - 1) + \delta(d_i + 1) + \cdots + \delta(d_i - (M-1)) + \delta(d_i + (M-1))\right] \tag{4.6}$$

$$i = 1, 2, \ldots, \delta - 1, \delta + 1, \ldots, n.$$

The integral $\int_A dA$ in (4.4) is given by:

$$\int_A dA = \int_d \ldots \int_{d_{\delta-1}} \int_{d_{\delta+1}} \ldots \int_{d_n} dd_1 \, dd_2 \ldots dd_{\delta-1} \, dd_{\delta+1} \, dd_n$$

Using (4.5) and (4.6) in (4.4), the M likelihood functions can be written as:

$$l_1 = \frac{1}{m} \sum_{k=1}^{m} \exp \left[\frac{2}{N_0} \int_0^{nT_s} r(t) \, S(t, d_\delta = +1, A_k) \, dt \right]$$

$$l_2 = \frac{1}{m} \sum_{k=1}^{m} \exp \left[\frac{2}{N_0} \int_0^{nT_s} r(t) \, S(t, d_\delta = -1, A_k) \, dt \right]$$

$$\vdots$$

$$\vdots \tag{4.7}$$

$$l_{M-1} = \frac{1}{m} \sum_{k=1}^{m} \exp \left[\frac{2}{N_0} \int_0^{nT_s} r(t) \, S(t, d_\delta = +(M-1), A_k) \, dt \right]$$

$$l_M = \frac{1}{m} \sum_{k=1}^{m} \exp \left[\frac{2}{N_0} \int_0^{nT_s} r(t) \, S(t, d_\delta = -(M-1), A_k) \, dt \right]$$

where $m = M^{n-1}$. The quantity $\frac{1}{m}$ which is common to all l_is can be ignored. The optimum receiver computes $l_1, l_2, \ldots, l_M$ and then computes:

$$l_k = \max\{l_1, l_2, \ldots, l_M\} \tag{4.8}$$

in order to arrive at an estimate $\hat{d}_\delta$ of d_δ using:

$$\hat{d}_\delta = \begin{cases} k, & \text{if } k \text{ is odd} \\[2mm] -(k-1), & \text{if } k \text{ is even} \end{cases} \tag{4.9}$$

The receiver structure dictated by (4.7) is shown in Fig. 4.1. The receiver correlates the received waveform with each of the m possible transmitted M-CPCM signals with the first symbol data $d_\delta = +1$, to produce $x_{+11}, x_{+12}, \ldots, x_{+1m}, (x_{+1k} = \int_0^{nT_s} r(t)S(t, d_\delta = +1, A_k) \, dt)$, and then computes the sum $\sum_{k=1}^{m} \exp(\frac{2}{N_0} x_{+1k})$ to produce the likelihood function l_1. A similar operation of correlation and summing is performed with first symbol data$=-1, \pm 3, \ldots, \pm(M-1)$ to produce the likelihood functions $l_2, \ldots, l_M$. Once these M likelihood functions are computed, the decision about d_δ is made based on the largest value of these functions. The optimum receiver shown in Fig. 4.1 is non-linear and requires a total of M^n correlation operations. The non-linearity of the receiver is due to the memory inherent in the M-CPCM signals. The performance of the optimum receiver is too complex to determine analytically. However, by making high and low SNR approximations in the likelihood functions, linear receivers can be obtained. In the next section, the performance analysis of the optimum receiver shown in Fig. 4.1 is presented using this approximation on SNR.

4.2.2 Symbol Error Probability Analysis

High SNR Upper bound

With reference to Fig. 4.1, the M likelihood functions can be written as:

$$
\begin{aligned}
l_1 &= \sum_{k=1}^{m} \exp\left[\frac{2}{N_0} x_{+1k}\right] \\
l_2 &= \sum_{k=1}^{m} \exp\left[\frac{2}{N_0} x_{-1k}\right] \\
&\qquad \vdots \\
&\qquad \vdots \\
l_{M-1} &= \sum_{k=1}^{m} \exp\left[\frac{2}{N_0} x_{+(M-1)k}\right] \\
l_M &= \sum_{k=1}^{m} \exp\left[\frac{2}{N_0} x_{-(M-1)k}\right]
\end{aligned}
\tag{4.10}
$$
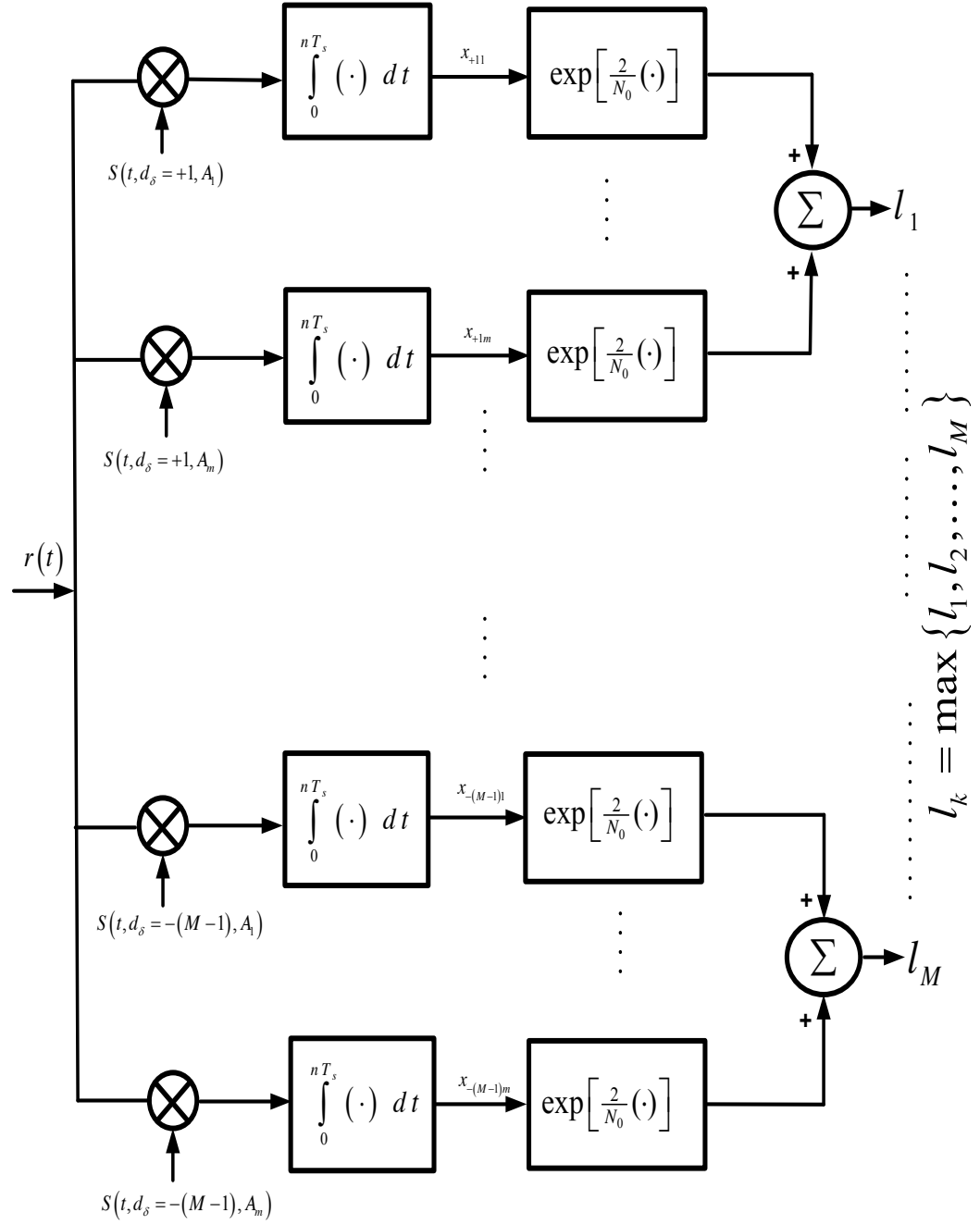
Figure 4.1: Optimum coherent M-CPCM receiver

where

$$
x_{\lambda k} = \begin{cases} \displaystyle\int\limits_{0}^{nT_s} r(t)S(t, d_\delta = \lambda, A_k) \, dt, & \lambda \text{ odd} \\[3em] \displaystyle\int\limits_{0}^{nT_s} r(t)S(t, d_\delta = -(\lambda - 1), A_k) \, dt, & \lambda \text{ even} \end{cases} \quad , \lambda = 1, 2, \ldots, M \qquad (4.11)
$$

For large values of SNR, the summations in (4.10) can be written as:

$$
\sum_{k=1}^{m} \exp\left(\frac{2}{N_0} \, x_{\lambda k}\right) \cong \exp\left(\frac{2}{N_0} \, \tilde{x}_\lambda\right), \qquad \lambda = 1, 2, \ldots, M \qquad (4.12)
$$

where

$$
\tilde{x}_\lambda = \max\{x_{\lambda k}; k = 1, 2, \ldots, m\} \qquad (4.13)
$$

Since $\exp(\cdot)$ is a monotonic function, $\tilde{x}_\lambda$ is an equivalent parameter to investigate. The high-SNR sub-optimum receiver dictated by (4.12)-(4.13) is shown in Fig. 4.2. This receiver computes all $x_{\lambda k}; \lambda = 1, 2, \ldots, M$ and $k = 1, 2, \ldots, m$, and chooses the largest of these to make a decision on d_δ. It is noted that this sub-optimum receiver is a linear receiver and requires as many correlators as the optimum receiver. Also, the sub-optimum receiver is optimum at high SNR, whereas the optimum receiver is optimum at all values of SNR. The sub-optimum receiver in Fig. 4.2 need not find the specific sequence A_k to choose $\hat{d}_\delta$ as an estimate of d_δ (Chapter 3, (3.11)). The symbol error rate performance of the receiver shown in Fig. 4.2 can be determined using high SNR upper bound. The upper bound can be constructed by observing that $x_{\lambda k}$s are Gaussian random variables. For a given transmitted symbol $d_\delta = u$ and a specific sequence A_k $(d_1, d_2, \ldots, d_{\delta-1}, d_{\delta+1}, \ldots, d_n)$, the receiver would be in error if it decides $d_\delta = v$, $v \neq u$ $(v, u = 1, 2, \ldots, M)$. Thus, the conditional probability of

this error using union bounding [40] is given by:

$$P_M(\epsilon \mid d_\delta = u, A_k) < \sum_{v=1}^{M} \sum_{j=1}^{m} P_r[x_{vj} > x_{uk} \mid d_\delta = u, A_k] \qquad (4.14)$$
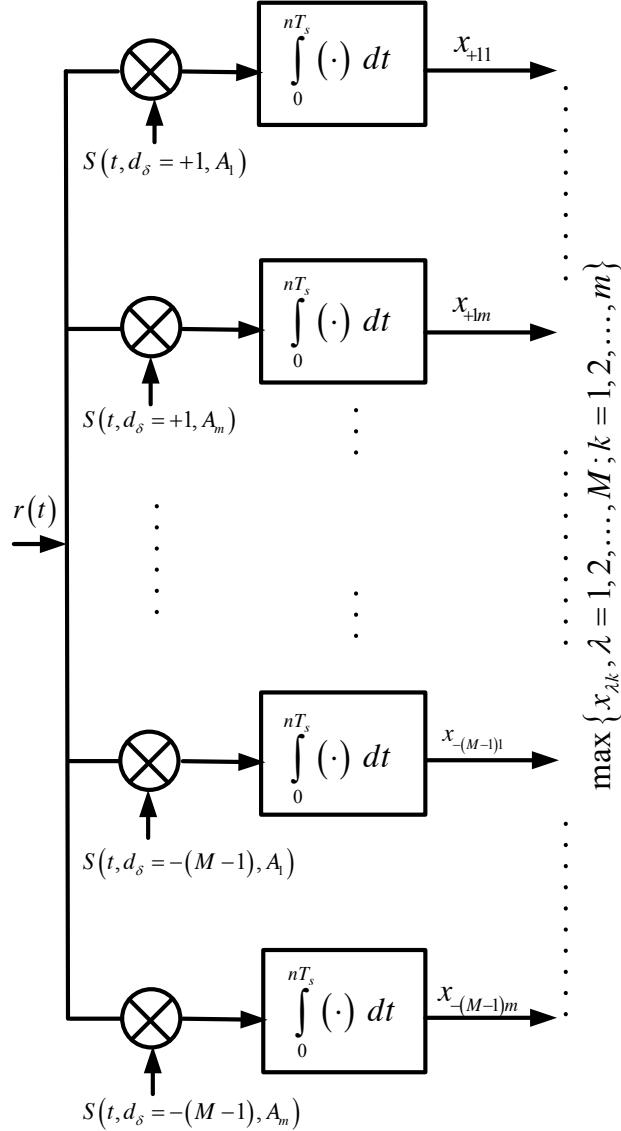
Figure 4.2: High-SNR sub-optimum coherent M-CPCM receiver

Averaging over all equally likely sequences A_k, the conditional probability of error

can be written as:

$$P_M(\epsilon \mid d_\delta = u) < \frac{1}{m} \sum_{v=1}^{M} \sum_{j=1}^{m} \sum_{k=1}^{m} P_r\left[x_{vj} > x_{uk} | d_\delta = u\right] \tag{4.15}$$

where $p(A_k) = \frac{1}{m}$, for $k = 1, 2, \ldots, m$. Averaging over all possible u, the average symbol error probability can be written as:

$$P_M(\epsilon) < \frac{1}{M} \frac{1}{m} \sum_{u=1}^{M} \sum_{\substack{v=1 \\ v \neq u}}^{M} \sum_{j=1}^{m} \sum_{k=1}^{m} P_r\left[x_{vj} > x_{uk}\right] \tag{4.16}$$

where

$$P_r[x_{vj} > x_{uk}] = Q\left[\sqrt{\frac{nE_s}{N_0}(1 - \rho(vj, uk))}\right] \tag{4.17}$$

The quantity $\rho(vj, uk)$ in (4.17) is given by:

$$\rho(vj, uk) = \frac{1}{nE_s} \int_0^{nT} S(t, d_\delta = v, A_j) S(t, d_\delta = u, A_k) \, dt \tag{4.18}$$

and represents the normalized correlation between the signals $S(t, d_\delta = v, A_j)$ and $S(t, d_\delta = u, A_k)$. It is noted that u and v take values $1, 2, \ldots, M$ and represent the decision symbol data d_δ. That is:

$$d_\delta = \begin{cases} u \text{ or } v, & u, v \text{ odd} \\ -(u-1) \text{ or } -(v-1), & u, v \text{ even} \end{cases} \tag{4.19}$$

$\rho(vj, uk)$ in (4.18) can be written as:

$$\rho(vj, uk) = \xi(\tilde{\gamma}) \tag{4.20}$$

where $\tilde{\gamma} = (\gamma_1, \gamma_2, \ldots, \gamma_\delta, \ldots, \gamma_n)$ is the difference sequence between data symbol sequences (u, A_k) and (v, A_j). Since $\gamma_\delta = u - v$ and $u \neq v$, it can take values from

the set $\{\pm 2, \pm 4, \ldots, \pm 2(M-1)\}$ and $\gamma_i = d_i^k - d_i^j$, $i = 1, 2, \ldots, (\delta-1), (\delta+1), \ldots, n$, and takes values from the set $\{0, \pm 2, \pm 4, \ldots, \pm 2(M-1)\}$. A closed form expression for $\xi(\tilde{\gamma})$ has been derived for M-CPCM and is given by:

$$\xi(\tilde{\gamma}) = \begin{cases} \cos\left(\sum_{i=1}^{n-1} \gamma_i \pi q\right), & \gamma_n = 0 \\ \sqrt{\dfrac{\pi}{2a}} \{\Psi_1 - \Psi_2\}, & \gamma_n \neq 0 \end{cases} \quad (4.21)$$

where

$$\Psi_1 = \cos\left(\frac{b^2 - ac}{a}\right) \mathbf{C}\left[\sqrt{\frac{2}{a\pi}}(a+b)\right] + \sin\left(\frac{b^2 - ac}{a}\right) \mathbf{S}\left[\sqrt{\frac{2}{a\pi}}(a+b)\right]$$

and

$$\Psi_2 = \cos\left(\frac{b^2 - ac}{a}\right) \mathbf{C}\left[\sqrt{\frac{2}{a\pi}}(b)\right] + \sin\left(\frac{b^2 - ac}{a}\right) \mathbf{S}\left[\sqrt{\frac{2}{a\pi}}(b)\right]$$

where

$$a = \gamma_n \pi w, \ \ b = -0.5 * \gamma_n \pi (q + w)$$

$$c = -\sum_{i=1}^{n-1} \pi q$$

Although, an explicit expression for computation of symbol error rate for M-CPCM has been derived, (4.17), the computation involved is too large. A simplified expression for (4.17) can be obtained by recognizing and identifying the Gaussian pairs which have the same correlation. Using (4.17)-(4.20) in (4.16), an equivalent expression for symbol error rate can be obtained and is given by:

$$P_M(\epsilon) < (m-1)M^{n-1} \int_{\tilde{\gamma}} Q\left[\sqrt{\frac{nE_s}{N_0}(1 - \xi(\tilde{\gamma}))}\right] p(\tilde{\gamma}) \, d\tilde{\gamma} \quad (4.22)$$

where

$$\int\limits_{\tilde{\gamma}} d\tilde{\gamma} = \int \ldots \int d\gamma_1 \ldots d\gamma_\delta \ldots d\gamma_n \tag{4.23}$$

and

$$p(\tilde{\gamma}) = p(\gamma_1) \ldots p(\gamma_\delta) \ldots p(\gamma_n) \tag{4.24}$$

with

$$p(\gamma_\delta) = \frac{1}{M(M-1)} \sum_{j=1}^{M-1} j \left[\delta(\gamma_\delta + 2(M-j)) + \delta(\gamma_\delta - 2(M-j)) \right] \tag{4.25}$$

and

$$p(\gamma_i) = \frac{1}{M} \delta(\gamma_i) + \frac{1}{M^2} \sum_{j=1}^{M-1} j \left[\delta(\gamma_i + 2(M-j)) + \delta(\gamma_i - 2(M-j)) \right] \tag{4.26}$$

$$i = 1, 2, \ldots, \delta-1, \delta+1, \ldots n$$

This simplified expression for symbol error probability requires less computations than the one given in (4.16).

High SNR lower bound

A lower bound on the symbol error probability of the coherent sub-optimum M-CPCM receiver (Fig. 4.2) can be constructed by supposing that for each transmitted symbol sequence, the receiver needs only to decide between this sequence and its nearest neighbor. Such a receiver would perform at least as good as the receiver that is not aware of two symbol sequences transmitted but must compare with all possible symbol sequences. The performance of this receiver is a lower bound to the

performance of the optimum receiver in Fig. 4.1 at high SNR. The lower bound on symbol error probability is given by:

$$P_M(\epsilon) > \frac{1}{M} \frac{1}{m} \sum_{u=1}^{M} \sum_{\substack{v=1 \\ v \neq u}}^{M} \sum_{k=1}^{m} Q \left[\sqrt{\frac{nE_s}{N_0}(1 - \rho^*(v, uk))} \right] \qquad (4.27)$$

where

$$\rho^*(v, uk) = \max \{\rho(vj, uk), j = 1, 2, \ldots, m\}$$

4.2.3 Numerical Results and Discussion

The symbol error rate upper bound of (4.16) is a function of: i) $\frac{E_b}{N_0}$, ii) n, iii) (q, w), and iv) M. For a given M, n, and a suitably high SNR, the set (q, w) that should be chosen is the one that minimizes (4.16). The optimum (q, w) sets have been determined at 6, 8, 10, and 12 dB for $2 \leq n \leq 5$ for 2-, 4-, 8-CPCM. The modulation parameter space is bounded by $0 < q \leq 2 \times 0 < w \leq 10$. Tables 4.1-4.3 summarize these results. It is observed that optimum (q, w) sets are nearly independent of SNR except for minor variations.

Table 4.1: Optimum (q, w) 2-CPCM systems as a function of observation intervals n and SNR (E_b/N_0)

SNR (dB)	(q_{opt}, w_{opt})			
	$n=2$	$n=3$	$n=4$	$n=5$
6	(0.28, 1.85)	(0.24, 2.07)	(0.23, 2.22)	(0.22, 2.33)
8	(0.27, 1.88)	(0.23, 2.16)	(0.21, 2.31)	(0.19, 2.37)
10	(0.26, 1.93)	(0.22, 2.20)	(0.19, 2.33)	(0.18, 2.39)
12	(0.26, 1.95)	(0.21, 2.20)	(0.18, 2.32)	(0.18, 2.39)

For purposes of symbol error rate performance illustration, the optimum sets computed at an SNR of 6 dB are used. It is noted that the high SNR upper bound given by (4.16) and the high SNR lower bound given by (4.27) become the same for SNR greater than or equal to 6 dB. Hence, the upper bound of (4.16) will be used to illustrate symbol error rate performance.

Table 4.2: Optimum (q, w) 4-CPCM systems as a function of observation intervals n and SNR (E_b/N_0)

SNR (dB)	(q_{opt}, w_{opt})			
	$n=2$	$n=3$	$n=4$	$n=5$
6	(0.24, 2.73)	(0.40, 2.43)	(0.39, 2.48)	(0.38, 2.49)
8	(0.25, 2.75)	(0.40, 2.48)	(0.39, 2.51)	(0.38, 2.50)
10	(0.25, 2.74)	(0.40, 2.51)	(0.38, 2.52)	(0.38, 2.51)
12	(0.25, 2.76)	(0.40, 2.50)	(0.38, 2.52)	(0.38, 2.50)

Table 4.3: Optimum (q, w) 8-CPCM systems as a function of observation intervals n and SNR (E_b/N_0)

SNR (dB)	(q_{opt}, w_{opt})		
	$n=2$	$n=3$	$n=4$
6	(1.12, 4.10)	(0.88, 4.71)	(0.88, 4.71)
8	(1.12, 4.10)	(0.88, 4.69)	(0.88, 4.69)
10	(1.12, 4.10)	(0.88, 4.68)	(0.88, 4.68)
12	(1.12, 4.11)	(0.88, 4.69)	(0.88, 4.68)

2-CPCM System

In Fig. 4.3, the high SNR upper bound on the performance of the optimum coherent receiver for observation intervals $n = 2, 3, 4$ and 5 are shown for 2-CPCM systems. It is observed that as n increases, the performance improves. However, in going from $n = 4$ to $n = 5$, the improvement in performance is only marginal but the complexity of the receiver increases considerably. This observation shows the trade off that exists between receiver complexity and performance. For $n = 2$, the optimum 2-CPCM system outperforms BPSK. The optimum 2-CPCM system for $5T_s$ observation length with $(q = 0.22, w = 2.33)$ outperforms BPSK by nearly 1.6 dB. In Chapter 3, the limiting SNR gain of 2-CPCM relative to BPSK was found out to be 1.66 dB. Thus, it is clear that nearly all the potential of 2-CPCM can be achieved with $n = 5$. An improvement of about 0.75 dB and 0.25 dB are possible in going from $2T_s$ to $5T_s$

and $3T_s$ to $5T_s$ observation lengths, respectively. When coherent receiver is used, the performance remains the same regardless of the position δ of the decision symbol. For example, for a 3-symbol observation length receiver, the performance is the same when decision is made on the first symbol ($\delta = 1$), second symbol ($\delta = 2$) or the third symbol ($\delta = 3$).
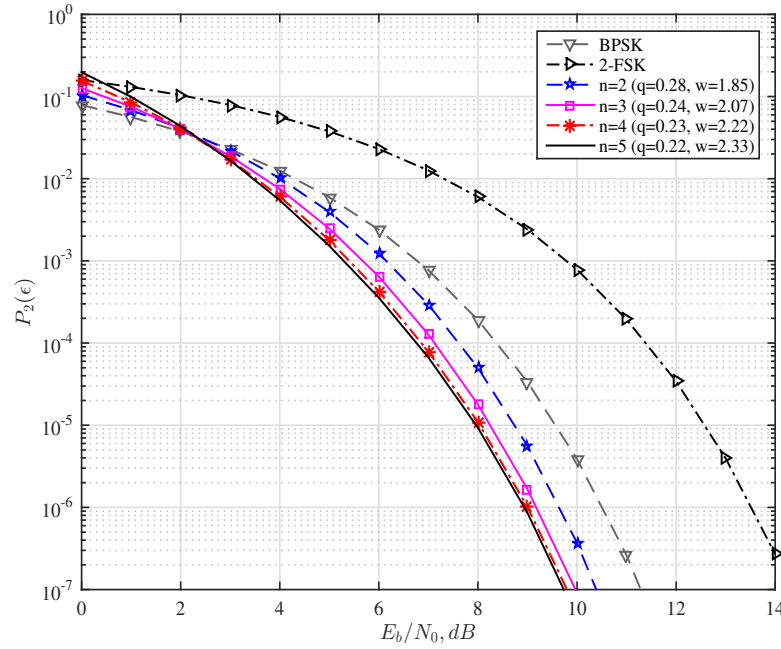
Figure 4.3: Error probability performance of optimum 2-CPCM systems for $n = 2, 3, 4$ and 5

In Fig. 4.4 error rate performance of 2-CPCM as a function of n is shown for specific SNRs of 6, 8, 10, and 12 dB. In Table 4.4, error probabilities of optimum 2-CPCM, BPSK and 2-FSK orthogonal are shown for $\frac{E_b}{N_0}$=6, 8, and 10 dB.
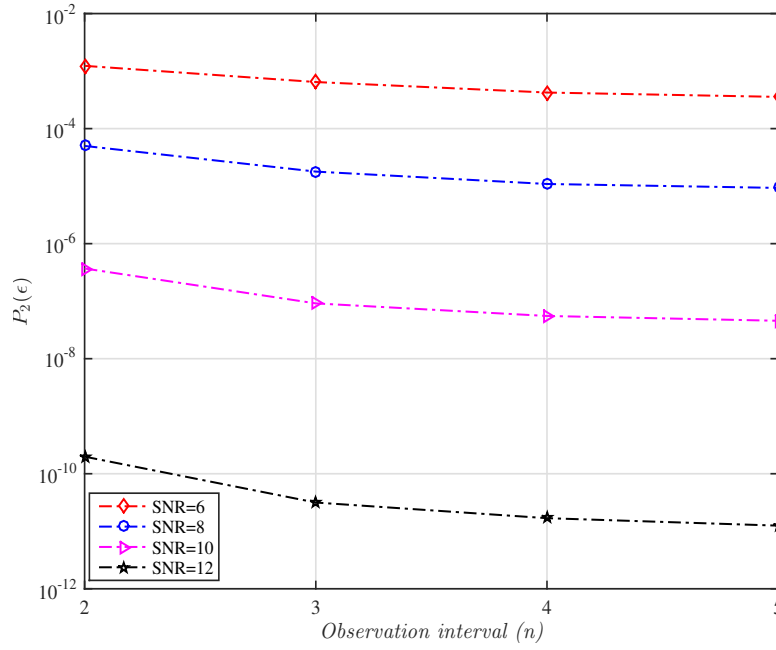
Figure 4.4: Error probability performance of optimum 2-CPCM systems as a function n at $\frac{E_b}{N_0} = $ 6, 8, 10 and 12 dB

Table 4.4: Error probabilities of 2-CPCM, BPSK, and 2-FSK at E_b/N_0=6, 8, and 10 dB

SNR (dB)	2-CPCM				BPSK	2-FSK
	$n=2$	$n=3$	$n=4$	$n=5$		
6	1.23×10^{-3}	6.46×10^{-4}	4.24×10^{-4}	3.65×10^{-4}	2.39×10^{-3}	2.30×10^{-2}
8	4.99×10^{-5}	1.79×10^{-5}	1.09×10^{-5}	9.30×10^{-6}	1.90×10^{-4}	6.00×10^{-3}
10	3.70×10^{-7}	9.15×10^{-8}	5.53×10^{-8}	4.56×10^{-8}	3.87×10^{-6}	7.83×10^{-4}

A good comparison of 2-CPCM can be made with 2-CPFSK. In Fig. 4.5, error rate performance of 2-CPFSK as a function of n is shown. From Figs. 4.3 and 4.5, it is observed that 2-CPCM outperforms 2-CPFSK by nearly 0.5 dB. In Table 4.5 error

probabilities of optimum 2-CPCM nd 2-CPFSK systems are given as a function of n for $\frac{E_b}{N_0} = 6$, 8, and 10 dB.
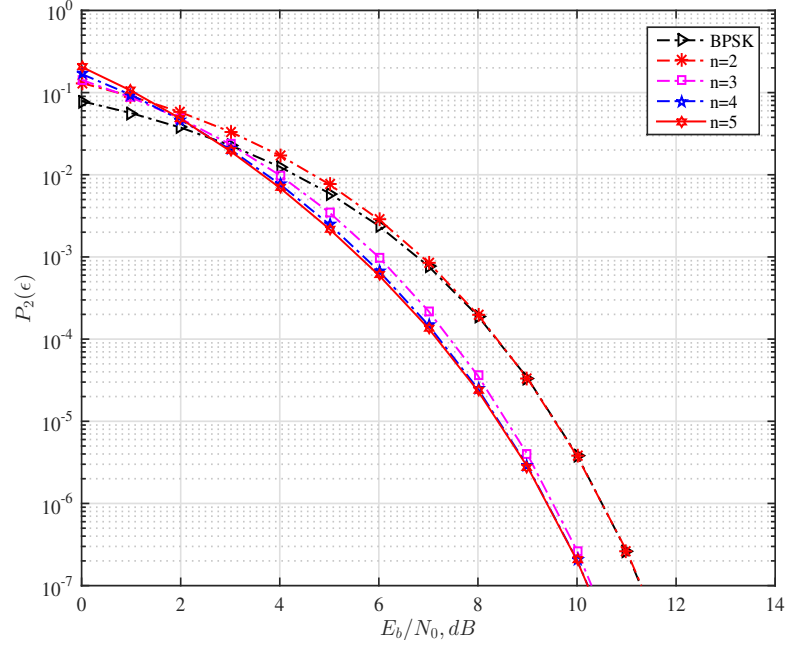
Figure 4.5: Error probability performance of 2-CPFSK ($h = 0.715$) for $n = 2, 3, 4$ and 5

Table 4.5: Probability of error comparison of 2-CPCM and 2-CPFSK

SNR (dB)	$n = 2$		$n = 3$		$n = 4$		$n = 5$	
	2-CPCM	2-CPFSK	2-CPCM	2-CPFSK	2-CPCM	2-CPFSK	2-CPCM	2-CPFSK
6	1.23×10^{-3}	2.86×10^{-3}	6.46×10^{-4}	9.94×10^{-4}	4.24×10^{-4}	6.76×10^{-4}	3.65×10^{-4}	6.00×10^{-4}
8	4.99×10^{-5}	1.98×10^{-4}	1.80×10^{-5}	3.59×10^{-5}	1.09×10^{-5}	2.48×10^{-5}	1.03×10^{-5}	2.35×10^{-5}
10	3.70×10^{-7}	3.78×10^{-6}	9.31×10^{-8}	2.66×10^{-7}	5.53×10^{-8}	2.05×10^{-7}	5.49×10^{-8}	2.03×10^{-7}

4-CPCM System

The sets of modulation parameters $(0.24, 2.73)$ and $(0.38, 2.49)$ are optimum for $n = 2$ and $n = 5$, respectively, for 4-CPCM system. These sets minimize the symbol error rate given in (4.16). It is observed that optimum $(0.38, 2.49)$ 4-CPCM system with $n = 5$ provides nearly 3.6 dB relative to coherent QPSK. In Fig. 4.6 symbol error rates for optimum 4-CPCM systems for $n = 2, 3, 4$, and 5 are shown. It is noted that energy normalization $E_s = 2E_b$ has been used for plotting error rates in Fig. 4.6.
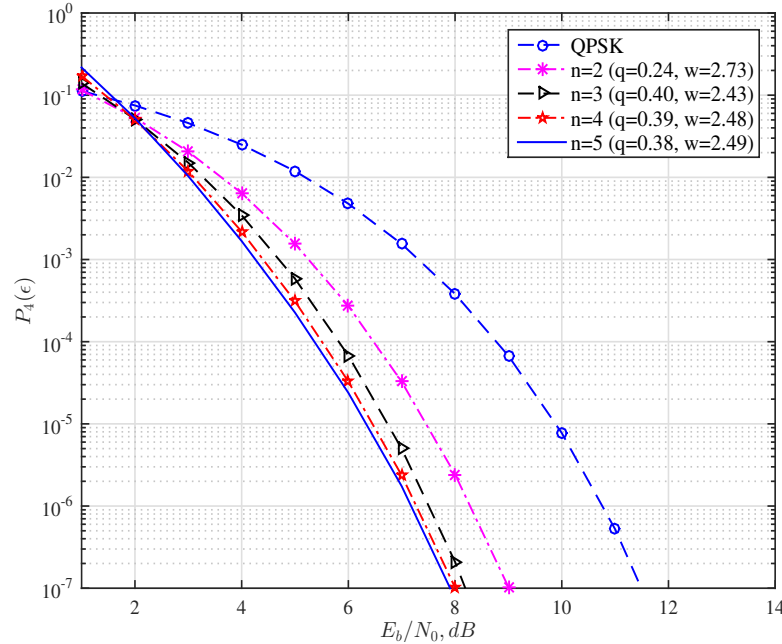
Figure 4.6: Symbol error probability performance of optimum 4-CPCM systems for $n = 2, 3, 4$ and 5

The optimum $(0.24, 2.73)$ 4-CPCM system (optimum for $n = 2$) with $2T_s$ observation length provides nearly 2.5 dB gain relative to coherent QPSK. A further advantage of nearly 1 dB can be obtained when the observation length of the receiver is increased from $n = 2$ to $n = 5$. An overall gain inherent in 4-CPCM system is 3.53 dB (Chapter 3, Table 3.1) and using the optimum receiver for 4-CPCM with $n = 5$, it is possible to realize almost all the potential available in a 4-CPCM system.

Table 4.6: Error probabilities of 4-CPCM and QPSK at E_b/N_0=6, 8, and 10 dB

SNR (dB)	4-CPCM				QPSK
	$n = 2$	$n = 3$	$n = 4$	$n = 5$	
6	2.73×10^{-4}	6.78×10^{-5}	3.27×10^{-5}	2.39×10^{-5}	4.78×10^{-3}
8	2.43×10^{-6}	2.09×10^{-7}	1.02×10^{-7}	7.47×10^{-8}	3.82×10^{-4}
10	2.24×10^{-9}	4.28×10^{-11}	1.99×10^{-11}	1.36×10^{-11}	7.74×10^{-6}

In Fig. 4.7, symbol error rates for 4-CPCM as a function of n are shown for $\frac{E_b}{N_0}$=6, 8, 10, and 12 dB. Table 4.6 shows symbol error probabilities at $\frac{E_b}{N_0}$=6, 8, and 10 dB for 4-CPCM system. For comparison purposes in Fig. 4.8 symbol error probability performance of 4-CPFSK for $n = 2, 3, 4$, and 5 are plotted as a function of SNR.
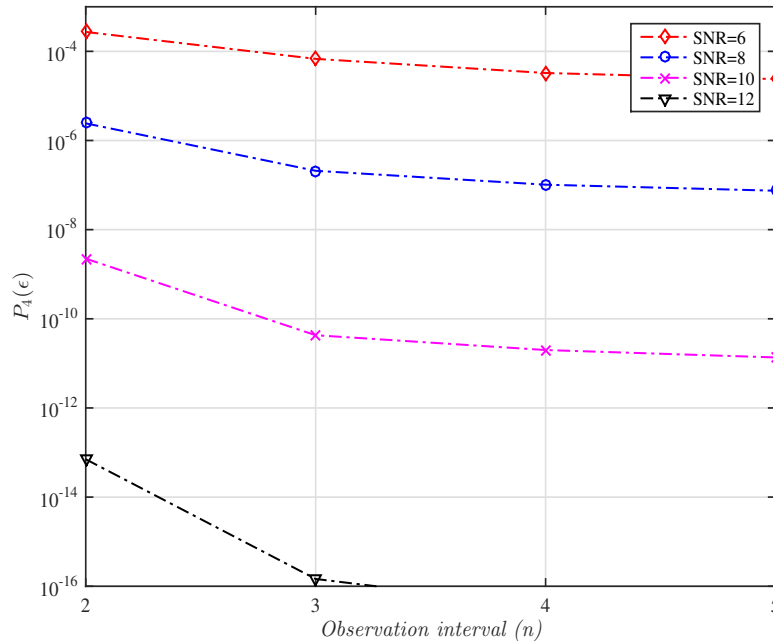
Figure 4.7: Error probability performance of optimum 4-CPCM systems as a function of n at $\frac{E_b}{N_0}$= 6, 8, 10, and 12 dB

Also, in Table 4.7, symbol error probabilities at $\frac{E_b}{N_0}$=6, 8, and 10 dB are shown for

both 4-CPCM and 4-CPFSK. It is observed that 4-CPCM outperforms 4-CPFSK for all observation intervals.
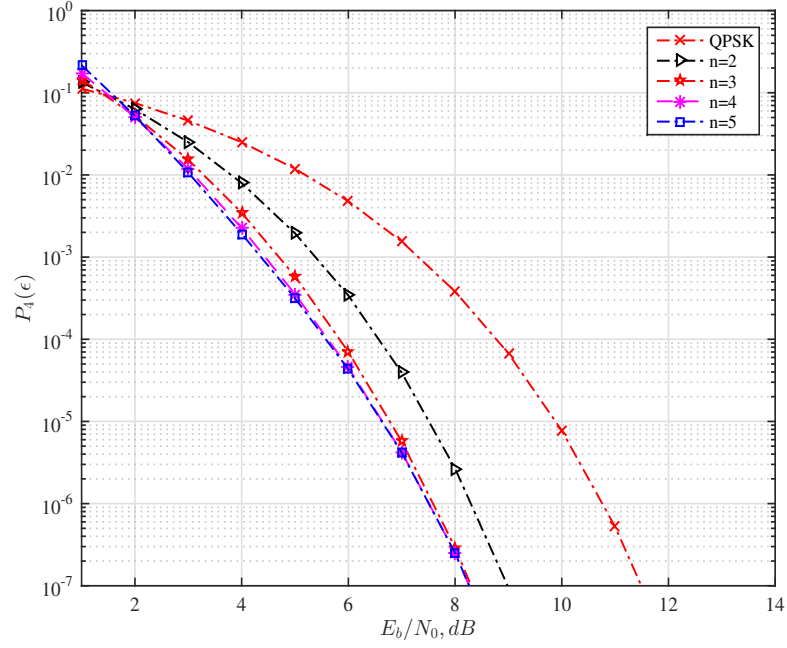
Figure 4.8: Error probability performance of 4-CPFSK for $n = 2, 3, 4$ and 5 [43]

Table 4.7: Probability of error comparison of 4-CPCM and 4-CPFSK

SNR (dB)	$n = 2$		$n = 3$		$n = 4$		$n = 5$	
	4-CPCM	4-CPFSK	4-CPCM	4-CPFSK	4-CPCM	4-CPFSK	4-CPCM	4-CPFSK
6	2.73×10^{-4}	3.40×10^{-4}	6.78×10^{-5}	7.02×10^{-5}	3.27×10^{-5}	4.30×10^{-5}	2.39×10^{-5}	4.30×10^{-5}
8	2.43×10^{-6}	2.67×10^{-6}	2.09×10^{-7}	2.93×10^{-7}	1.02×10^{-7}	2.50×10^{-7}	7.47×10^{-8}	2.50×10^{-7}
10	2.24×10^{-9}	1.50×10^{-9}	4.28×10^{-11}	1.12×10^{-10}	1.99×10^{-11}	1.10×10^{-10}	1.36×10^{-11}	1.10×10^{-10}

8-CPCM System

In Fig. 4.9, the symbol error rates for optimum 8-CPCM systems for $n = 2$ and $n = 3$ are shown. In the same figure is shown the performance of 8-PSK. Again

energy normalization of $E_s = 3E_b$ has been used in plotting the graphs in Fig. 4.9.
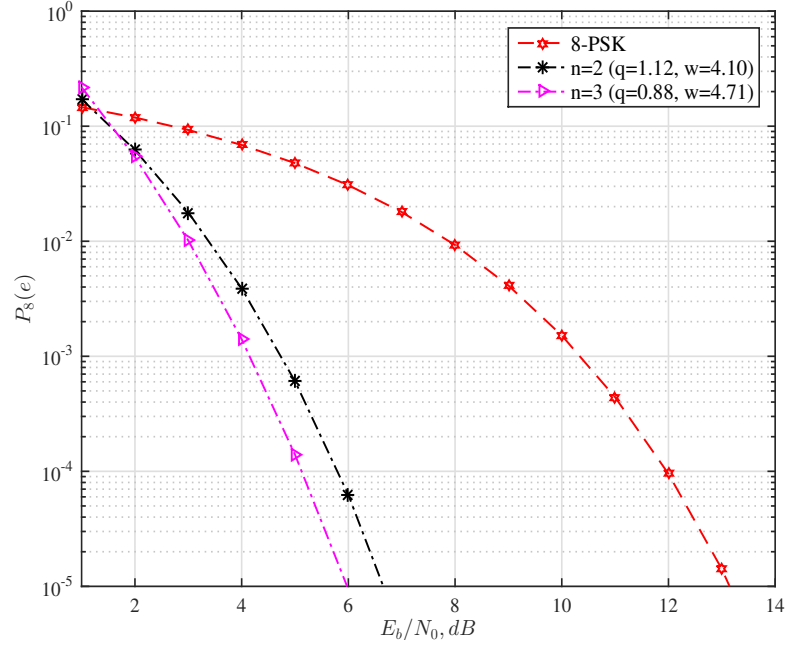
Figure 4.9: Symbol error probability performance of 8-CPCM for $n = 2$ and 3 and 8-PSK

Table 4.8: Error probabilities of 8-CPCM and 8-PSK

SNR (dB)	8-CPCM		8-PSK
	$n = 2$	$n = 3$	
6	6.23×10^{-5}	9.39×10^{-6}	3.07×10^{-2}
8	1.22×10^{-7}	8.05×10^{-9}	9.27×10^{-3}
10	9.04×10^{-12}	1.95×10^{-13}	1.52×10^{-3}

In Fig. 4.10 symbol error probability performance of 8-CPFSK for $n = 2$ and $n = 3$ are shown. Tables 4.8 and 4.9 shows error probabilities at $\frac{E_b}{N_0} = 6$, 8, and 10 dB for 8-CPCM, 8-CPFSK and 8-PSK. The 8-CPCM system with the set of modulation parameters $(0.88, 4.71)$, optimum for $n = 3$, is superior to coherent 8-PSK by nearly 7 dB. In going from $n = 2$ to $n = 3$, 8-CPCM system can offer an advantage of

nearly 1 dB. As a comparison with 8-CPFSK, optimum 8-CPCM is only marginally inferior. Further investigation of 8-CPCM is needed for $n \geq 4$ to assess the modulation completely.
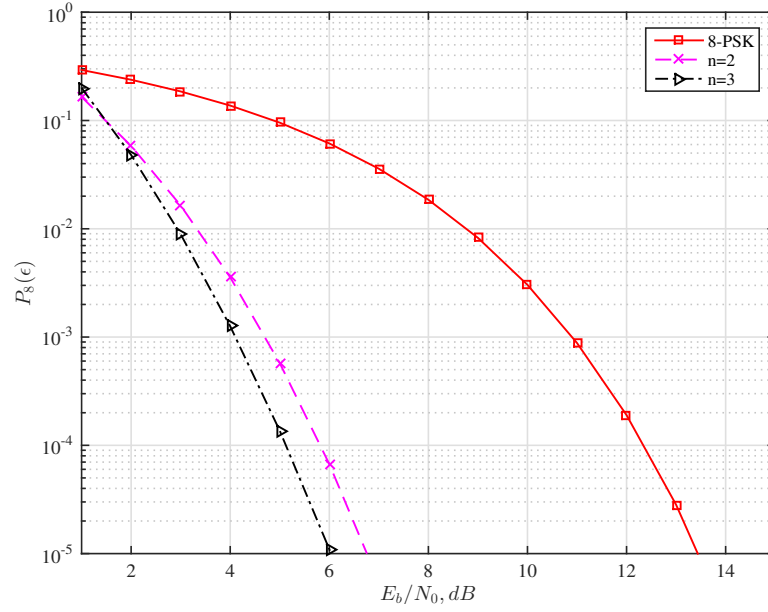
Figure 4.10: Symbol error probability performance of 8-CPFSK for $n = 2$ and 3 [43]

Table 4.9: Probability of error comparison of 8-CPCM and 8-CPFSK

SNR (dB)	$n = 2$		$n = 3$	
	8-CPCM	8-CPFSK	8-CPCM	8-CPFSK
6	6.23×10^{-5}	6.71×10^{-5}	9.39×10^{-6}	1.10×10^{-5}
8	1.22×10^{-7}	2.81×10^{-7}	8.05×10^{-9}	1.78×10^{-8}
10	9.04×10^{-12}	9.04×10^{-11}	1.95×10^{-13}	1.21×10^{-12}

4.3   Non-coherent Detection of M-CPCM in AWGN

4.3.1   Optimum Non-coherent Receiver

The received M-CPCM signal in AWGN for non-coherent detection can be written as:

$$r(t) = S(t, d_\delta, A, \theta), \quad 0 \le t \le nT_s \tag{4.28}$$

where d_δ, $\delta \in \{1, 2, \ldots, n\}$ is the decision symbol, $A = (d_1, d_2, \ldots, d_{\delta-1}, d_{\delta+1}, \ldots, d_n)$ represents one of the $m = M^{n-1}$ possible symbol sequences, θ is the starting phase considered to be an independent random variable uniformly distributed in $(0, 2\pi)$, and $n(t)$ is the AWGN with two-sided power spectral density of $\frac{N_0}{2}$ watts/Hz and mean equal to zero. Following arguments similar to those in Chapter 2, the solution to the detection problem stated in (4.28) is the likelihood ratio test, modified by taking expectation over composite parameters A and θ. The likelihood functions can be written as:

$$l_1 = \int_\theta \sum_{k=1}^m \exp\left[\frac{2}{N_0} \int_0^{nT_s} r(t)\ S(t, d_\delta = +1, A_k, \theta)\ dt \right] p_\theta(\theta)\ d\theta$$

$$l_2 = \int_\theta \sum_{k=1}^m \exp\left[\frac{2}{N_0} \int_0^{nT_s} r(t)\ S(t, d_\delta = -1, A_k, \theta)\ dt \right] p_\theta(\theta)\ d\theta$$

$$\vdots$$

$$\tag{4.29}$$

$$\vdots$$

$$l_{M-1} = \int_\theta \sum_{k=1}^m \exp\left[\frac{2}{N_0} \int_0^{nT_s} r(t)\ S(t, d_\delta = +(M-1), A_k, \theta)\ dt \right] p_\theta(\theta)\ d\theta$$

$$l_M = \int_\theta \sum_{k=1}^m \exp\left[\frac{2}{N_0} \int_0^{nT_s} r(t)\ S(t, d_\delta = -(M-1), A_k, \theta)\ dt \right] p_\theta(\theta)\ d\theta$$

where

$$
p_\theta(\theta) = \begin{cases} \dfrac{1}{2\pi} & 0 \leq \theta \leq 2\pi \\[2ex] 0, & \text{otherwise} \end{cases} \tag{4.30}
$$

Upon performing integration in (4.29), the likelihood functions become:

$$
l_j = \sum_{k=1}^{m} I_0 \left(\frac{2}{N_0} Z_{jk} \right), \qquad j = 1, 2, \ldots, M \tag{4.31}
$$

where

$$
Z_{jk}^2 = I_{jk}^2 + Q_{jk}^2 \tag{4.32}
$$

with

$$
I_{jk} = \begin{cases} \displaystyle\int_0^{nT_S} r(t)\, S(t, d_\delta = +j, A_k, 0)\, dt, & j \ \text{odd} \\[4ex] \displaystyle\int_0^{nT_S} r(t)\, S(t, d_\delta = -(j-1), A_k, 0)\, dt, & j \ \text{even} \end{cases} \tag{4.33}
$$

and

$$
Q_{jk} = \begin{cases} \displaystyle\int_0^{nT_s} r(t)\, S(t, d_\delta = +j, A_k, \frac{\pi}{2})\, dt, & j \ \text{odd} \\[4ex] \displaystyle\int_0^{nT} r(t)\, S(t, d_\delta = -(j-1), A_k, \frac{\pi}{2})\, dt, & j \ \text{even} \end{cases} \tag{4.34}
$$

In (4.31) $I_0(\cdot)$ is the modified zero-order Bessel function.

The structure of the optimum receiver implied by (4.31) is shown in Fig. 4.11. The optimum non-coherent receiver derived from (4.31) essentially consists of a bank M^{n-1} matched filters, for each d_δ ($\pm 1, \ldots, \pm(M-1)$), whose outputs are envelope-detected and weighted with the nonlinearity $I_0(\cdot)$ to form M sum terms, $l_1, l_2, \ldots, l_M$,

before a decision on d_δ is made. Mathematically, the decision rule for the optimum non-coherent receiver for M-CPCM is given by:

$$l_k = \max\{l_1, l_2, \ldots, l_m\} \tag{4.35}$$

and the decision based on this is:

$$\hat{d}_\delta = \begin{cases} k, & k \text{ odd} \\ -(k-1), & k \text{ even} \end{cases} \tag{4.36}$$

The optimum non-coherent receiver for M-CPCM is twice as complex as that of the corresponding optimum coherent receiver. However, in the case of the former no phase recovery circuit is required.

4.3.2 Symbol Error Probability Analysis

At high values of SNR, a sub-optimum receiver with symbol error rate performance close to the optimum receiver can be obtained. That is, at high SNR:

$$\sum_{i=1}^{m} I_0\left(\frac{2}{N_0} Z_{ji}\right) \cong I_0\left(\frac{2}{N_0} \tilde{Z}_j\right) \tag{4.37}$$

where

$$\tilde{Z}_j = \max\{Z_{j1}, Z_{j2}, \ldots, Z_{jm}\} \tag{4.38}$$

since $I_0(x)$ is a monotonic function of x, the decision rule for the sub-optimum receiver is to choose $\max\{Z_{ji}; j = 1, \ldots, M, i = 1, \ldots, m\}$. The sub-optimum receiver is shown in Fig. 4.12. An exact evaluation of the performance of this receiver is not possible. However, the union bound [40] will provide a tight performance estimate at high SNR. Given $d_\delta = u$, and A_k, the conditional probability of symbol error is bounded by:
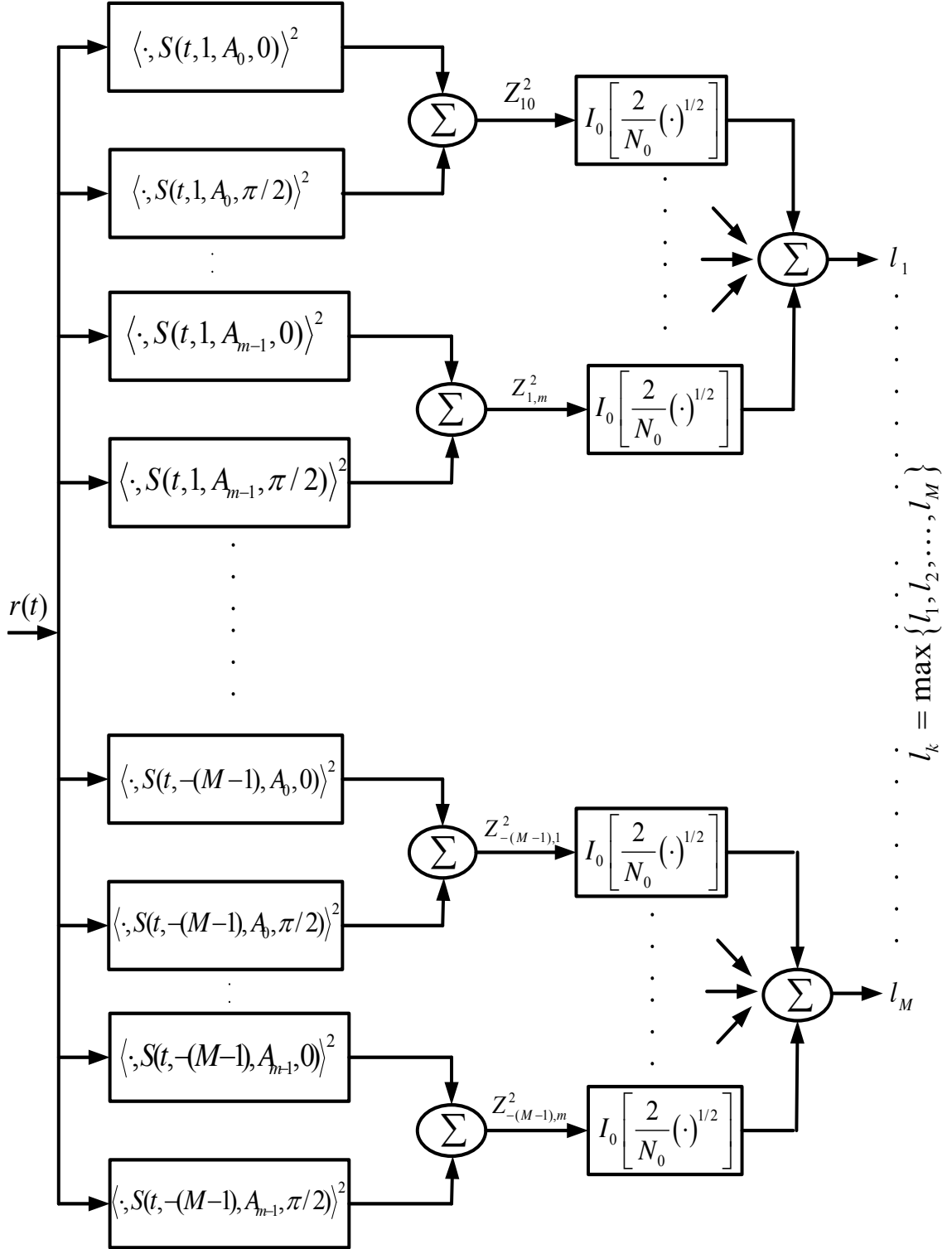
Figure 4.11: Optimum non-coherent M-CPCM receiver structure

$$\left(\langle x(t), y(t) \rangle^2 \triangleq \left[\int\limits_{0}^{nT_s} x(t)y(t)dt \right]^2 \right)$$

$$P_M(\epsilon|u, A_k) < \sum_{v=1}^{M} \sum_{j=1}^{m} P_r \left[Z_{vj} > Z_{uk} | u, A_k \right] \tag{4.39}$$

Averaging over all A_k, $k = 1, 2, \ldots, n$, we get:

$$P_M(\epsilon|u) < \frac{1}{m} \sum_{u=1}^{M} \sum_{j=1}^{m} \sum_{k=1}^{m} P_r \left[Z_{vj} > Z_{uk} | u \right] \tag{4.40}$$

where $P(A_k) = \frac{1}{m}$, $k = 1, 2, \ldots, m$. Averaging over all u, $v \neq u$, the symbol error rate can be written as:

$$P_M(\epsilon) < \frac{1}{M} \frac{1}{m} \sum_{u=1}^{M} \sum_{\substack{v=1 \\ v \neq u}}^{M} \sum_{j=1}^{m} \sum_{k=1}^{m} P_r \left[Z_{vj} > Z_{uk} \right] \tag{4.41}$$

By observing that $Z_{\lambda,k}$, $\lambda = 1, 2, \ldots, M$ and $k = 1, 2, \ldots, n$ are Rician random variables, probability of one Rician random variable [3] exceeding another in (4.41) is given by:

$$P_r \left[Z_{vj} > Z_{uk} \right] = \frac{1}{2} \left(1 - Q(\sqrt{b}, \sqrt{a}) + Q(\sqrt{a}, \sqrt{b}) \right) \tag{4.42}$$

where

$$a = \frac{nE_s}{2N_0} \left[1 - \sqrt{1 - |\rho_c(vj, uk)|^2} \right] \tag{4.43}$$

$$b = \frac{nE_s}{2N_0} \left[1 + \sqrt{1 - |\rho_c(vj, uk)|^2} \right] \tag{4.44}$$
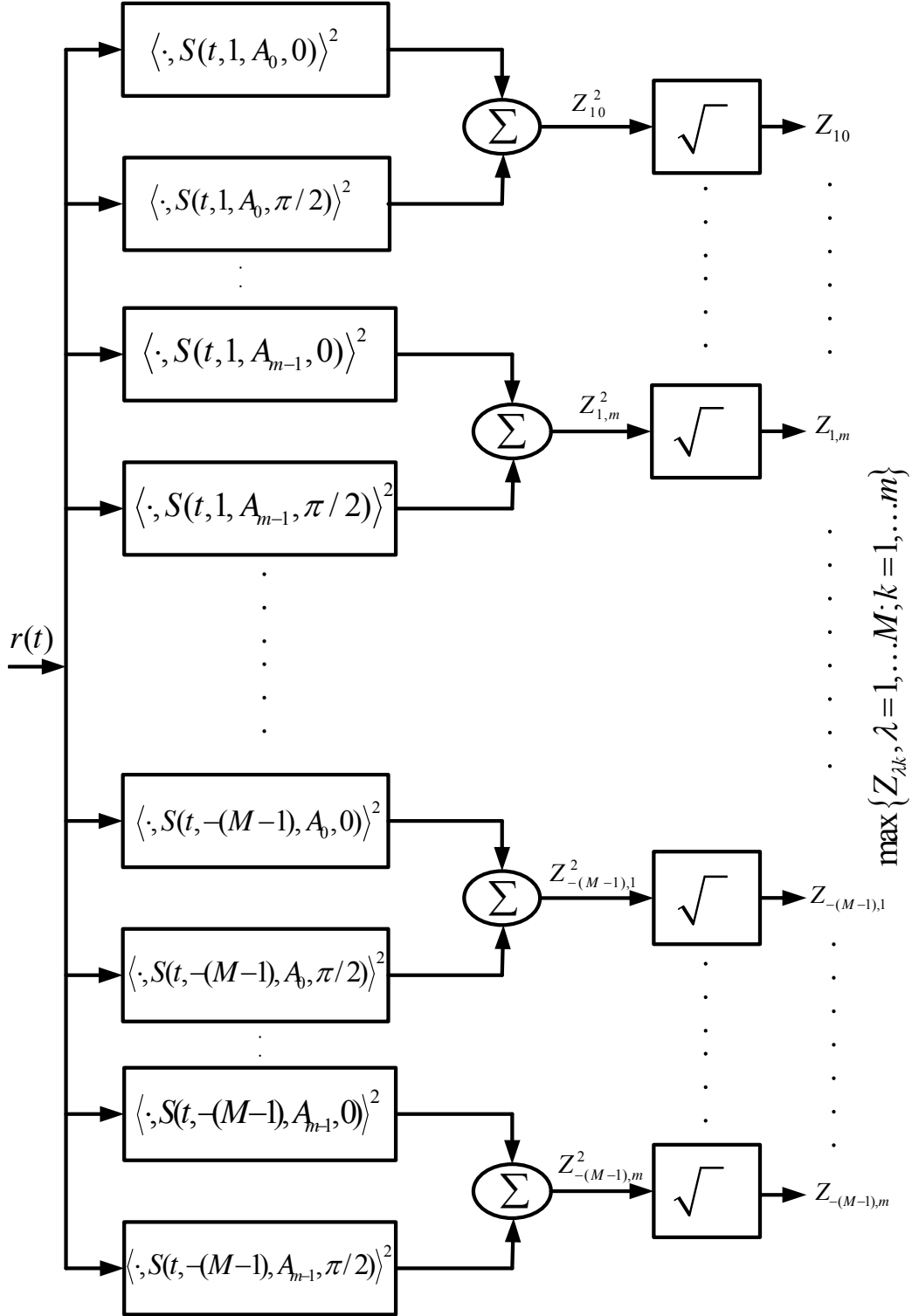
Figure 4.12: Sub-optimum non-coherent M-CPCM receiver structure

$$\left(\langle x(t), y(t) \rangle^2 \triangleq \left[\int\limits_{0}^{nT_s} x(t)y(t)dt \right]^2 \right)$$

In (4.43) and (4.44), $\frac{nE_s}{N_0}$ represents the signal-to-noise ratio and $\rho_c(vj, uk)$ is the correlation between complex envelopes $S_c(t, d_\delta = v, A_j)$ and $S_c(t, d_\delta = u, A_k)$ respectively. The complex envelopes are given by:

$$S_c(t, \lambda, A) = \sqrt{\frac{2E_s}{T_s}} \exp\left[j\phi(t, \lambda, A)\right] \tag{4.45}$$

In (4.42), $Q(\cdot, \cdot)$ represents the Marcum-Q function [3] given by:

$$Q(x, y) = \int_y^\infty \exp - \left[\frac{x^2 + u^2}{2}\right] I_0(xu) \ u \ du \tag{4.46}$$

The quantity $\rho(\cdot, \cdot)$ in (4.43) and (4.44) for M-CPCM is given by:

$$\rho_c(vj, uk) = \frac{1}{2nE_s} \int_0^{nT_s} S_c(t, d_\delta = v, A_j) \ S_c(t, d_\delta = u, A_k) \ dt \tag{4.47}$$

That is,

$$\rho(vj, uk) = \frac{1}{n} \sum_{i=1}^n \frac{1}{T_s} \int_0^{T_s} \exp\left[j\phi(t, vj, uk)\right] \ dt \tag{4.48}$$

using (4.1), the phase can be written as:

$$\phi_i(t, vj, uk) = (d_i^j - d_i^k)g(t - (i-1)T_s) + \pi q \sum_{r=1}^{i-1}(d_r^j - d_r^k) \tag{4.49}$$

and represents the phase difference during the ith symbol interval between signals $S(t, d_\delta = v, A_j)$ and $S(t, d_\delta = u, A_k)$. It is noted that the complex correlation is a function of the difference of the jth and k^{th} data sequences. Denoting these sequences as $(d_1^j, d_2^j, \ldots, d_{\delta-1}^j d_{\delta+1}^j, \ldots, d_n^j)$ and $(d_1^k, d_2^k, \ldots, d_{\delta-1}^k d_{\delta+1}^k, \ldots, d_n^k)$, the correlation in (4.46) can be written as:

$$\rho(vj, uk) = \zeta(\tilde{\gamma}) = \sum_{i=1}^n \zeta(\gamma_i) \tag{4.50}$$

where $\tilde{\gamma} = (\gamma_1, \gamma_2, \ldots, \gamma_{\delta-1}, \gamma_\delta, \gamma_{\delta+1}, \ldots, \gamma_n)$ with $\gamma_\delta = v - u$ and $\gamma_i = d_i^j - d_i^k$; $i = 1, 2, \ldots, \delta - 1, \delta + 1, \ldots, n$. For M-CPCM signals:

$$\zeta(\gamma_i) = \begin{cases} \exp(jP_i), & \gamma_i = 0 \\[2mm] (2\pi|\gamma_i|w)^{-1/2} \exp j \left[P_i + \text{sgn}(\gamma_i)\frac{\pi}{4w}|\gamma_i|(q+w)^2 \right] \times & \\[2mm] \{[\mathbf{C}(X) + \mathbf{C}(Y)] - j\,\text{sgn}(\gamma_i)\,[\mathbf{S}(X) + \mathbf{S}(Y)]\}, & \gamma_i \neq 0 \end{cases} \tag{4.51}$$

where

$$P_i = \pi q \sum_{r=1}^{i-1} \gamma_r$$

$$X = (|\gamma_i|/2w)^{1/2}(w - q)$$

$$Y = (|\gamma_i|/2w)^{1/2}(w + q)$$

Using (4.51), an expression easy for computation of symbol error rate can be written. That is:

$$P_M(\epsilon) < (M - 1)\, M^{n-1} \int_{\tilde{\gamma}} \frac{1}{2} \left[1 - Q(\sqrt{b}, \sqrt{a}) + Q(\sqrt{a}, \sqrt{b}) \right] p(\tilde{\gamma})\, d\tilde{\gamma} \tag{4.52}$$

where $\int_{\tilde{\gamma}} d\tilde{\gamma}$ and $p(\tilde{\gamma})$ are as given in (4.23) and (4.24).

4.3.3 Numerical Results and Discussion

The general error probability upper bound on the performance of optimum non-coherent M-CPCM receiver can be computed using (4.52). As in the coherent case, the symbol error probability is a function of: i) n, ii) E_b/N_0, iii) M, iv) δ, and (q, w). The set of signal modulation parameters (q, w) that should be chosen is obviously the one that minimizes the symbol error probability upper bound of (4.52). Optimum

sets of modulation parameters have been determined numerically, as analytical minimization of (4.52) is difficult to perform. The minimization have been carried out over $(0, 0) < (q, w) \leq (2, 10)$ and at SNR=8 dB. Optimum (q, w) sets for 2-, 4-, and 8-CPCM non-coherent systems as a function of n and δ are shown in Tables 4.10 to 4.12.

Table 4.10: Optimum (q, w) sets for non-coherent 2-CPCM system as a function of n and δ

n	δ	optimum (q, w)
2	1	(0.53, 3.45)
	2	(0.48, 1.25)
3	1	(0.78, 3.85)
	2	(0.50, 3.45)
	3	(0.31, 1.70)
4	1	(0.21, 2.00)
	2	(0.69, 3.90)
	3	(0.69, 5.00)
	4	(0.85, 4.00)
5	3	(0.26, 2.60)

Table 4.11: Optimum (q, w) sets for non-coherent 4-CPCM system as a function of n and δ

n	δ	optimum (q, w)
2	2	(0.86, 4.80)
3	2	(0.76, 4.80)
4	2	(0.76, 4.65)
5	3	(0.75, 4.65)

Table 4.12: Optimum (q, w) sets for non-coherent 8-CPCM system as a function of n and δ

n	δ	optimum (q, w)
2	2	(0.92, 4.00)
3	2	(0.88, 4.70)

2-CPCM System

It is noted that for non-coherent 2-CPCM system, the optimum modulation parameters is a function of the choice of the position of the decision symbol. For n odd, best error rates are achieved when decision is made on the middle symbol. For example, if $n = 3$, and $n = 5$, $\delta = 2$ and $\delta = 3$, respectively, provide the least symbol error rates. However, when n is even, decision made on one of the middle bits provides the best performance. That is, for $n = 4$, δ could be either 2 or 3. The symbol error probability upper bound on the performance of the optimum non-coherent 2-CPCM receiver is shown in Fig. 4.13 for $n = 3$ and $n = 5$ using the optimum (q, w) sets.
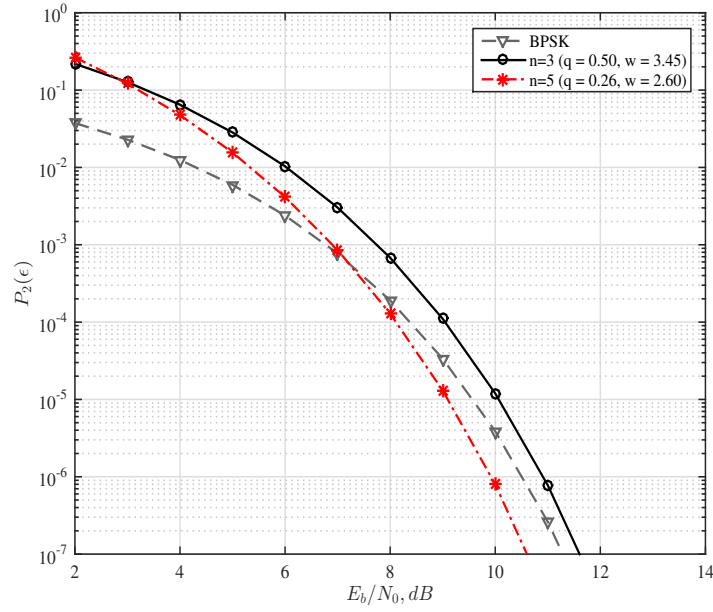
Figure 4.13: Error probability performance of non-coherent 2-CPCM for $n = 3$ and 5

An overall gain of about 1 dB is possible with non-coherent 2-CPCM (with $n = 5$) relative to coherent BPSK. Also, the same 2-CPCM system is superior to non-coherent orthogonal FSK by nearly 4.3 dB. In Fig. 4.14, symbol error rates for non-coherent 2-CPFSK for $n = 3$ and 5 using $h = 0.715$ are shown and Table 4.13 shows a comparison of symbol error rates between 2-CPCM and 2-CPFSK non-coherent systems. It is observed that the 2-CPCM is marginally superior to 2-CPFSK, when non-coherent detection is employed.
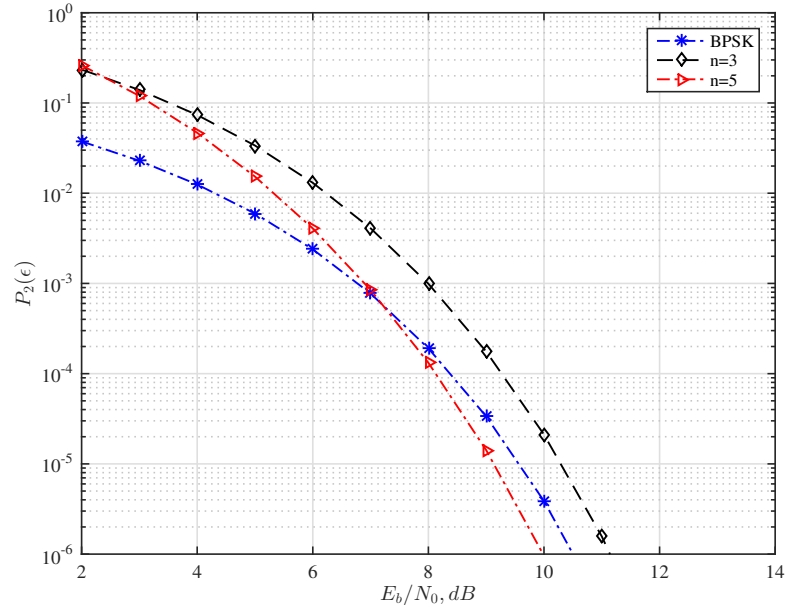
Figure 4.14: Error probability performance of non-coherent 2-CPFSK for $n = 3$ and 5) [43]

Table 4.13: Error probability of 2-CPCM and 2-CPFSK at SNR= 6, 8, and 10 dB

SNR (dB)	**2-CPCM** $(n = 3)$	**2-CPFSK** $(n = 3)$	**2-CPCM** $(n = 5)$	**2-CPFSK** $(n = 5)$	**BPSK**
6	$1.03{\times}10^{-2}$	$1.30{\times}10^{-2}$	$4.14{\times}10^{-3}$	$4.07{\times}10^{-3}$	$1.03{\times}10^{-2}$
8	$6.79{\times}10^{-4}$	$9.92{\times}10^{-4}$	$1.29{\times}10^{-4}$	$1.32{\times}10^{-4}$	$6.79{\times}10^{-4}$
10	$1.20{\times}10^{-5}$	$2.11{\times}10^{-5}$	$7.95{\times}10^{-7}$	$9.57{\times}10^{-7}$	$1.19{\times}10^{-5}$

4-CPCM System

For 4-CPCM non-coherent system upper bound symbol error rates are shown in Fig. 4.15 for $n = 3$ and $n = 5$. In the same figure, the performance of coherent QPSK is also shown. It is noted that the plots in this figure show symbol error rates vs. SNR per bit. In Fig. 4.16, upper bound symbol error rates for 4-CPFSK ($n = 3$ and $n = 5$)

non-coherent receiver are shown. From these figures, it is observed that 4-CPCM non-coherent system marginally outperforms 4-CPFSK when $n = 5$ is employed. Both these systems outperform coherent QPSK. There is an advantage of nearly 1 dB is going from $n = 3$ to $n = 5$ in the case of non-coherent 4-CPCM system.
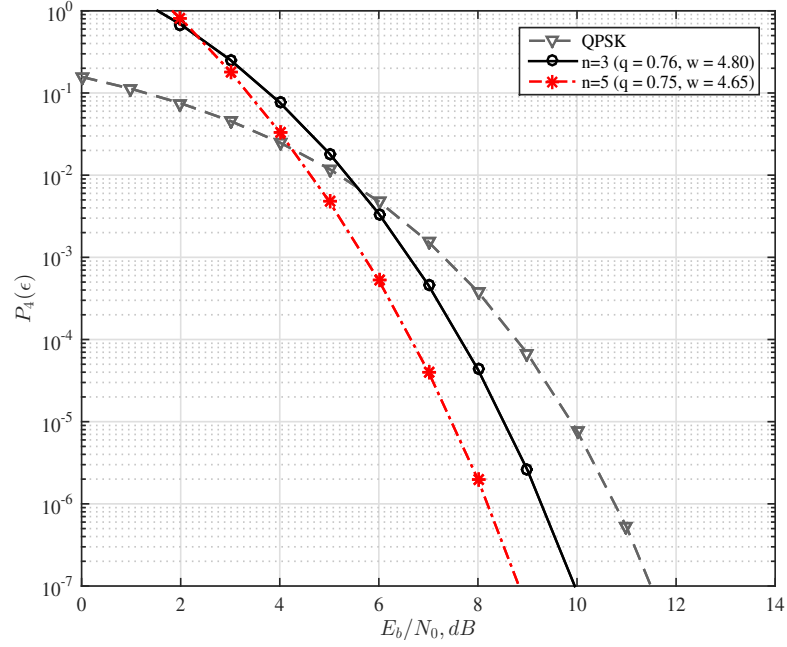
Figure 4.15: Error probability performance of non-coherent 4-CPCM systems for $n = 3$ and 5
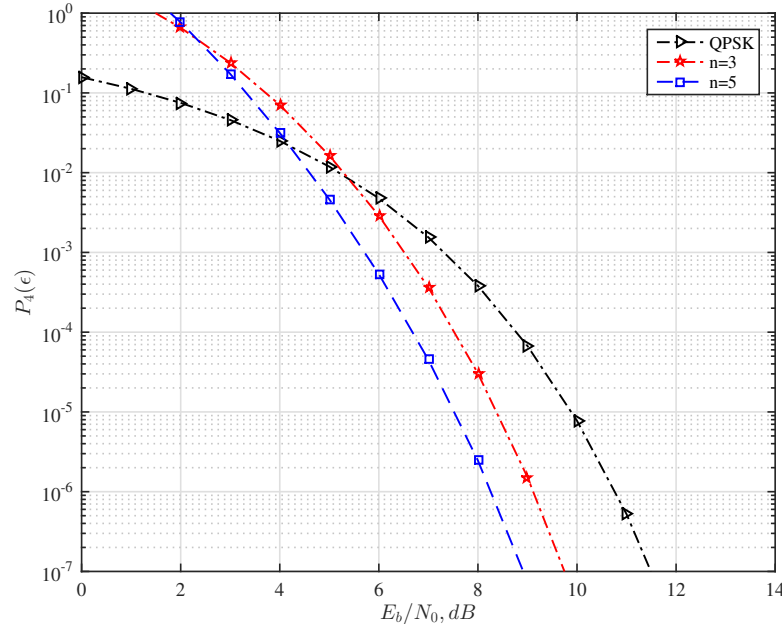
Figure 4.16: Error probability performance of non-coherent 4-CPFSK $h = 0.715$ for $n = 3$ and 5 [43]

Table 4.14: Error probabilities for non-coherent 4-CPCM and 4-CPFSK at $\frac{E_b}{N_0} = 6, 8$, and 10 dB

SNR (dB)	4-CPCM $(n = 3)$	4-CPFSK $(n = 3)$	4-CPCM $(n = 5)$	4-CPFSK $(n = 5)$	QPSK
6	3.39×10^{-3}	2.89×10^{-3}	5.24×10^{-4}	5.35×10^{-4}	4.78×10^{-3}
8	4.32×10^{-5}	3.04×10^{-5}	1.98×10^{-6}	2.46×10^{-6}	3.82×10^{-4}
10	8.56×10^{-8}	3.97×10^{-8}	6.77×10^{-10}	1.02×10^{-9}	7.74×10^{-6}

4.4 Conclusions

In this Chapter, coherent and non-coherent detection of M-CPCM signals in AWGN are addressed. Structures of optimum coherent and non-coherent receivers are de-

rived. Precise performance analysis of these receivers is too complex to carry out analytically and hence upper bounds on their performance are determined, at high SNR, using union bounding technique. Closed-form expressions for symbol error probability are derived that are simpler from the viewpoint of numerical computation. Symbol error rates, for both coherent and non-coherent receivers are functions of: i) Signal-to-noise ratio $\frac{E_b}{N_0}$, ii) observation length of the receiver n, iii) Number of levels used in the modulator M, iv) Signal modulation parameters (q, w), and v) the location of the decision symbol δ, within the observation length. Optimum coherent and non-coherent M-CPCM systems have been identified, through minimization of the symbol error rates, as a function of observation length of the receivers and the location of the decision symbol.

Coherent 2-, 4-, and 8- CPCM designs exist and can offer SNR advantage of 1.6, 3.6 and 7 dB relative to coherent BPSK, coherent QPSK, and coherent 8-PSK systems. In the case of coherent M-CPCM receivers, the location of decision symbol (δ) has no effect on the symbol error rate. Similarly, non-coherent 2-, 4-, 8-CPCM systems can be designed that are superior in performance relative to coherent BPSK, coherent QPSK, and octal PSK systems, respectively. In the case of M-CPCM non-coherent receiver, it is observed that the location of decision symbol δ plays an important role and the optimum decision symbol location is given by $\delta = \mathrm{int}(\frac{n}{2}) + 1$, for n odd and $\delta = (\frac{n}{2})$ or $\delta = (\frac{n}{2}) + 1$ for n even. However, for coherent M-CPCM receiver, the symbol error rate is independent of the location, $1 \leq \delta \leq n$, of the decision symbol.

Chapter 5

Multi-Mode Multi-Level Continuous Phase Chirp Modulation: Coherent Detection

5.1   Introduction

In Chapters 3 and 4, multi-level chirp modulation with memory is examined. In this modulation, the phase of the modulated signals is constrained to be continuous. It is this phase continuity that introduces memory into the signals. In M-CPCM, the set of signal modulation parameters (q, w) is held the same from symbol-to-symbol intervals. However, it is well known [3], [25] that impressive gains in performance can be obtained by using time-varying modulation parameters. The purpose of this Chapter is to use this concept of time-varying modulation parameters in multi-level chirp modulation and examine its performance in AWGN channel. The class of modulation considered is referred to as multi-mode M-CPCM.

5.2   Multi-mode M-CPCM Signals

Multi-mode M-CPCM signals can be written as:

$$S(t, d) = \sqrt{\tfrac{2E_s}{T_s}} \, \cos(w_c t + \phi(t, d) + \theta), \quad 0 \le t \le nT_s \tag{5.1}$$

where E_s, T_s, w_c, d, and θ have the same meaning as explained in Chapter 3. The set of modulation parameters used during any symbol interval is chosen cyclically from a set Ω_k of K sets of modulation parameter. That is, from the set:

$$\Omega_K = \{(q_1, w_1), (q_2, w_2), \ldots, (q_K, w_K)\} \tag{5.2}$$

For example, the set used during the first symbol interval is (q_1, w_1) and during the $2nd$, $3^{rd}, \ldots, K^{th}$ symbol intervals sets $(q_2, w_2), (q_3, w_3), \ldots, (q_K, w_K)$ are used. From $(K+1)$ to $(K+K)$, again sets $(q_1, w_1), \ldots, (q_K, w_K)$ are going to be employed. This process goes on and on. In other words, the set of modulation parameters used during the $(i + K)^{th}$ symbol interval is same as that used during the ith symbol interval. That is:

$$(q_{i+K}, w_{i+K}) = (q_i, w_i), \quad i = 1, 2, \ldots \tag{5.3}$$

In (5.1), the information carrying phase is given by:

$$\phi(t, d) = d_i g(t - (i - 1)T_s) + \pi \sum_{l=0}^{i-1} q_l \, d_l, \quad (i - 1)T_s \le t \le iT_s \tag{5.4}$$

where

$$g(t) = \begin{cases} 0, & t \le (i - 1)T_s, \quad t > iT_s \\ 2\pi \int_0^t f(\tau)d\tau, & (i - 1)T_s \le t \le iT_s \\ \pi q_i = \pi(h_i - w_i), & t = iT_s \end{cases} \tag{5.5}$$

and $f(\cdot)$ is the instantaneous frequency during the ith interval and is given by:

$$f(t) = \begin{cases} 0, & t \le (i - 1)T_s, \quad t > iT_s \\ \left(\frac{h_i}{2T_s}\right) - \left(\frac{w_i}{T_s^2}\right)t, & (i - 1)T_s \le t \le iT_s \end{cases} \tag{5.6}$$

using (5.6) in (5.5), the phase function $g(t)$ can be written as:

$$
g(t) = \begin{cases}
0, & t \leq (i-1)T_s, \quad t > iT_s \\[2mm]
\pi \left\{ h_i \left(\frac{t}{T_s} \right) - w_i \left(\frac{t}{T_s} \right)^2 \right\}, & (i-1)T_s \leq t \leq iT_s \\[2mm]
\pi q_i = \pi(h_i - w_i), & t = iT_s
\end{cases} \tag{5.7}
$$

The number of sets of modulation parameters K defines how many modes exist. For example, if $K = 2$, the modulation is referred to as 2-mode M-CPCM or dual-mode M-CPCM, if $K = 3$ we get 3-mode (or triple-mode) M-CPCM, and so on. In Fig. 5.1 are shown instantaneous phase and frequency for a dual-mode 2-CPCM system.
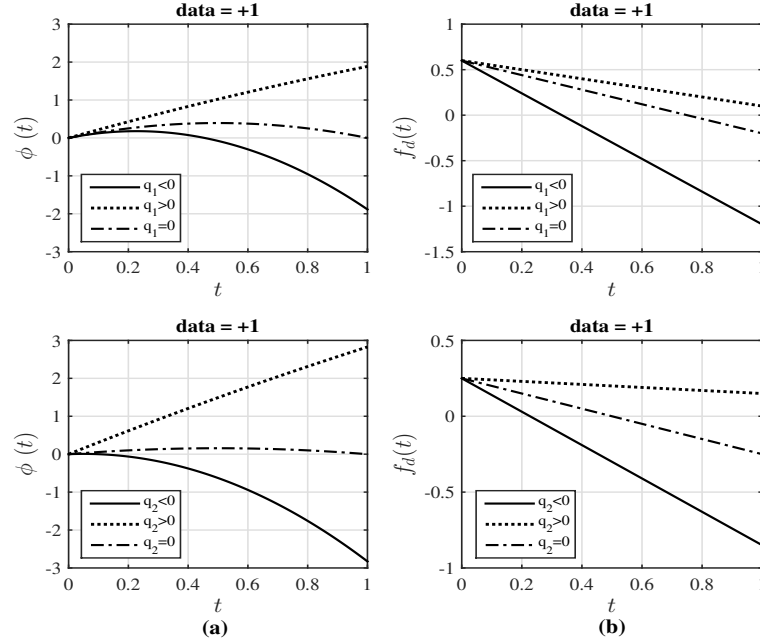
Figure 5.1: Phase (a) and instantaneous frequency (b) for a dual-mode 2-CPCM system

In Fig. 5.2 is shown the evolution of phase as a function of time for a dual-mode 2-CPCM system (with the starting phase $\theta = 0$). One of the important features of dual-mode 2-CPCM is observed in Fig. 5.2. The first merge in the phase tree occurs for dual-mode 2-CPCM after 3-symbol intervals, unlike after 2 symbols for 2-CPCM (Fig. 3.5). Mono-mode M-CPCM or simply M-CPCM signals in Chapter 4 (Section

4.2) were modeled as $S(t, d_\delta, A, \theta)$, $0 \le t \le nT_s$. However, in the case of multi-mode M-CPCM slight modification is required to reflect the sequence of sets of modulation parameters used. Thus, the transmitted signal in the case of multi-mode M-CPCM is modeled as $S^p(t, d_\delta, A, \theta)$, where p denotes the specific sequence of signal parameter sets $((q_1, w_1), (q_2, w_2), \ldots, (q_n, w_n))$ used over n symbol intervals of the signal. For $\Omega_K = \{(q_1, w_1), \ldots, (q_K, w_K)\}$, it is fairly easy to see that $p = K$, regardless of n.
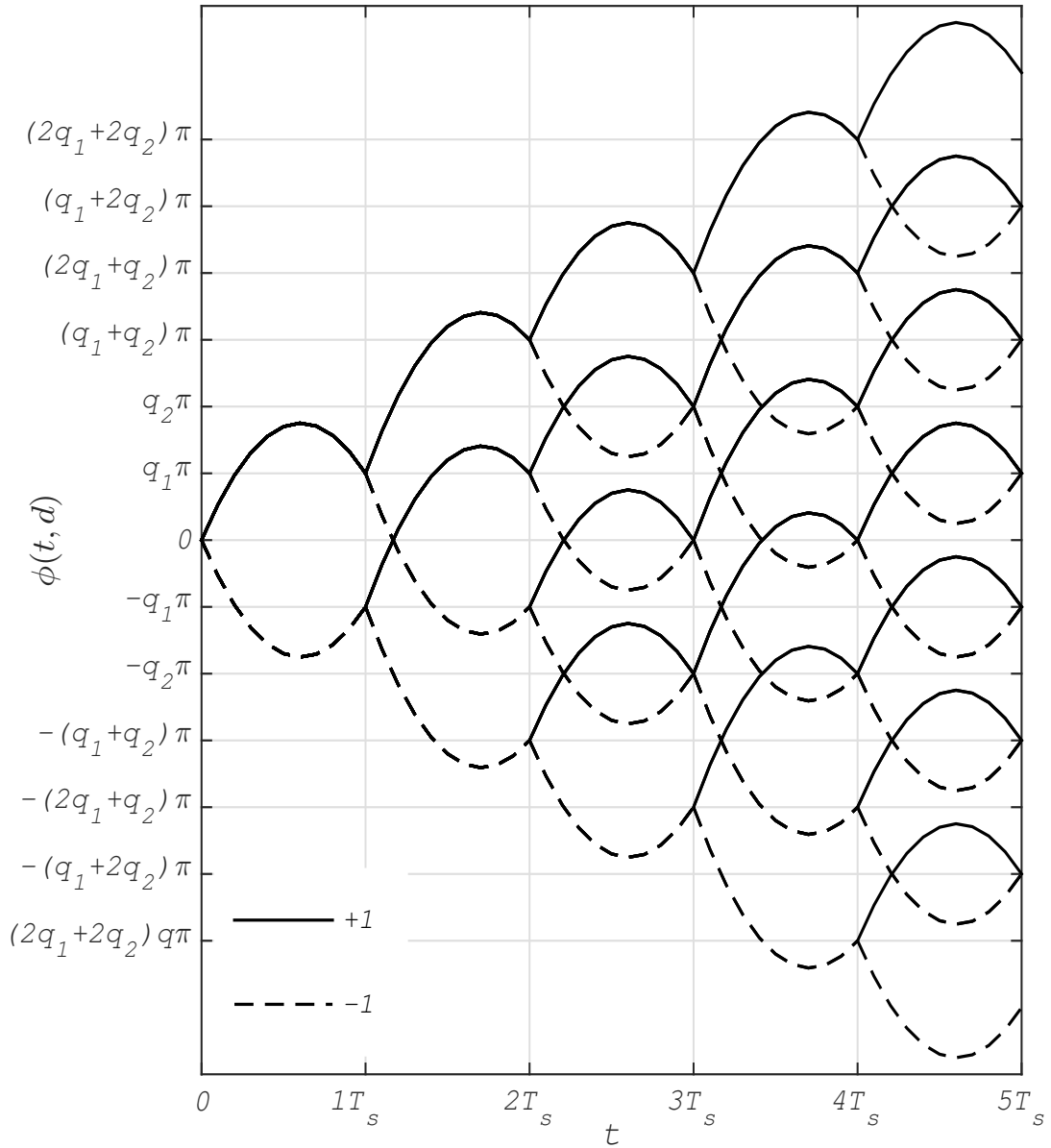
Figure 5.2: Phase tree for dual-mode 2-CPCM system

For example, for $\Omega_2 = \{(q_1, w_1), (q_2, w_2)\}$ and $n = 4$ (say), the unique permutations possible are:

$$(q_1, w_1), (q_2, w_2), (q_1, w_1), (q_2, w_2)$$

$$(q_2, w_2), (q_1, w_1), (q_2, w_2), (q_1, w_1)$$

The delay merges in the phase tree results in better distance properties and hence better SNR gain in the case of dual-mode 2-CPCM when compared to mono-mode 2-CPCM. In this thesis, only dual-mode M-CPCM systems are considered.

5.3 Optimum Coherent Receiver and Performance Analysis

The received waveform over n-symbol intervals can be written as:

$$r(t) = S^p(t, d_\delta, A) + n(t), \quad 0 \le t \le nT_s \tag{5.8}$$

where $S^p(\cdot, \cdot, \cdot)$ denotes the transmitted multi-mode M-CPCM signal. $n(t)$ is the AWGN with two-sided power spectral density of $\frac{N_0}{2}$ watts/Hz, d_δ is the decision symbol taking values from the set $\{\pm 1, \pm 3, \ldots, \pm(M-1)\}$ and $A = (d_1, d_2, \ldots, d_{\delta-1}, d_{\delta+1}, d_n)$ denotes one of the $m = M^{n-1}$ possible sequences. Again, the detection strategy is to observe $r(t)$, $0 \le t \le nT_s$, and arrive at a optimum decision on d_δ. In (5.8), p denotes one of the K possible sequences of signal modulation parameters sets. Following the developments presented in Chapter 4 for coherent detection of M-CPCM, the M likelihood functions are given by:

$$l_\lambda^p = \sum_{k=1}^{m} \exp\left[\frac{2}{N_0} x_{\lambda k}^p\right] \tag{5.9}$$

where $\lambda = 1, 2, \ldots, M$ and

$$
x^p_{\lambda k} =
\begin{cases}
\displaystyle\int_0^{nT} r(t) S^p(t, d_\delta = \lambda, A_k) \, dt, & \lambda \text{ odd} \\[2em]
\displaystyle\int_0^{nT} r(t) S^p(t, d_\delta = -(\lambda - 1), A_k) \, dt, & \lambda \text{ even}
\end{cases}
\tag{5.10}
$$

The receiver structure dictated by (5.9) is shown in Fig. 5.3 computes
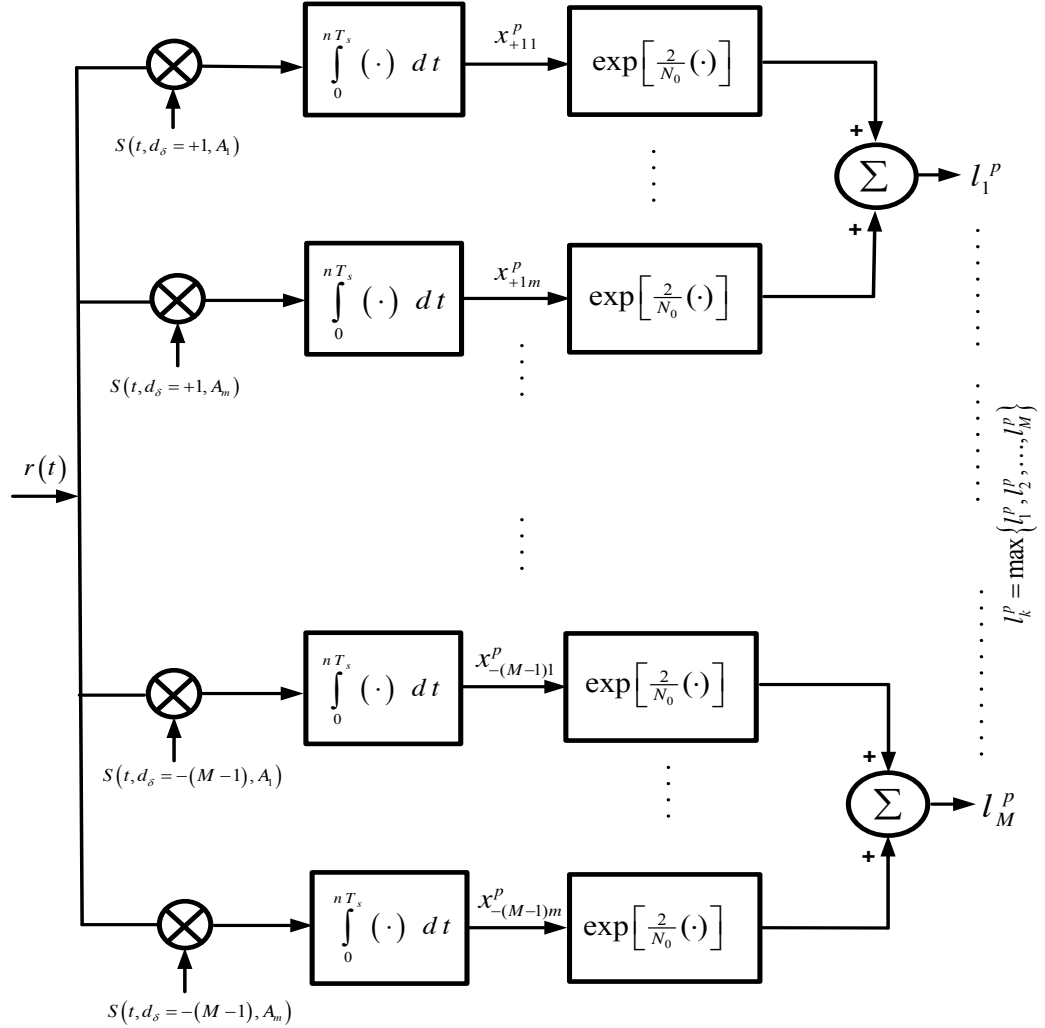
Figure 5.3: Optimum coherent multi-mode M-CPCM receiver

$l_\lambda^p, \lambda = 1, 2, \ldots M$ and chooses the largest of these to arrive at an estimate $\hat{d}_\delta$ of d_δ. That is, the receiver computes:

$$l_k^p = \max\{l_1^p, l_2^p, \ldots, l_M^p\} \tag{5.11}$$

and decides

$$\hat{d}_\delta = \begin{cases} k, & k \text{ odd} \\ -(k-1), & k \text{ even} \end{cases} \tag{5.12}$$

It is noted that the transmitter and the receiver must know p precisely. The performance of the optimum receiver can be bounded at high SNR using union bounding technique used in Chapter 4 and the upper and lower bounds for symbol error rate are given by:

$$P_M(\epsilon) < \frac{1}{KmM} \sum_{p=1}^{K} \sum_{u=1}^{M} \sum_{\substack{v=1 \\ v \neq u}}^{M} \sum_{j=1}^{m} \sum_{k=1}^{m} Q\left[\sqrt{\frac{nE_s}{N_0}(1 - \rho^p(vj, uk))}\right] \tag{5.13}$$

and

$$P_M(\epsilon) > \frac{1}{K} \frac{1}{M} \frac{1}{m} \sum_{p=1}^{K} \sum_{u=1}^{M} \sum_{\substack{v=1 \\ v \neq u}}^{M} \sum_{k=1}^{m} Q\left[\sqrt{\frac{nE_s}{N_0}(1 - \rho^{p*}(v, uk))}\right] \tag{5.14}$$

where

$$\rho^{p*}(v, uk) = \max\{\rho^p(vj, uk), j = 1, 2, \ldots, m\} \tag{5.15}$$

The normalized correlation $\rho^p(vj, uk)$ is given by:

$$\rho^p(vj, uk) = \frac{1}{nE_s} \int_0^{nT_s} S^p(t, d_\delta = v, A_j) S^p(t, d_\delta = u, A_k)\, d(t) \tag{5.16}$$

For multi-mode M-CPCM, a closed-form expression for (5.16) has been obtained and
is given by:

$$\rho^p(vj, uk) = \begin{cases} \cos(\pi \sum\limits_{r=1}^{l-1} \gamma_r q_r^p), & \gamma_l = 0 \\[4mm] \dfrac{1}{\sqrt{2|\gamma_l|w_k^p}}[\cos(\Upsilon_l^p)\Phi_l^p + \sin(\Upsilon_l^p)\Theta_l^p], & \gamma_l \neq 0 \end{cases} \qquad (5.17)$$

where

$$\Upsilon_l^p = \frac{1}{4w_l^p}\pi|\gamma_l|(w_l^p - q_l^p)^2 + \text{sgn}(a_l^j - a_l^k)\pi \sum_{r=1}^{l-1} \gamma_r q_r^p$$

$$\Phi_l^p = C(\chi) + C(\beta)$$

$$\Theta_k^p = S(\chi) + S(\beta)$$

and

$$\chi = \sqrt{\frac{|\gamma_l|}{2w_l^p}}(w_l^p - q_l^p)$$

$$\beta = \sqrt{\frac{|\gamma_l|}{2w_l^p}}(w_l^p + q_l^p)$$

The parameters w_l^p and q_l^p belongs to the lth set of the pth of K possible sequences
of sets $\{(q_1, w_1), (q_2, w_2), \ldots, (q_n, w_n)\}$.

5.4   Numerical Results and Discussion

The expressions given in (5.13) and (5.14) can be used to compute upper and lower
bounds on symbol error probability at high SNR. It is noted that these two bounds
become the same for SNRs $\geq$ 6 dB, thereby implying the bounds are tight and hence

we work with high SNR upper bound. The symbol error rate performance of the optimum coherent receiver is a function of i) $\frac{E_s}{N_0}$, ii) M, iii) δ, iv) n, and v) Ω_k, the set of K sets of signal modulation parameters. In order to find the optimum $\Omega = \{(q_1, w_1), \ldots, (q_K, w_K)\}$. The upper bound expression given in (5.13) can be minimized as a function of M, Ω_k, and n at high-SNR. This exercise has been carried out at $\frac{E_b}{N_0} = 6, 8,$ and 10 dB for dual-mode ($K = 2$) 2-, 4-, and 8-CPCM systems. The minimization has been carried out in the signal parameter range given by $0 < w \leq 5$ and $0 < q_1, q_2 \leq 2$ and the results are given in Table 5.1 to 5.3 for $M = 2, 4,$ and 8-CPCM, respectively.

Table 5.1: Optimum dual-mode 2-CPCM modulation parameter sets

SNR (dB)	$(q_1, q_2; w_1)$			
	$n=2$	$n=3$	$n=4$	$n=5$
6	(0.28, 0.28; 1.85)	(0.26, 0.49; 1.37)	(0.27, 0.49; 1.62)	(0.30, 0.49; 1.63)
8	(0.27, 0.27; 1.88)	(0.26, 0.49; 1.36)	(0.27, 0.49; 1.68)	(0.30, 0.50; 1.68)
10	(0.26, 0.26; 1.93)	(0.26, 0.49; 1.35)	(0.28, 0.50; 1.66)	(0.31, 0.50; 1.58)

$(q_1, q_2; w_1)$ is used to denote $\Omega_2 = \{(q_1, w_1), (q_2, w_1)\}$

Table 5.2: Optimum dual-mode 4-CPCM modulation parameter sets

SNR (dB)	$(q_1, q_2; w_1)$		
	$n=2$	$n=3$	$n=4$
6	(0.24, 0.25; 2.73)	(0.41, 0.40; 2.46)	(0.40, 0.39; 2.49)
8	(0.25, 0.24; 2.73)	(0.39, 0.40; 2.45)	(0.41, 0.39; 2.51)
10	(0.25, 0.25; 2.72)	(0.40, 0.40; 2.46)	(0.38, 0.40; 2.49)

$(q_1, q_2; w_1)$ is used to denote $\Omega_2 = \{(q_1, w_1), (q_2, w_1)\}$

To reduce number of computation in the evaluation of upper bound, a simplified expression for the probability of error similar to the expression used in Chapter 4 has been used. Fig. 5.4 shows the error probability performance of dual-mode 2-CPCM system for observation intervals $n = 2, 3, 4$ and 5. Fig. 5.5 shows the performance

Table 5.3: Optimum dual-mode 8-CPCM modulation parameter sets

SNR (dB)	$(q_1, q_2; w_1)$	
	$n=2$	$n=3$
6	(1.11, 1.12; 4.13)	(0.87, 0.89; 4.71)
8	(1.10, 1.11; 4.10)	(0.89, 0.89; 4.69)
10	(1.10, 1.12; 4.12)	(0.88, 0.89; 4.68)

$(q_1, q_2; w_1)$ is used to denote $\Omega_2 = \{(q_1, w_1), (q_2, w_1)\}$

of mono-mode 2-CPCM along with dual mode 2-CPCM for $n = 4$ and 5. The optimum dual-mode 2-CPCM with 4 observation intervals outperforms the mono-mode 2-CPCM with 5 observation intervals by nearly 0.5 dB. Table 5.4 shows symbol error probabilities for both systems at $\frac{E_b}{N_0} = 6$, 8, and 10 dB.

Figure 5.4: Error probability performance of dual-mode 2-CPCM for $n = 2, 3, 4$ and 5 and BPSK

Figure 5.5: Error probability performance of dual-mode and mono-mode 2-CPCM for $n = 4$ and 5

Table 5.4: Error probabilities of dual-mode and mono-mode 2-CPCM systems at $\frac{E_b}{N_0} =$ 6, 8, 10 dB

SNR (dB)	Dual-mode 2-CPCM			Mono-mode 2-CPCM		
	$n = 3$	$n = 4$	$n = 4$	$n = 3$	$n = 4$	$n = 5$
6	5.14×10^{-4}	2.33×10^{-4}	1.50×10^{-4}	6.45×10^{-4}	4.24×10^{-4}	3.56×10^{-4}
8	1.11×10^{-5}	2.89×10^{-6}	1.37×10^{-6}	1.79×10^{-5}	1.09×10^{-5}	9.31×10^{-6}
10	3.24×10^{-8}	4.38×10^{-9}	1.30×10^{-9}	9.15×10^{-8}	5.53×10^{-8}	4.56×10^{-8}

In Fig. 5.6, performance of dual-mode 4-CPCM for $n = 2, 3$, and 4, along with the performance of coherent QPSK are shown. It is observed that dual-mode 4-CPCM outperforms coherent QPSK by almost 4, 3.5, and 2 dB for observation intervals $n = 2, 3$, and 4, respectively.
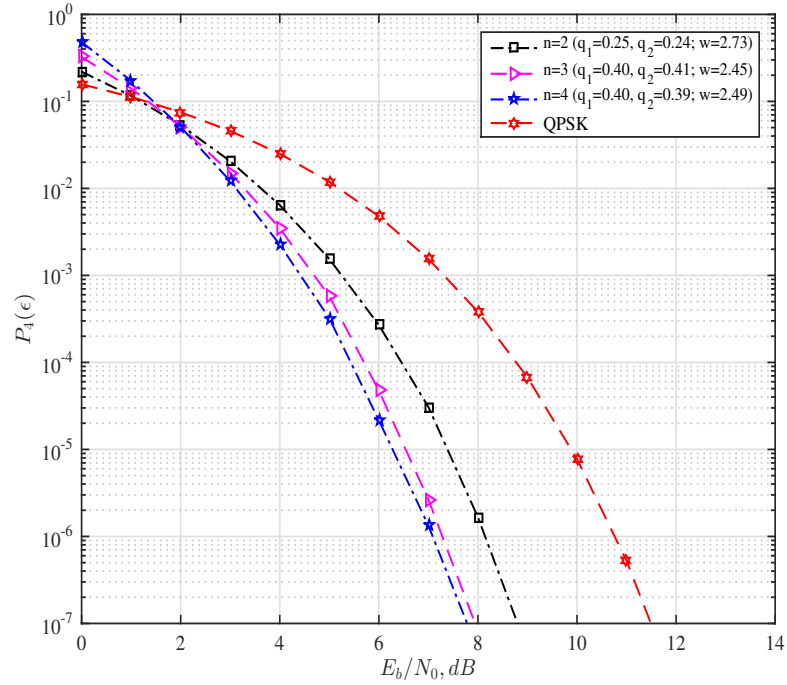
Figure 5.6: Error probability performance of dual-mode 4-CPCM for $n = 2, 3$, and 4

To compare dual-mode 4-CPCM with corresponding mono-mode system, in Fig. 5.7 performances of these systems for $n = 3$, and 4 are shown. The performance of dual-mode system with $n = 3$ is almost identical to the performance of mono-mode system with $n = 4$. This improvement in the performance comes at the cost of increased complexity of dual-mode system. Also, it is observed that dual-mode 4-CPCM outperforms corresponding mono-mode system by nearly 0.25 dB. Table 5.5 shows error probabilities of both mono- and dual-mode 4-CPCM systems at $\frac{E_b}{N_0} = 6$, 8, and 10 dB.

Figure 5.7: Error probability performance of dual-mode and mono-mode 4-CPCM for $n = 3$ and 4

Table 5.5: Error probabilities of dual-mode and mono-mode 4-CPCM at $\frac{E_b}{N_0} = 6$, 8, 10 dB

SNR (dB)	Dual-mode 4-CPCM			Mono-mode 4-CPCM		
	$n = 2$	$n = 3$	$n = 4$	$n = 2$	$n = 3$	$n = 4$
6	2.69×10^{-4}	4.74×10^{-5}	2.04×10^{-5}	2.73×10^{-4}	6.78×10^{-5}	3.27×10^{-5}
8	1.66×10^{-6}	8.16×10^{-8}	4.77×10^{-8}	2.43×10^{-6}	2.09×10^{-7}	1.02×10^{-7}
10	6.26×10^{-10}	3.49×10^{-12}	1.73×10^{-12}	2.24×10^{-9}	4.28×10^{-11}	1.99×10^{-11}

In Fig. 5.8, performance of dual-mode 8-CPCM for $n = 2$ and 3 is shown. In the same figure performance of coherent 8-PSK is also shown. Fig. 5.9 shows performances of both mono-mode and dual-mode 8-CPCM. It is observed that dual-mode system outperform mono-mode by nearly 0.2 dB for $n = 2$ and 3. Table 5.6 summarizes the performance of both mono- and dual-mode 8-CPCM systems.
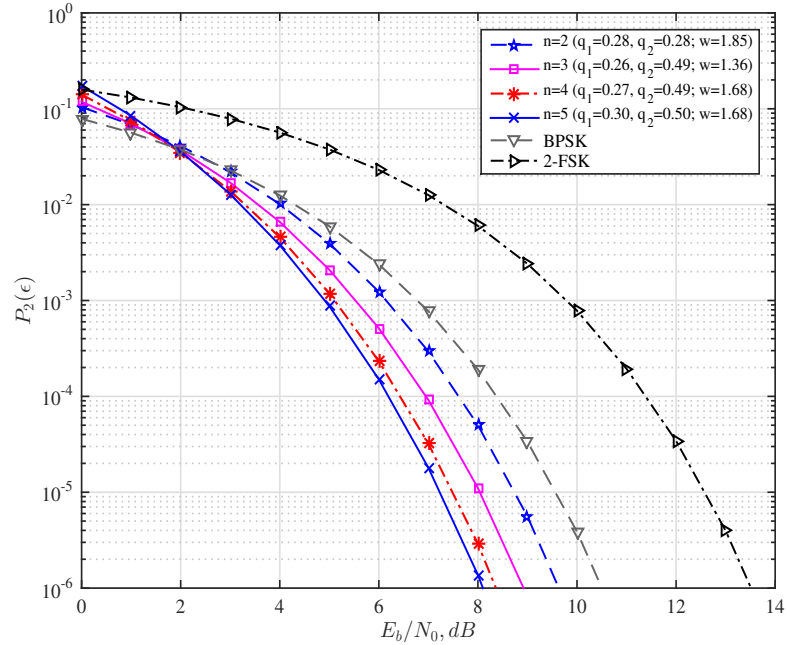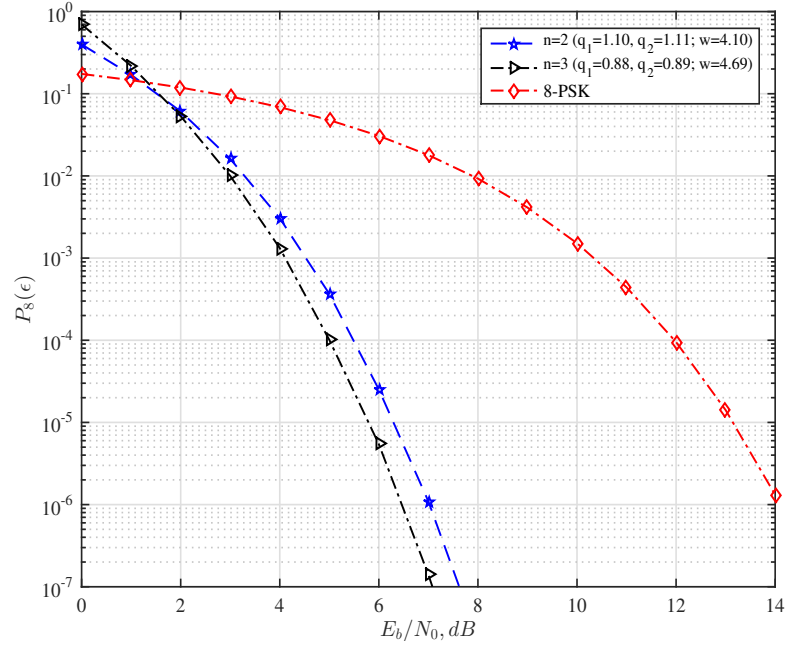
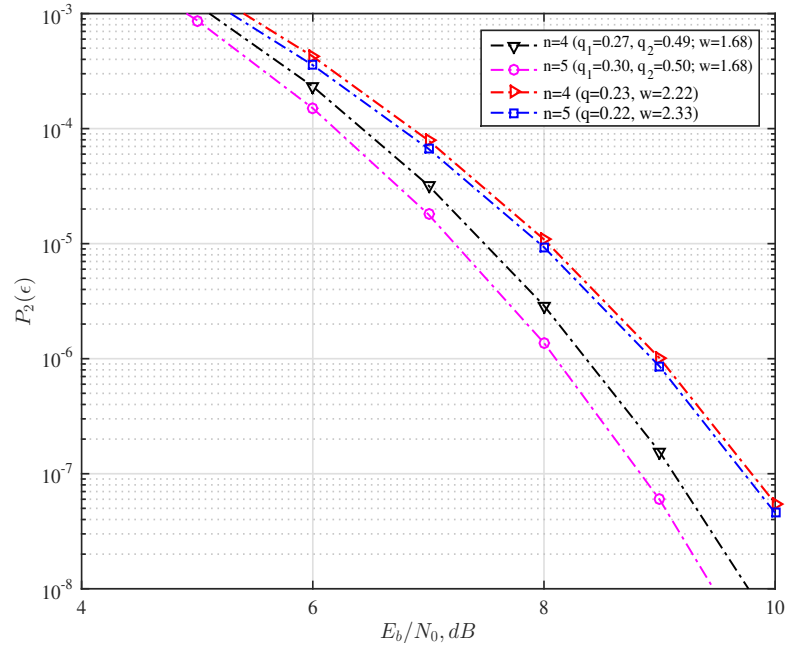Figure 5.8: Error probability performance of dual-mode 8-CPCM for $n = 2$ and 3
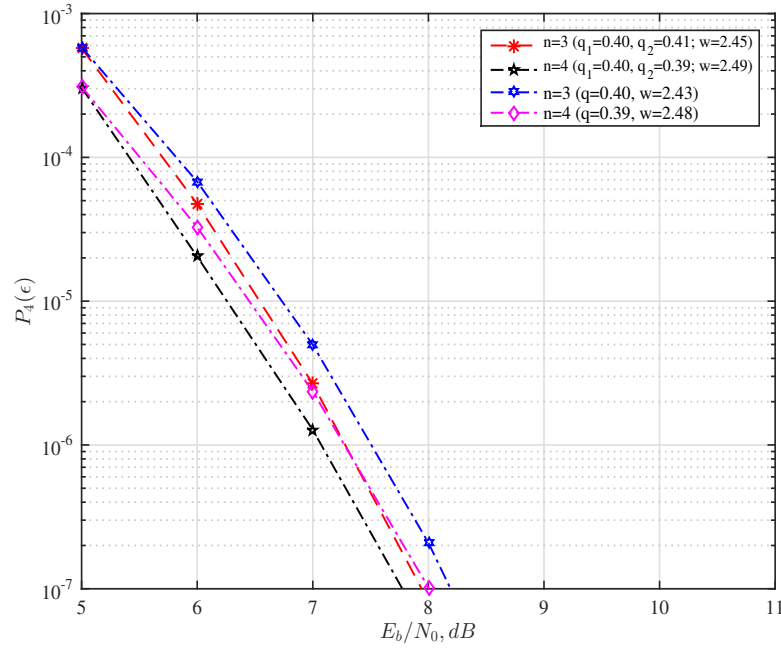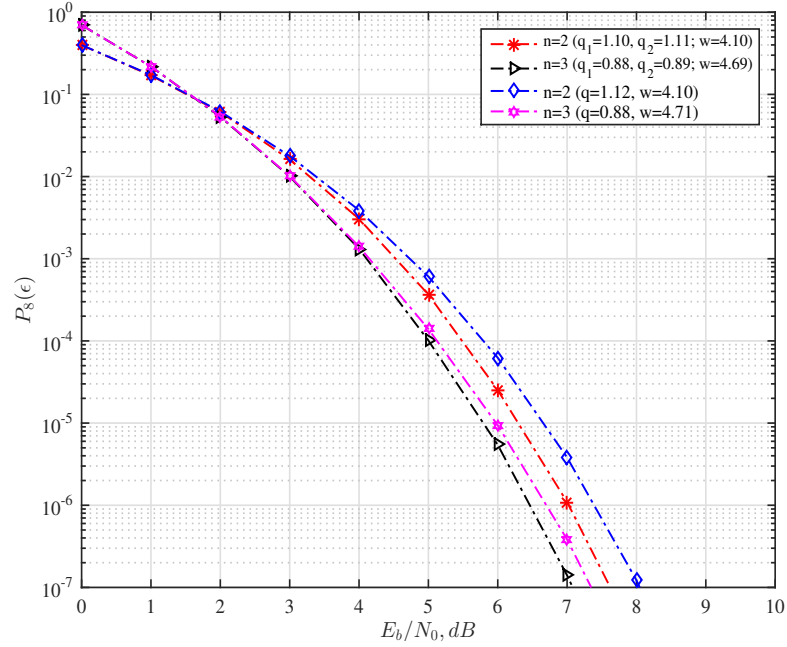

Figure 5.9: Error probability performance of dual-mode and mono-mode 8-CPCM for $(n = 2$ and 3$)$

Table 5.6: Error probabilities of dual-mode and mono-mode 8-CPCM at $\frac{E_b}{N_0}$ = 6, 8, 10 dB

SNR (dB)	Dual-mode 8-CPCM		Mono-mode 8-CPCM	
	$n = 2$	$n = 3$	$n = 2$	$n = 3$
6	2.52×10^{-5}	5.43×10^{-6}	6.23×10^{-5}	9.39×10^{-6}
8	2.35×10^{-8}	2.21×10^{-9}	1.22×10^{-7}	8.05×10^{-9}
10	4.69×10^{-13}	1.66×10^{-14}	9.04×10^{-12}	1.95×10^{-13}

5.5   Conclusions

In this Chapter, the concept of time varying modulation parameters has been applied to multi-level chirp modulation. The performance of these signals in AWGN is examined. Structure of the optimum coherent multi-mode M-CPCM receiver is derived and its performance analysis is presented. Closed-form expression for symbol error probability is derived for multi-mode M-CPCM. Optimum dual-mode M-CPCM systems have been identified, through minimization of symbol error rate, as a function of observation length of the receiver, number of levels of data, and the received signal-to-noise ratio $\frac{E_b}{N_0}$. It has been found that dual-mode 2-, 4-, and 8-CPCM outperform corresponding mono-mode 2-, 4-, and 8-CPCM by nearly 0.5 dB, 0.25 dB and 0.2 dB, respectively. In the case of multi-mode M-CPCM coherent receiver, the location of decision symbol, δ, has no effect on its performance.

Chapter 6

Memoryless Multi-level Chirp Modulation over Fading Channels

6.1 Introduction

In Chapter 2, memoryless multi-level chirp modulated signals are proposed for data transmission and investigated over AWGN channel. Closed-form expression for symbol error rate of a digital communication system employing M-CPCM is derived and used to determine optimum chirp signaling techniques. However, the dominant consideration in the design of communication systems employing wireless technologies will be their ability to perform over channels perturbed by a lot of impairments, not the least of which is the multi-path fading and shadowing. Thus, the objective of this Chapter is to examine the performance of multi-level chirp modulation. In particular, closed-form expressions for symbol error rates are derived over: i) Rayleigh, ii) Nakagami-m, and iii) Generalized-K (K_G) fading and shadowing environments for communication systems employing multi-level chirp modulation. Illustrations are then provided using these expressions to assess the performance of M-CPCM over fading channels.

6.2 Fading Channel Models

Wireless channel introduces various impairments and effects including short-term fading and long-term fading (shadowing) which cause serious degradation of signal-to-noise ratio (SNR) leading to poor BER performance. Over here, the performance of

the optimum M-CPCM receiver over short-term and long-term fading (shadowing) is evaluated. The received M-CPCM signal over the fading channel can be written as:

$$r(t) = h(t) * S(t, d_\delta, A, \theta) + n(t), \quad 0 \leq t \leq nT_s \tag{6.1}$$

where $h(t) = \alpha\delta(t)$ is the impulse response of the channel and $n(t)$ is AWGN. The instantaneous SNR per symbol and the average SNR are $\gamma = \alpha^2 E_s/N_0$ and $\bar{\gamma} = \Omega E_s/N_0$, where $\Omega = E\{\alpha^2\}$ and $E_s = E_b \log_2(M)$. The average symbol error probability of M-CPCM ($P_M(\epsilon)$) over fading channel is determined by averaging the conditional error probability over the Probability Density Function (PDF) of the fading model and is given by [44]:

$$P_{av} = \int\limits_0^\infty p_\gamma(\gamma) \ P_M(\epsilon|\gamma) \ d\gamma \tag{6.2}$$

where $p_\gamma(\gamma)$ is the density of γ and $P_M(\epsilon|\gamma)$ is the conditional symbol error probability of M-CPCM over AWGN channel.

6.2.1   Rayleigh Fading Channel

Rayleigh fading channel is used to model multi-path fading channel when there is no Line-of-Sight (LOS) path between the transmitter and the receiver antennas. It is commonly used in many different environments. The density that describes the Rayleigh fading channel is given by [44]:

$$p_\alpha(\alpha) = \frac{2\alpha}{\Omega} \ \exp\left(-\frac{\alpha^2}{\Omega}\right), \quad \alpha \geq 0 \tag{6.3}$$

6.2.2   Nakagami-m Fading Channel

Nakagami-m distribution is used to model a variety of fading environments. In particular, it is used to model a multi-path fading channel when there is a direct Line-of-Sight (LOS) path between the transmitter and receiver. Also, it is a general distribution used to model different fading environments by changing the parameter m of

the model. For example, when $m = 1$, Nakagami-m distribution reduces to Rayleigh distribution and as $m \to +\infty$, Nakagami-m distribution becomes identical to AWGN. The Nakagami-m density is given by [44]:

$$p_\alpha(\alpha) = \frac{2m^m \alpha^{2m-1}}{\Omega^m \Gamma(m)} \exp\left(-\frac{m\alpha^2}{\Omega}\right), \quad \alpha \geq 0 \tag{6.4}$$

where $0.5 \leq m < \infty$ is the Nakagami-m fading parameter.

6.2.3 Generalized-K Fading and Shadowing Channel

The Generalized-K is a composite model used to describe both fading and shadowing channel characteristics. This model represents a wireless channel subjected to short and long-term fading. The density of the Generalized-K model is given by:

$$p_\alpha(\alpha) = 2 \left(\frac{cm}{\Omega}\right)^{\frac{c+m}{2}} \frac{\alpha^{\frac{c+m-2}{2}}}{\Gamma(c)\Gamma(m)} K_{c-m}\left(2\sqrt{\frac{cm}{\Omega}}\alpha\right), \gamma \geqslant 0 \tag{6.5}$$

where $K_{c-m}(.)$ is the modified Bessel function of order $c-m$, and $\Gamma(.)$ is the Gamma function [45]. The coefficients c and m are the shadowing and fading parameters, respectively. As m and c increase, the fading and shadowing become less sever. For m and $c \to \infty$, the channel approaches that of AWGN.

To compute the average symbol error probability in (6.2), the integral must be evaluated for each fading model. In the next Section, closed-form expressions for the average symbol error probabilities for M-CPCM communication system are derived for the three fading environments described in this Section.

6.3 Average Symbol Error Rate Expressions for Memoryless M-CPCM

6.3.1 Rayleigh Fading Channel

When α in (6.1) is Rayleigh, the density given in (6.3) of γ is given by:

$$p_\gamma(\gamma) = \frac{1}{\bar{\gamma}} \exp\left(-\frac{\gamma}{\bar{\gamma}}\right), \quad \gamma \geqslant 0 \tag{6.6}$$

where $\gamma = \alpha^2 \frac{E_s}{N_0}$ and $\bar{\gamma} = \Omega \frac{E_s}{N_0}$ ($\Omega = E\{\alpha^2\}$). The symbol error probability expression for M-CPCM is given by (2.39) and is reproduced here for convenience:

$$P_M(\epsilon) < \frac{1}{M} \sum_{j=1}^{M} \sum_{\substack{i=1 \\ i \neq j}}^{M} Q\left[\sqrt{\frac{E_s}{N_0}(1 - \rho(i,j))}\right] \tag{6.7}$$

since received M-CPCM signal over fading channel is $r(t) = \alpha S(t, d_\delta, A, \theta) + n(t)$, the conditional symbol error probability is given by:

$$P_M(\epsilon|\gamma) < \frac{1}{M} \sum_{j=1}^{M} \sum_{\substack{i=1 \\ i \neq j}}^{M} Q\left[\sqrt{\frac{E_s}{N_0}(1 - \rho(i,j))}\right] \tag{6.8}$$

where $\gamma = \frac{\alpha^2 E_s}{N_0}$. For M-CPCM signal $\rho(i,j)$ is given in (2.16) and:

$$Q(x) \triangleq \frac{1}{\sqrt{2\pi}} \int_x^\infty e^{-\frac{t^2}{2}} dt$$

which also can be written as [44]:

$$Q(x) = \frac{1}{\pi} \int_0^{\frac{\pi}{2}} e^{\left(-\frac{x^2}{2sin^2(\theta)}\right)} d\theta \tag{6.9}$$

Using (6.6), and (6.8), in (6.2), the average symbol error rate can be expressed as:

$$P_{av} = \frac{1}{\pi \bar{\gamma} M} \sum_{j=1}^{M} \sum_{\substack{i=1 \\ i \neq j}}^{M} \int_{0}^{\frac{\pi}{2}} \int_{0}^{\infty} \exp\left(-\frac{(1 - \rho(i,j))\gamma}{2\sin^2(\theta)} - \frac{\gamma}{\bar{\gamma}}\right) d\gamma \, d\theta \quad (6.10)$$

performing the integrations in (6.10), the average symbol error rate can be written as:

$$P_{av} = \frac{1}{M} \sum_{j=1}^{2M} \sum_{\substack{i=1 \\ i \neq j}}^{M} \left[1 - \sqrt{\frac{1}{1 + \frac{1}{\frac{\Omega E_s}{2N_0}(1 - \rho(i,j))}}} \right] \quad (6.11)$$

6.3.2 Performance analysis over Nakagami-m Fading Channel

The exponential function in (6.4) can be written as [46]:

$$\exp\left(-m\frac{\gamma}{\bar{\gamma}}\right) = G_{0,1}^{1,0}\left(\frac{m\gamma}{\bar{\gamma}} \mid {0}\right) \quad (6.12)$$

where $G_{a,b}^{q,p}\left(x \mid {\cdots \atop \cdots}\right)$ is the Meijer G-function [45]. $Q(\cdot)$ term in (6.8) can be written as [47]:

$$Q(\sqrt{(1 - \rho(i,j))\gamma}) = \frac{1}{\sqrt{\pi}} G_{1,2}^{2,0}\left((1 - \rho(i,j))\gamma \mid {1 \atop 0, \ 1/2}\right) \quad (6.13)$$

using (6.12) and (6.13) in (6.2), the average symbol error rate can be written as:

$$P_{av} = \frac{1}{M\sqrt{\pi}} \sum_{j=1}^{M} \sum_{\substack{i=1 \\ i \neq j}}^{M} \int_{0}^{\infty} \gamma^{m-1} G_{1,2}^{2,0}\left((1 - \rho(i,j))\gamma \mid {1 \atop 0, \ 1/2}\right) G_{0,1}^{1,0}\left(\frac{m\gamma}{\bar{\gamma}} \mid {0}\right) d\gamma$$

$$(6.14)$$

By solving the integral in (6.14), a closed form expression for the symbol error rate over Nakagami-m channel can be written as:

$$P_{av} = \frac{1}{M\sqrt{\pi}\Gamma(m)} \sum_{j=1}^{M} \sum_{\substack{i=1 \\ i \neq j}}^{M} G_{2,2}^{2,1} \left(\frac{(1-\rho(i,j))}{m} \frac{\Omega E_s}{2N_0} \, \middle| \, \begin{matrix} 1,\ 1-m \\ 0,\ 1/2 \end{matrix} \right) \tag{6.15}$$

6.3.3 Generalized-K Fading and Shadowing Channel

The average symbol error rate P_{av} can be evaluated by using (6.8), (6.9), (6.2), (6.5) and expressing the modified Bessel function in (6.5) as [46]:

$$K_{c-m} \left(2\sqrt{\frac{cm}{\overline{\gamma}}\gamma} \right) = \frac{1}{2} G_{0,2}^{2,0} \left(\frac{cm}{\overline{\gamma}}\gamma \, \middle| \, \frac{(c-m)}{2}, \frac{-(c-m)}{2} \right) \tag{6.16}$$

Thus, the integral of (6.2) can be expressed in terms of Miejer G-function as:

$$I = \frac{1}{2\sqrt{\pi}} \int_0^\infty \gamma^{\frac{c+m}{2}-1} G_{1,2}^{2,0} \left((1-\rho(i,j))\gamma \, \middle| \, \begin{matrix} 1 \\ 0,\ 1/2 \end{matrix} \right) G_{0,2}^{2,0} \left(\frac{cm}{\overline{\gamma}}\gamma \, \middle| \, \frac{(c-m)}{2}, \frac{-(c-m)}{2} \right) d\gamma \tag{6.17}$$

solving (6.17), and the average symbol error probability (P_{av}) over K_G-channel is obtained in a closed form as:

$$P_{av} \leq \frac{1}{M\sqrt{\pi}\Gamma(c)\Gamma(m)} \sum_{j=1}^{M} \sum_{\substack{i=1 \\ i \neq j}}^{M} G_{3,2}^{2,2} \left(\frac{(1-\rho(i,j))}{m} \frac{\Omega E_s}{2N_0} \, \middle| \, \begin{matrix} 1,\ 1-c,\ 1-m \\ 0,\ 1/2 \end{matrix} \right) \tag{6.18}$$

6.4 Numerical Results and Discussion

In Fig. 6.1 average symbol error rates for 2-level chirp ($q = 0.36, w = 1.52$), BPSK, 2-FSK, and DPSK over Rayleigh fading channel is shown as a function of normalized SNR. Also, in the same figure performance of 2-level chirp over AWGN is shown. It is observed that the performance of 2-level chirp is nearly the same as that of BPSK and is better than 2-FSK and DPSK systems, over Rayleigh fading channel.

Figure 6.1: Average symbol error rate performance of optimum 2-level chirp system $(q = 0.36, w = 1.52)$ over Rayleigh fading channel
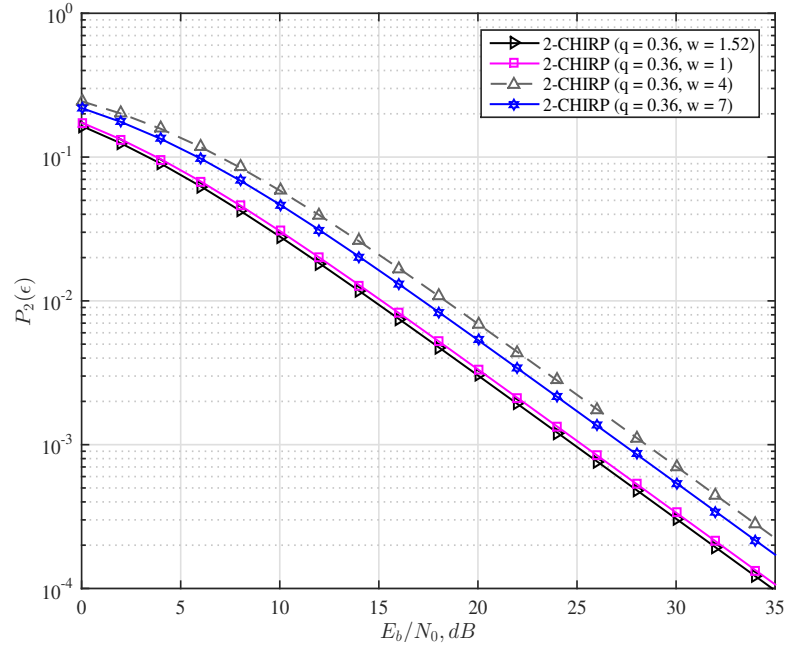
Figure 6.2: Average symbol error rate performance of 2-level chirp system over Rayleigh fading channel as a function of $w = \mathbf{1.52}$ (optimum), 1, 4, 7, for a fixed value of $q = 0.36$
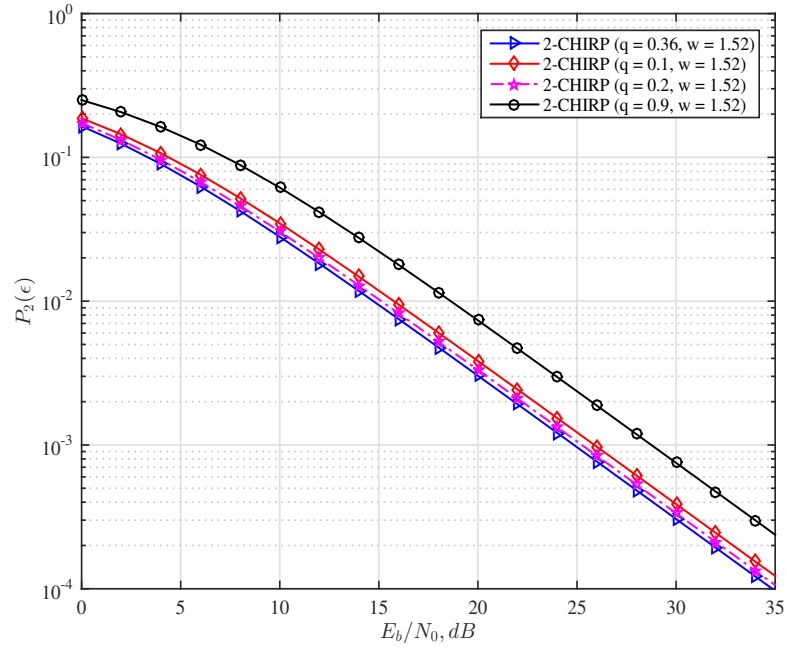
Figure 6.3: Average symbol error rate performance of 2-level chirp system over Rayleigh fading channel as a function of $q = \mathbf{0.36}$ (optimum), 0.1, 0.2, 0.9, for a fixed value of $w = 1.52$

Fig. 6.4 and Fig. 6.5 show symbol error probability performance of 4-level ($q = 0.40, w = 2.40$) and 8-level ($q = 0.95, w = 0.25$) chirp systems, respectively. These chirp system perform poorly relative to 4-PSK and 8-FSK, respectively over Rayleigh fading channel.
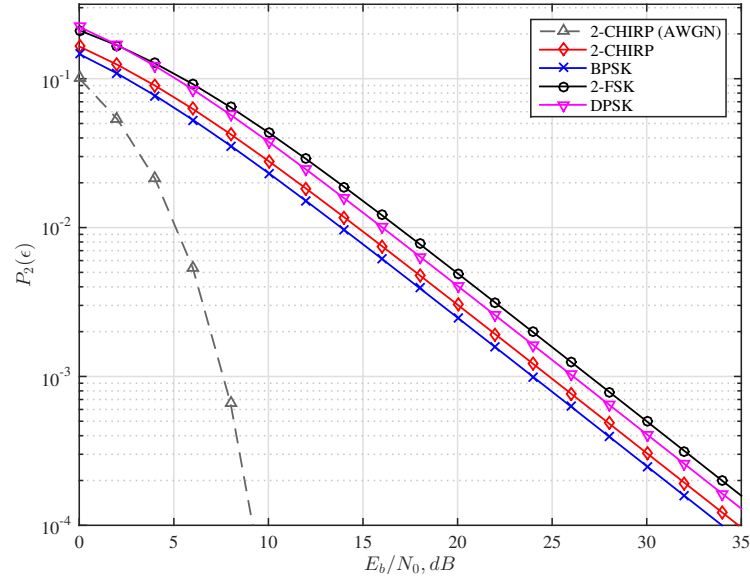
Figure 6.4: Average symbol error rate performance of 4-level chirp system $(q = 0.40, w = 2.40)$ over Rayleigh fading channel
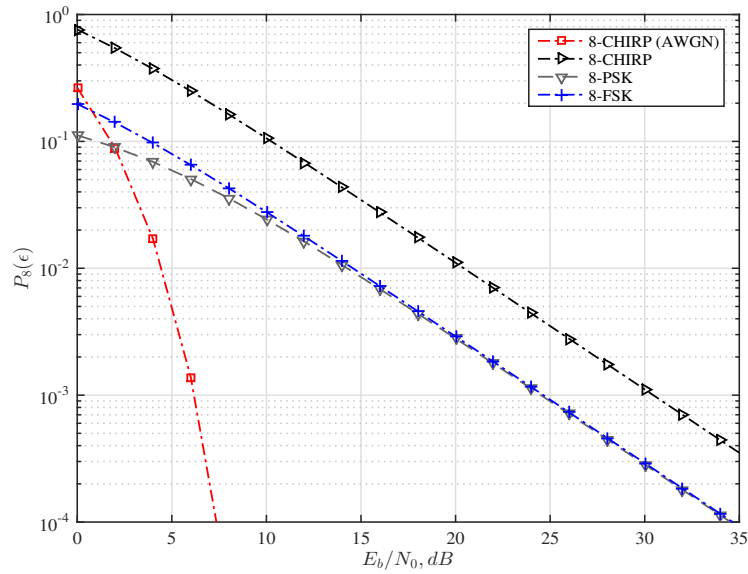
Figure 6.5: Average symbol error rate performance of 8-level chirp system $(q = 0.95, w = 0.25)$ over Rayleigh fading channel

Figs. 6.6 to 6.8 show average symbol error rates for 2, 4, and 8-level chirp systems over Nakagami-m fading channel. For the special case when $m = 1$, Nakagami-m reduces to the well known Rayleigh model. The performance approaches AWGN performance

Figure 6.6: Average symbol error rate performance of 2-level chirp system ($q = 0.36, w = 1.52$) over Nakagami-m fading channel as a function of m

Figure 6.7: Average symbol error rate performance of 4-level chirp system ($q = 0.40, w = 2.40$) over Nakagami-m fading channel as a function of m

as $m \to \infty$ because the line of sight (LOS) path dominates the received signal. Also, it is noted that as M increases the symbol error rate increases for some fading parameters m, at a fixed value of SNR. This observation can be utilized to design

an adaptive modulation technique by changing the modulation order to increase the bandwidth efficiency or to improve the error rate performance to meet a certain quality of service [48].

Figure 6.8: Average symbol error rate performance of 8-level chirp system $(q = 0.95, w = 0.25)$ over Nakagami-m fading channel as a function of m

Figs. 6.9 to 6.11 show average symbol error rates for $2, 4$ and 8-ary chirp system over K_G fading channel as a function of c and m. For comparison purposes, symbol error rate over Rayleigh fading and AWGN channel are also plotted. Because of the shadowing effect, the performance over K_G channel is poorer than the performance over AWGN and Rayleigh channels. Several techniques may be used to mitigate the effect of shadowing and fading on the performance. For example, at a symbol error rate of 10^{-4} for 2-level chirp system, performance deteriorates by 5, 14, and 27 dB for generalized-K with $c = 6$, $m = 8$, generalized-K with $c = 6, m = 2$, and Rayleigh channel model, respectively, with relative to the performance over AWGN channel. To compensate for this degradation in performance, channel coding and/or diversity techniques could be used. However, these techniques increase the channel bandwidth and system complexity.
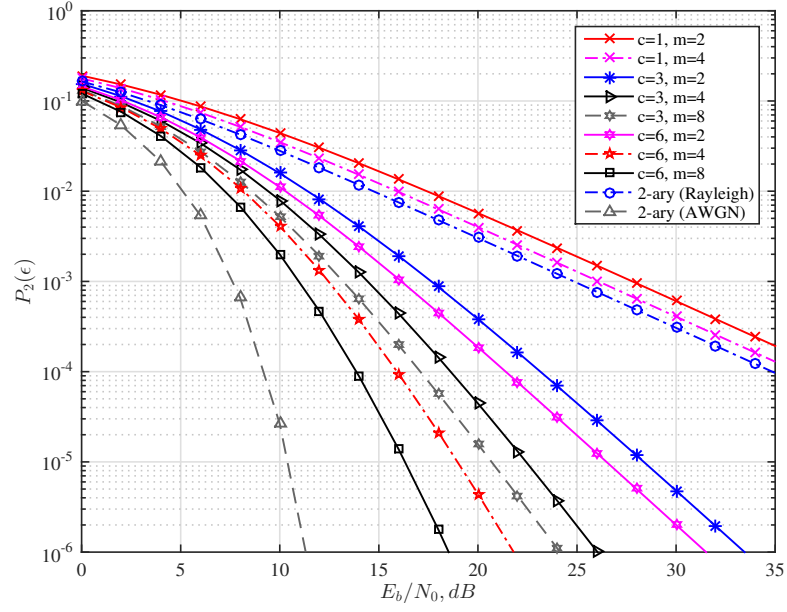
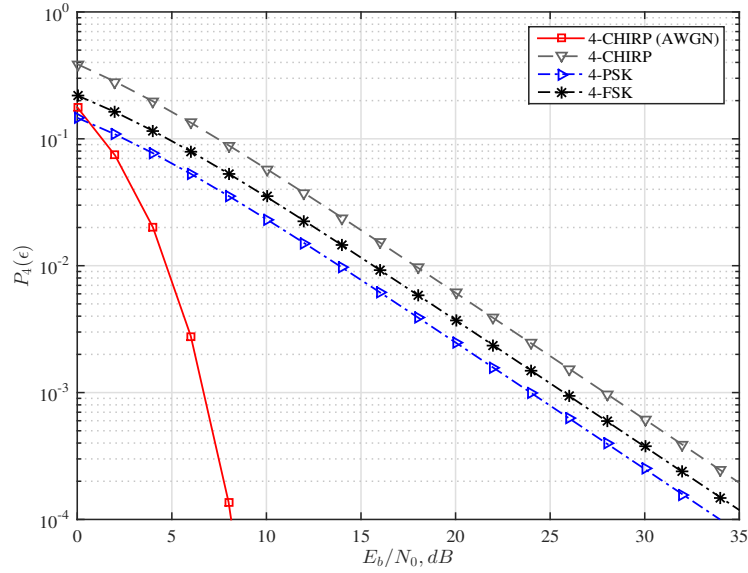Figure 6.9: Average symbol error rate performance of 2-level chirp system $(q = 0.36, w = 1.52)$ over K_G fading channel as a function of c and m
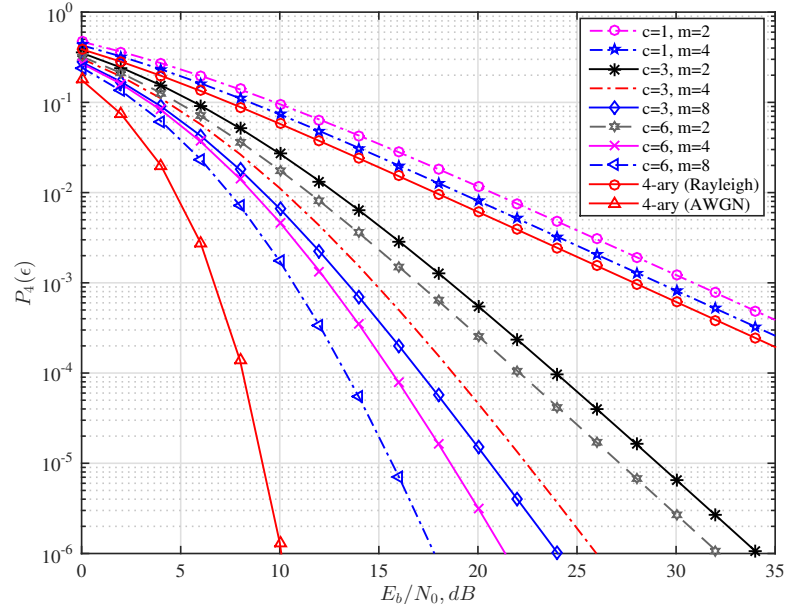
Figure 6.10: Average symbol error rate performance of 4-level chirp system $(q = 0.40, w = 2.40)$ over K_G fading channel as a function of c and m
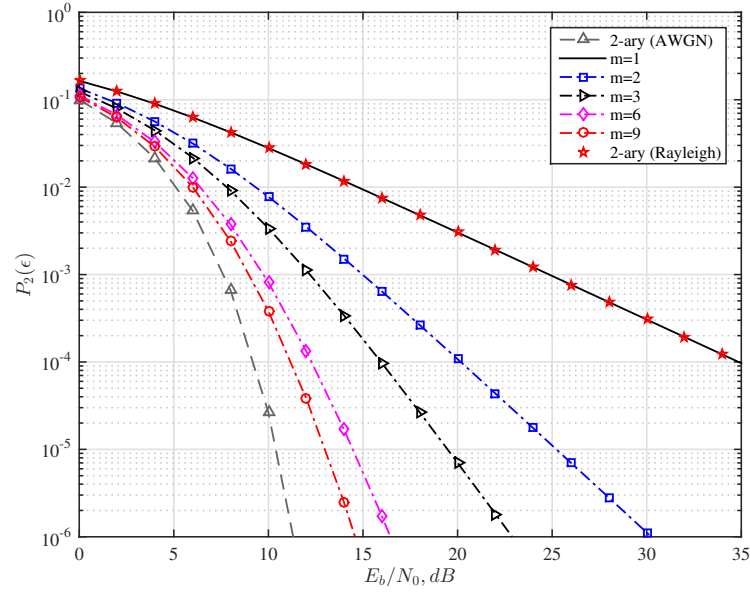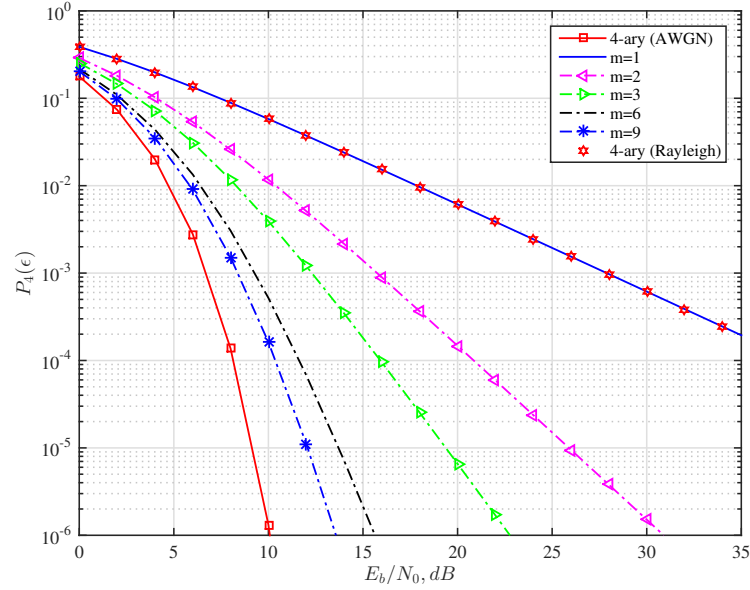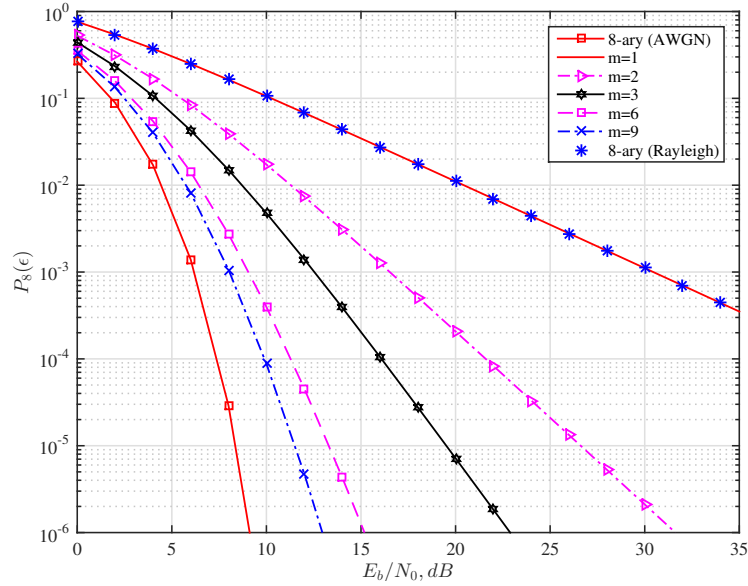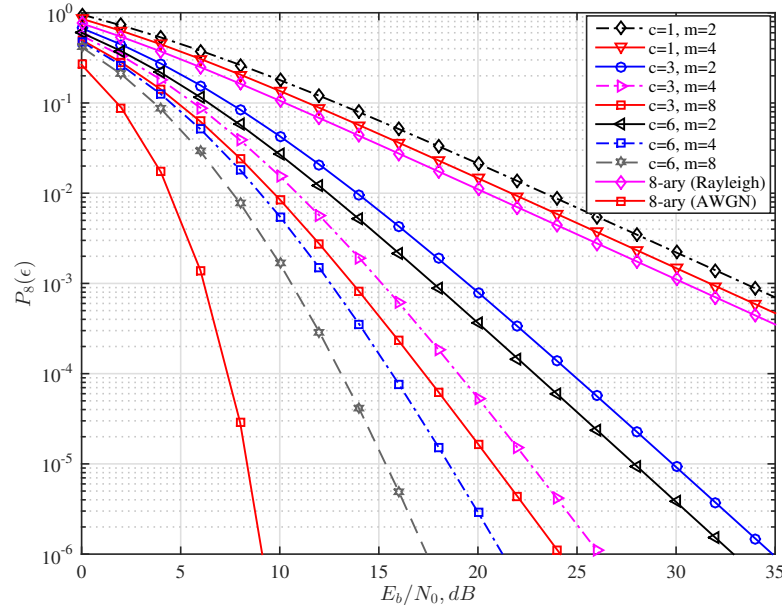
Figure 6.11: Average symbol error rate performance of 8-level chirp system $(q = 0.95, w = 0.25)$ over K_G fading channel as a function of c and m

6.5   Conclusions

In this Chapter, average symbol error rate performance of M-level chirp signals over Rayleigh, Nakagami-m and Generalized-K fading and shadowing channels are considered. In particular, the performance of the optimum coherent symbol-by-symbol detection receiver is examined for memoryless M-level chirp signals. New and easy-to-compute closed-form expressions for average symbol error probability for digital M-level chirp communication system impaired by additive white Gaussian noise and three fading models are derived. The selected fading models represent most practical wireless channels. The closed-form expressions derived are then used to illustrate the performance of 2-, 4-, and 8-level chirp systems as a function of average bit energy to noise ratio, and modulation and fading environment. It is found that the performance of binary chirp system is very close to the performance of BPSK modulation and better than the performance of 2-FSK and DPSK systems, over Rayleigh fading channel . Also, it is noted that the effect of shadowing on the performance is worse than fading and as M increases, the symbol error rate increases for some fading parameters m at

a fixed value of SNR. The technique used to estimate average symbol error rates over fading channels can be used to design efficient communication systems. Although the results presented in this Chapter is for memoryless M-level chirp modulation, it is fairly easy to extend the results to M-CPCM and multi-mode M-CPCM systems treated in Chapter 4 and 5.

Chapter 7

Spectral Characteristics of M-CPCM Signals

7.1 Introduction

Like the error rate performance, the bandwidth that a signal occupies is considered an important aspect of the total system performance. M-CPCM signals are constant-envelop signals that do not have a limited bandwidth. As a result, different measures, like power outside a certain frequency or the position of spectral nulls are useful to assess the spectral efficiency. In this Chapter, different ways to compute the distribution of energy as a function of frequency in a digital signal are explored and the direct method to compute the power spectral density for M-CPCM signals is presented.

7.2 Spectral Calculation Methods

Power spectral density (PSD) describes the energy distribution for a signal with respect to frequency. It is used to calculate the bandwidth that a signal occupies and hence its bandwidth efficiency. In the literature, there are many methods that are used to calculate the power spectrum. Some of these are simple and straightforward and some require complicated mathematical calculations. One approach is the auto-correlation method in which the Fourier transform of time-averaged autocorrelation is computed. This approach can only be applied to a system whose data produces wide-sense stationary output. Another approach is the so-called direct approach in which the Fourier transform of the signal is computed and then averaged. The limitations of this method come from the complicated equations and the two-dimensional

numerical integrations which are required for most schemes. Also, there are many other approaches such as the simulation approach and the Markov chain which can be used to measure the power spectra for any scheme. These approaches have not proved satisfactory as they do not produce closed-form expressions for the spectra or produce expression that are very difficult to be translated into computer formulas. Moreover, some approaches apply only to frequency pulses that integrate to zero and some require very long computation especially for high level M of modulation and for pulses with changeable modulation parameters. In the next Section, a general method to calculate the power spectrum is introduced. This method can handle arbitrary M-level data and works for arbitrary set of modulation parameters [27].

7.3 Spectra of M-CPCM

The power spectrum of a stochastic signal $x(t)$ is defined as [49]:

$$G(f) = \lim_{\lambda \to \infty} \left[\frac{2}{\lambda} G_\lambda(f) \right], \quad f > 0 \tag{7.1}$$

where

$$G_\lambda(f) = \mathbb{E} \left\{ | \int_0^\lambda x(t) \exp\left[-j2\pi ft\right] \ dt|^2 \right\} \tag{7.2}$$

and $\mathbb{E}$ denotes the expectation operator. Using this definition of power spectrum, many authors have derived closed-form expressions for the spectra of digital signals. Applying the direct method developed in [27] to M-CPCM signals, the power spectra of M-CPCM signals can be obtained. The method can handle arbitrary M-level data and works for arbitrary sets of modulation parameters q and w. The one-sided low pass spectrum is given by:

$$G(f) = \frac{2}{\hat{T}}[p(f) + 2Re\{F(f)F_b^*(f)\exp(-j2\pi f\hat{T}) + F(f)F_b^*(f)\Lambda(f)\}] \tag{7.3}$$

where

$$\Lambda(f) = \exp(-j4\pi f\hat{T}) \frac{C(\hat{T})}{1 - C(\hat{T})exp(-j2\pi f\hat{T})} \tag{7.4}$$

and

$$b_n(t) = \pi \int_0^t [d_{1n}f(\tau) + d_{2n}f(\tau - T_s) + \ldots$$

$$+d_{kn}f(\tau - kT_s)] \ d\tau, \quad n = 1, 2, \ldots M^k \tag{7.5}$$

$$F_n(f) = \int_0^{\hat{T}} \exp(-j2\pi ft + jb_n(t)) \ dt \tag{7.6}$$

$$C(T) = E\{\exp(iB_n)\} \tag{7.7}$$

$$B_n = b_n(\hat{T}) \tag{7.8}$$

$$F(f) = E\{F_n(f)\} = M^{-k}\sum_n F_n(f) \tag{7.9}$$

$$F_b^*(f) = E\{F_n^*(f)\exp(jB_n)\} = M^{-k}\sum_n F_n^*(f)\exp(jB_n) \tag{7.10}$$

$$P(f) = E\{|F_n(f)|^2\} = M^{-k}\sum_n |F_n(f)|^2 \tag{7.11}$$

E denotes the expectation operator with respect to index $n = 1, 2, \cdots M^k$, $\hat{T} = kT$ is the signal interval in seconds and the factor k represents the cycle length (equal 1 for the single-mode signalling). In (7.5), the function $f(\tau), f(\tau - T_s), \ldots, f(\tau - kT_s)$ denotes the frequency function of M-CPCM during each time interval which were defined in (Chapter 3, 3.6). The expressions (7.3) to (7.11) have been evaluated using

Matlab to find the spectra of M-CPCM. Eqn. 7.6 involves numerical integration and for which the adaptive Simpson quadrature method was used to solve the integration. As a cross check, the result of the well known power and bandwidth efficient modulation scheme MSK is considered first. In the chirp pulse, if the modulation parameter w is set to zero, and q is 0.5, the pulse shape becomes same as the pulse shape of MSK. The spectra of binary chirp ($q = 0.5$ and $w = 0$) is sketched by using the direct method and by using the closed-form expression of the squared magnitude of the Fourier transform given in [3]. In Fig. 7.1, power spectrum of 2-CPCM along with spectrum of MSK are shown. It is noted that both spectra are identical.

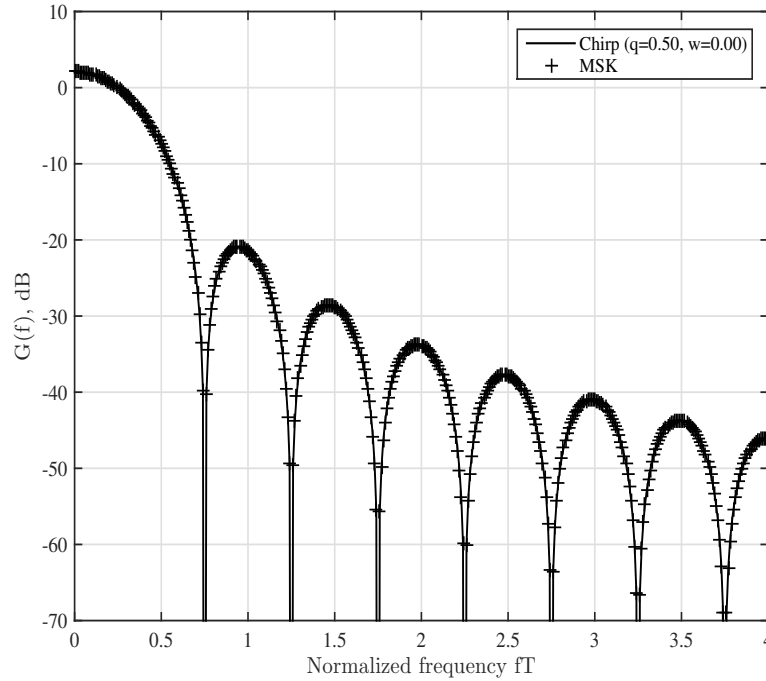Figure 7.1: Power spectra of 2-CPCM ($q = 0.5, w = 0.0$) and MSK

In the next Section, spectra for some M-CPCM systems are plotted for $M = 2, 4$ and 8 and compared with other conventional systems. Note that, the spectra for systems with values other than M=2 should be compared at the same bit rate. Thus, all given plots are normalized to the bit rate which is given by:

$$T_b = \frac{T_s}{\log_2(M)} \tag{7.12}$$

7.4 Spectra of Mono-mode M-CPCM Signals

Fig. 7.2 shows the power spectra for 2-CPCM systems using sets of modulation parameters that minimizes the probability of error. It is observed that 2-CPCM can offer different bandwidth occupancy by varying modulation parameter sets. Optimum 2-level CPCM with bit by bit detection can offer 99% bandwidth at normalized frequency of 0.56 Hz/bit/s, which is slightly better than the bandwidth offered by MSK (0.60 Hz/bits/s) but has a wider main lobe. However, this set of modulation parameter does not provide a gain in dB relative to MSK. Also, it is noted that other sets of modulation parameters can have different energy distributions and thus power/bandwidth trades-offs are possible with these signals. Fig. 7.3 shows the power spectra for modulation parameter sets that maximizes Euclidean distance over different observation lengths. It is noted that the difference between the maximum value of power in the main lobe and the maximum value in the first side lobe is nearly 20 dB for 2-CPCM with ($q = 0.30, w = 1.90$) and 22 dB with ($q = 0.20, w = 2.40$). This show significant signal energy distribution in side lobes. To examine the sensitivity of 2-CPCM system with respect to modulation parameters, Fig. 7.4 shows the power spectra for different modulation parameters sets with a fixed value of $w = 1.5$. It is noted that the spectra are very sensitive to small change in the modulation parameters q.
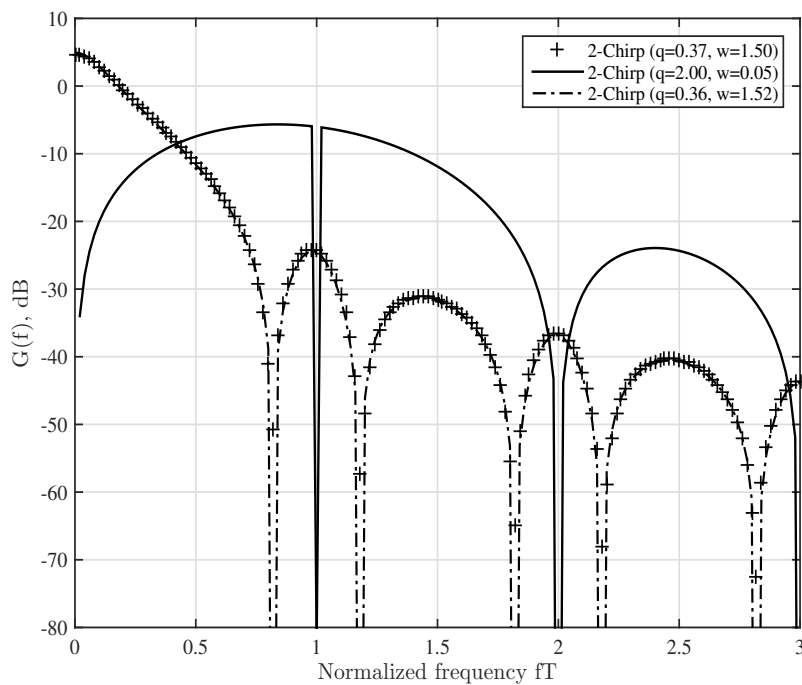
Figure 7.2: Power spectra of 2-CPCM system
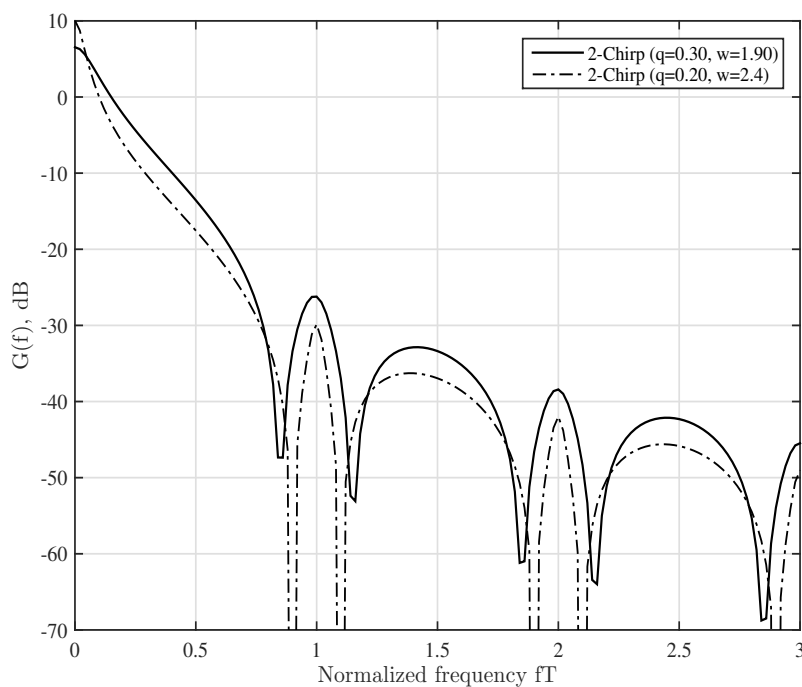
Figure 7.3: Power spectra of 2-CPCM system
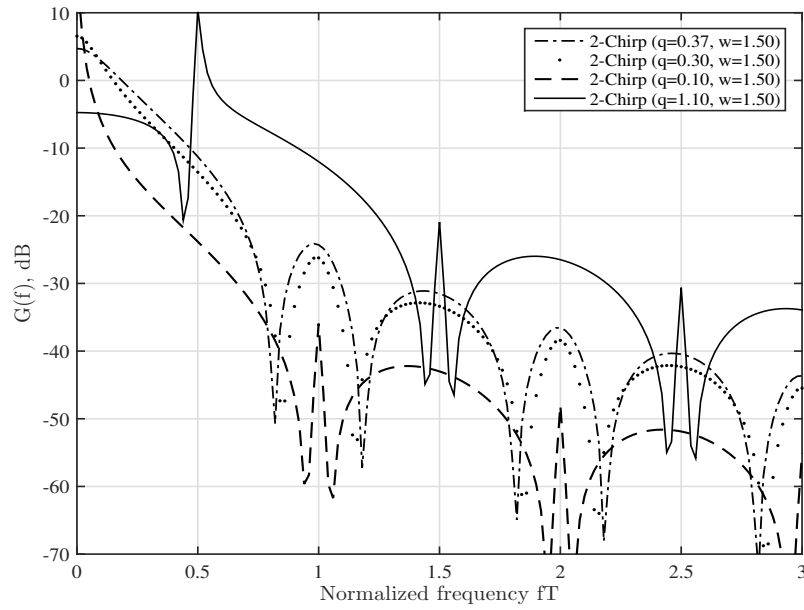
Figure 7.4: Power spectra of 2-CPCM system for a fixed value of w

To compare different power spectra as a function of modulation level M, the spectra of 4-CPCM and 8-CPCM systems are shown in Fig.7.5 to 7.7. It is found that as M increases, spectra become smoother and smoother; however, the signal energy distribution is almost the same throughout the spectrum.
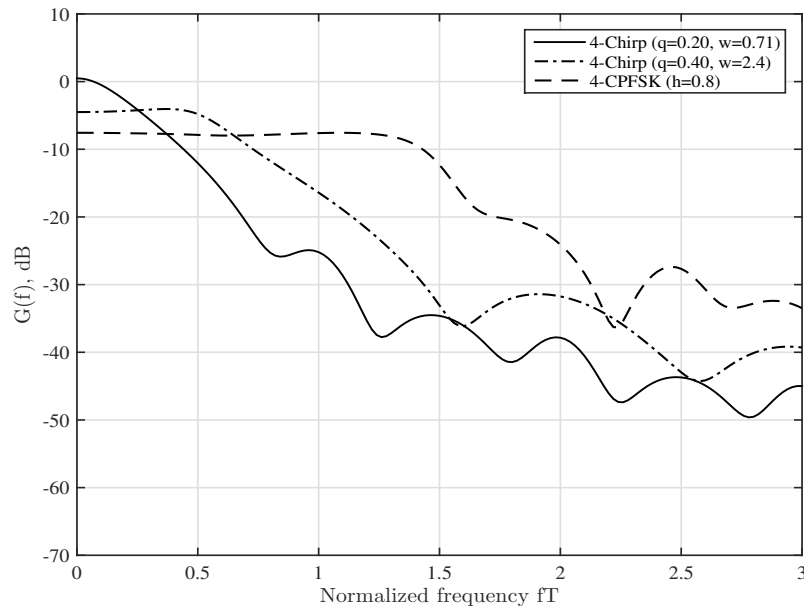
Figure 7.5: Power spectra of 4-CPCM system
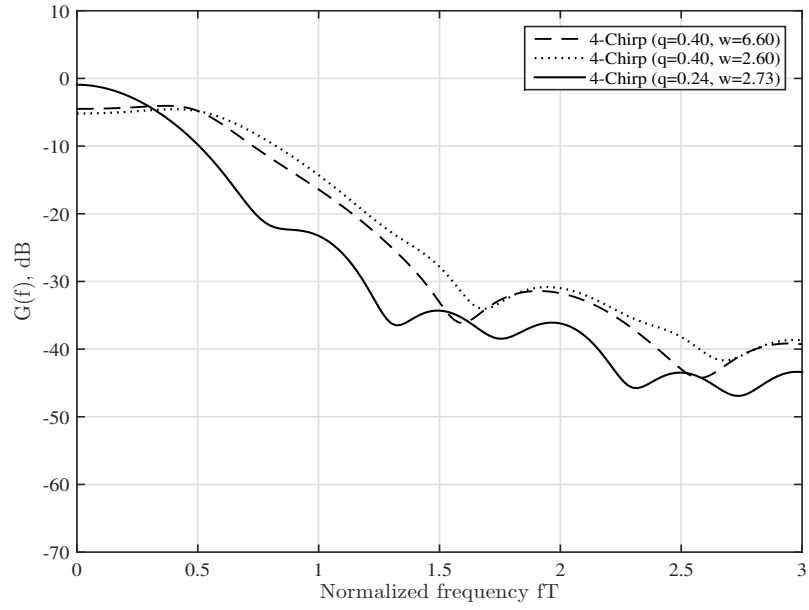
Figure 7.6: Power spectra of 4-CPCM system
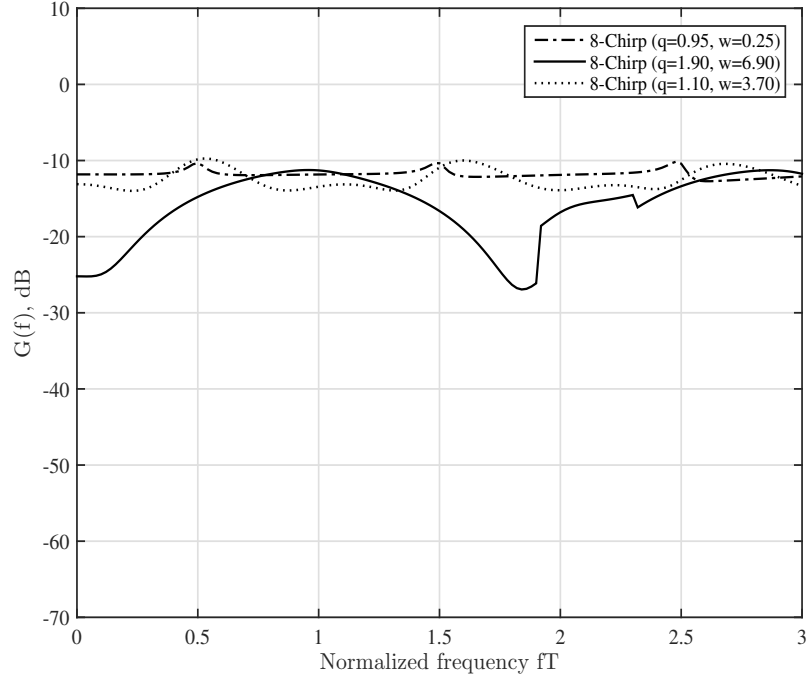
Figure 7.7: Power spectra of 8-CPCM system

7.5 Conclusions

In this Chapter, the direct method to calculate the power spectra of M-CPCM is investigated. Numerical results are exhibited for a variety of chirp signals of interest. It is observed that M-level chirp signals can offer different bandwidth occupancy by varying modulation parameters. These variations can be exploited to provide a trade-off between the error rate performance and the bandwidth efficiency. It has been shown that there exist some sets of modulation parameters that offer bandwidth occupancy better than conventional scheme and thus making M-CPCM signals an attractive modulation technique from the viewpoint of power and bandwidth trade-offs.

Chapter 8
Conclusion

8.1 Introduction

This Chapter summarizes the contributions of this thesis and the conclusions from the results obtained. Also, the areas for further research in the light of the needs of modern wireless communication systems are outlined. In Section 8.2, summary of contributions to the thesis is given and in Section 8.3, suggestions for further research work are outlined.

8.2 Summary of Contributions

In Chapter 2, a class of memoryless constant-envelope multi-level chirp signals is proposed for data communication. The parameters of these signals are described and illustrated. The ability of these signals to operate over AWGN is assessed using minimum Euclidean distance criteria. Optimum modulation parameter sets (q, w) that maximize the minimum distance have been determined for 2-, 4-, 8-, and 16-level chirp modulated signals. Next, detection of these signals in AWGN is addressed for coherent and non-coherent receptions. Error rate analyses are presented and closed-form expressions for symbol error rates are derived for the optimum receivers. Optimum multi-level coherent and non-coherent chirp systems have been determined that minimize symbol error rate. It is found that M-level chirp systems are attractive for data transmission by virtue of its power/bandwidth performance.

In Chapter 3, a class of signals referred to as M-CPCM is proposed and described. A detailed investigation of the minimum Euclidean distance properties of these signals is presented. Closed-form expression for Euclidean distance is derived,

as a function of the modulation parameters q and w and observation length n for 2-, 4-, 8-CPCM. Upper bounds on the minimum Euclidean distance of this class of signals are derived and sets of modulation parameters that maximize Euclidean distance are identified. A significant property of 2-CPCM is that it provides a distance larger than the 2-CPFSK modulation. Also, it is shown that 4- and 8-CPCM have distance larger than the distances of 4- and 8-CPFSK, for observation lengths of 2 to 5. In all cases, the minimum Euclidean distance is an increasing function of the observation interval n and the maximum values of distance does not just occur at a specific set of modulation parameters. This observation is very useful and provides a flexibility in the design of chirp communication system by choosing a set of modulation parameters of practical interest.

In Chapter 4, multiple-symbol detection of M-CPCM signals over AWGN is addressed. First, optimum coherent receiver structure for arbitrary observation length is derived and its error rate performances analysis is given. Upper bound on symbol error probability performance of optimum coherent M-CPCM receiver is given in closed-form, as a function of signal modulation parameters (q, w), the receiver decision observation length n, number of levels of data M, location of decision symbol (δ), and the received signal-to-noise ratio $\frac{E_b}{N_0}$. It is shown that the 2-CPCM system, for $5T$ observation interval, offers nearly 2 dB improvement in performance relative to coherent PSK and about 4 dB improvement relative to coherent binary FSK. It is observed that, by increasing the observation length, gain in the SNR can be achieved but this gain comes at the cost of increased complexity of the receiver. 4-CPCM system has nearly 3.5 dB gain over coherent QPSK and 8-CPCM system offers nearly 7 dB improvement relative to coherent octal PSK. Next, a similar analysis for non-coherent reception is given. Upper bound on symbol error probability performance of optimum non-coherent M-CPCM receiver is given in the closed-form. It is observed that the location of decision symbol δ plays an important role and the optimum decision symbol location is given by $\delta = \text{int}(\frac{n}{2})+1$, for n odd and $\delta = (\frac{n}{2})$ or $\delta = (\frac{n}{2})+1$ for n even. It is observed that non-coherent 2-CPCM system performs better than BPSK by nearly 1.2 dB when the observation length is $5T$. The performance of non-coherent 2-CPCM and non-coherent 2-CPFSK are nearly the same when the

observation lengths are $3T$ and $5T$, respectively.

In Chapter 5, a class of time-varying M-CPCM referred to as multi-mode M-CPCM is proposed for data transmission. A general description of this M-CPCM system is given and the independent sets of modulation parameters that characterize such a system are identified and described. The symbol error probability upper bound on the performance of the optimum coherent dual-mode M-CPCM receiver is derived as a function of the sets of modulation parameters (q, w), the receiver decision observation length n, number of levels of data M, and the received signal-to-noise ratio $\frac{E_b}{N_0}$. It is found that dual-mode 2-CPCM system outperforms corresponding mono-mode system. This improvement can be only achieved at certain sets of modulation parameters.

In Chapter 6, performances of M-level chirp systems over Rayleigh, Nakagami-m and Generalized-K fading and shadowing channel are presented. New and easy-to-compute closed-form expressions for average symbol error probability for M-level chirp communication system for three fading models are derived. The fading models represent most practical wireless channels. It is found that the performance of binary chirp is very close to the performance of BPSK modulation over Rayleigh fading channel and better than the performance of 2-FSK and DPSK systems. Also, it is found that the effect of shadowing on the performance of M-level chirp system is worse than that in fading. The results presented can be used to design an efficient and reliable M-level chirp communication system for application over fading channels.

In Chapter 7, direct method to calculate the power spectra of M-CPCM is presented. Numerical results are given for the classes of chirp signals considered in the thesis. It is observed that bandwidth occupancy of M-CPCM can be changed by varying modulation parameters. This observation can be exploited to obtain a trade-off between the error rate performance and the bandwidth efficiency. It is shown that there exist some sets of modulation parameters that offer bandwidth occupancy better than the conventional modulations and thus making M-CPCM an attractive modulation technique from the viewpoint of power and bandwidth trade-off.

8.3   Suggestions for Future Work

- Space time coding (STC) is an attractive area of research in recent years. CPM with STC are proposed and studied. However, utilizing M-level chirp signals in STC to enhance system performance is an interesting area of research.

- In this thesis, error rate performance analysis and some properties of constant-envelope chirp signals have been analyzed and examined using analytical methods. It would be interesting to examine the performance and properties of this class of signals using practical implementations of chirp systems.

- M-level chirp modulation with coding can be used for application in a multiple user environment. In a multi-user environment, co-channel interference and adjacent channel interference are major sources of performance degradation. It would be interesting to design and analyze multi-user communication systems using M-level chirp modulation.

References

[1] T. Rappaport, *Wireless Communications: Principles and Practice*, 2nd ed. Upper Saddle River, NJ, USA: Prentice Hall PTR, 2001.

[2] A. Goldsmith, *Wireless Communications.* Cambridge University Press, 2005.

[3] J. G. Proakis, *Digital communications, 4th ed.* McGraw-Hill, 2001.

[4] R. C. Dixon, *Spread spectrum systems.* Wiley, 1976.

[5] L. M. Dao, "Wireless communications using chirp signals," Master's thesis, School of Global Information and Telecommunications Studies, Waseda University, 2008.

[6] M. Huemer, A. Koppler, C. C. W. Ruppel, L. Reindl, A. Springer, and R. Weigel, "Saw based chirp fourier transform for ofdm systems," in *Ultrasonics Symposium, 1999. Proceedings. 1999 IEEE*, vol. 1, October 1999, pp. 373–376 vol.1.

[7] J. Burnsweig and J. Wooldridge, "Ranging and data transmission using digital encoded fm-"chirp" surface acoustic wave filters," *IEEE Transactions on Microwave Theory and Techniques*, vol. 21, no. 4, pp. 272–279, April 1973.

[8] [Online]. Available: http://www.ieee802.org/15/pub/TG4a.html

[9] [Online]. Available: http://www.nanotron.com/EN/PR_nN_TRX.php

[10] M. R. Winkler, "Chirp signals for communications," in *Western Electronic Show and Convention*, August 1962.

[11] A. Berni and W. Gregg, "On the utility of chirp modulation for digital signaling," *Communications, IEEE Transactions on*, vol. 21, no. 6, pp. 748 – 751, June 1973.

[12] C. Cook, "Linear fm signal formats for beacon and communication systems," *Aerospace and Electronic Systems, IEEE Transactions on*, vol. AES-10, no. 4, pp. 471 –478, July 1974.

[13] G. Gott and J. Newsome, "H. f. data transmission using chirp signals," *Electrical Engineers, Proceedings of the Institution of*, vol. 118, no. 9, pp. 1162 –1166, September 1971.

[14] G. Gott and A. Karia, "Differential phase-shift keying applied to chirp data signals," *Electrical Engineers, Proceedings of the Institution of*, vol. 121, no. 9, pp. 923 –928, September 1974.

[15] D. Dayton, "Fm "chirp" communications: Multiple access to dispersive channels," *Electromagnetic Compatibility, IEEE Transactions on*, vol. EMC-10, no. 2, pp. 296 –297, June 1968.

[16] M. Kowatsch, F. Seifert, and J. Lafferl, "Comments on transmission system using pseudonoise modulation of linear chirps," *Aerospace and Electronic Systems, IEEE Transactions on*, vol. AES-17, no. 2, pp. 300 –303, March 1981.

[17] M. Kowatsch and J. Lafferl, "A spread-spectrum concept combining chirp modulation and pseudonoise coding," *Communications, IEEE Transactions on*, vol. 31, no. 10, pp. 1133 – 1142, October 1983.

[18] S. El-Khamy and S. Shaaban, "Matched chirp modulation: detection and performance in dispersive communication channels," *Communications, IEEE Transactions on*, vol. 36, no. 4, pp. 506 –509, April 1988.

[19] A. K. Elhakeem and A. Targi, "Performance of hybrid chirp/ds signals under doppler and pulsed jamming," in *Global Telecommunications Conference and Exhibition 'Communications Technology for the 1990s and Beyond' (GLOBECOM), 1989. IEEE*, November 1989, pp. 1618–1623 vol.3.

[20] X. Wang, M. Fei, and X. Li, "Performance of chirp spread spectrum in wireless communication systems," in *Communication Systems, 2008. ICCS 2008. 11th IEEE Singapore International Conference on*, November 2008, pp. 466 –469.

[21] W. Hirt and S. Pasupathy, "Continuous phase chirp (cpc) signals for binary data communication-part i: Coherent detection," *Communications, IEEE Transactions on*, vol. 29, no. 6, pp. 836 – 847, June 1981.

[22] ——, "Continuous phase chirp (cpc) signals for binary data communication–part ii: Noncoherent detection," *Communications, IEEE Transactions on*, vol. 29, no. 6, pp. 848 – 858, June 1981.

[23] T. Aulin and C.-E. W. Sundberg, "Continuous phase modulation–part i: Full response signaling," *Communications, IEEE Transactions on*, vol. 29, no. 3, pp. 196–209, March 1981.

[24] T. Aulin, N. Rydbeck, and C.-E. W. Sundberg, "Continuous phase modulation–part ii: Partial response signaling," *Communications, IEEE Transactions on*, vol. 29, no. 3, pp. 210–225, March 1981.

[25] K. Raveendra, "Digital transmission using multimode phase-continuous chirp signals," *Communications, IEE Proceedings-*, vol. 143, no. 2, p. 87, April 1996.

[26] B. A. Dave and R. K. Rao, "Data transmission using digital asymmetric phase continuous chirp signals," *World Wireless Congress, Palo Alto*, vol. 24-27, pp. 383–388, May 2005.

[27] S. Wilson and R. Gaus, "Power spectra of multi-h phase codes," *Communications, IEEE Transactions on*, vol. 29, no. 3, pp. 250–256, March 1981.

[28] U. Mengali and M. Morelli, "Decomposition of m-ary cpm signals into pam waveforms," *Information Theory, IEEE Transactions on*, vol. 41, no. 5, pp. 1265–1275, September 1995.

[29] A. Hengstler, "A novel chirp modulation spread spectrum technique for multiple access," January 2001.

[30] A. Springer, W. Gugler, M. Huemer, R. Koller, and R. Weigel, "A wireless spread-spectrum communication system using saw chirped delay lines," *Microwave Theory and Techniques, IEEE Transactions on*, vol. 49, no. 4, pp. 754 –760, April 2001.

[31] H. Shen, S. Machineni, C. Gupta, and A. Papandreou-Suppappola, "Time-varying multichirp rate modulation for multiple access systems," *IEEE Signal Processing Letters*, vol. 11, no. 5, pp. 497 – 500, May 2004.

[32] H. Liu, "Multicode ultra-wideband scheme using chirp waveforms," *Selected Areas in Communications, IEEE Journal on*, vol. 24, no. 4, pp. 885 – 891, April 2006.

[33] M. Fanyu and G. Xuemai, "A combined chirp signal modulation technique for multiple access system," *Information Technology Journal 10(2)*, pp. 416–422, 2011.

[34] R. K. R. A. Kadri and J. Jiang, "Low-power chirp spread spectrum signals for wireless communications within nuclear power plants," *ANS, Nuclear Technology*, vol. 166, no. 2, pp. 156–169, May 2009.

[35] M. A. Khan, R. K. Rao, and X. Wang, "Closed-Form Error Probability for M-ary Chirp Modulation in Frequency-Selective and -Nonselective Fading Channels," in *26th IEEE Canadian Conference on Electrical and Computer Engineering (CCECE)*, May 2013, pp. 1–4.

[36] ——, "Performance Analysis of MRC-Chirp System over Independent and Correlated Fading Channels," in *26th IEEE Canadian Conference on Electrical and Computer Engineering (CCECE)*, May 2013, pp. 1–4.

[37] ——, "Performance of quadratic and exponential multiuser chirp spread spectrum communication systems," in *8th IEEE International Symposium on Performance Evaluation of Computer and Telecommunication Systems (SPECTS)*, July 2013, pp. 58–63.

[38] ——, "Non-linear trigonometric and hyperbolic chirps in multiuser spread spectrum communication systems," in *9th IEEE International Conference on Emerging Technologies (ICET)*, December 2013, pp. 1–6.

[39] A. Mohammad, "M-ary chirp modulation for data transmission," Master's thesis, The University of Western Ontario, London, Ontario, Canada, 2011.

[40] H. Van Trees, *Detection, Estimation, and Modulation Theory*, ser. Detection, Estimation, and Modulation Theory. Wiley, 2001, no. pt. 1. [Online]. Available: https://books.google.ca/books?id=7mXEMgEACAAJ

[41] M. Abramowitz and I. Stegun, *Handbook of Mathematical Functions: With Formulas, Graphs, and Mathematical Tables*, ser. Applied mathematics series. Dover Publications, 1964. [Online]. Available: https://books.google.ca/books?id=MtU8uP7XMvoC

[42] J. Anderson, T. Aulin, and C. Sundberg, *Digital Phase Modulation*, ser. Applications of Communications Theory. Springer US, 1986. [Online]. Available: https://books.google.ca/books?id=RwMpVSOXdJQC

[43] T. Schonhoff, "Symbol error probabilities for m-ary cpfsk: Coherent and noncoherent detection," *Communications, IEEE Transactions on*, vol. 24, no. 6, pp. 644–652, June 1976.

[44] M. Simon and M. Alouini, *Digital Communication over Fading Channels*, ser. Wiley Series in Telecommunications and Signal Processing. Wiley, 2005. [Online]. Available: https://books.google.ca/books?id=OYrDN0Q6BacC

[45] [Online]. Available: http://functions.wolfram.com

[46] A. Prudnikov, I. Brychkov, and O. Marichev, *Integrals and Series: Special functions*, ser. Integrals and Series. Gordon and Breach Science Publishers, 1998. [Online]. Available: https://books.google.ca/books?id=2t2cNs00aTgC

[47] M. Alsharef, A. M. Hamed, and R. K. Rao, "Error rate performance of digital chirp communication system over fading channels," in *Error Rate Performance of Digital Chirp Communication System over Fading Channels*, vol. II, October 2015.

[48] A. Hamed, R. Rao, and S. Primak, "Adaptive multidimensional modulation over faded shadowing channels," in *Electrical and Computer Engineering (CCECE), 2014 IEEE 27th Canadian Conference on*, May 2014, pp. 1–4.

[49] W. Bennett and S. Rice, "Spectral density and autocorrelation functions associated with binary frequency-shift keying," *Bell System Technical Journal, The*, vol. 42, no. 5, pp. 2355–2385, September 1963.

Appendix A
Squared Euclidean Distance for M-Level Chirp Signals

The squared Euclidean distance between signals $S_i(t)$ and $S_j(t)$ is derived here. The squared Euclidean distance is given by:

$$D^2(S_i, S_j) = 2E_s(1 - \rho(S_i, S_j)) \tag{A.1}$$

where the quantity $\rho(S_i, S_j)$ represents the normalized correlation between S_i and S_j. Assume the the transmitted signal represents data symbol d_j and the received signal represents data symbol d_i. These signals are given by:

$$S(t, d_i) = \sqrt{\frac{2E_s}{T}} \, \cos\left[w_c t + d_i \pi \left\{ h\left(\tfrac{t}{T}\right) - w\left(\tfrac{t}{T}\right)^2 \right\}\right]$$

$$\tag{A.2}$$

$$S(t, d_j) = \sqrt{\frac{2E_s}{T}} \, \cos\left[w_c t + d_j \pi \left\{ h\left(\tfrac{t}{T}\right) - w\left(\tfrac{t}{T}\right)^2 \right\}\right]$$

The normalized cross correlation between these signals is defined by:

$$\rho(i, j) = \frac{1}{E_s} \int_0^T S(t, d_i) \, S(t, d_j) dt \tag{A.3}$$

Substitute (A.2) in (A.3)

$$\rho(i,j) = \frac{1}{E_s} \int\limits_{0}^{T} \sqrt{\frac{2E_s}{T}} \, \cos\left[w_c t + d_i \pi \left\{ h\left(\frac{t}{T}\right) - w\left(\frac{t}{T}\right)^2 \right\} \right]$$

$$\times \sqrt{\frac{2E_s}{T}} \, \cos\left[w_c t + d_j \pi \left\{ h\left(\frac{t}{T}\right) - w\left(\frac{t}{T}\right)^2 \right\} \right] dt \quad \text{(A.4)}$$

Using the identity:

$$\cos\alpha \cos\beta = \frac{1}{2}\left[\cos(\alpha+\beta) + \cos(\alpha-\beta)\right] \tag{A.5}$$

and ignoring the high frequency term. (A.4) can be written as:

$$\rho(i,j) = \frac{1}{T} \int\limits_{0}^{T} \cos\left[(d_i - d_j)\pi \left\{ h\left(\frac{t}{T}\right) - w\left(\frac{t}{T}\right)^2 \right\} \right] dt \tag{A.6}$$

if $(d_i - d_j) = 0 \qquad \Rightarrow \rho = 1$

if $(d_i - d_j) \quad +ve \quad$ or $\quad (d_i - d_j) \quad -ve$

$$\rho(i,j) = \frac{1}{T} \int\limits_{0}^{T} \cos\left[|(d_i - d_j)|\pi w \left(\frac{t}{T}\right)^2 - \pi|d_i - d_j|h\left(\frac{t}{T}\right) \right] dt \tag{A.7}$$

Let $a = \pi|d_i - d_j|w$, $b = \pi|d_i - d_j|$ and $x = \frac{t}{T}$ (A.7) can be written as:

$$\rho(i,j) = \int\limits_{0}^{1} \cos\left(ax^2 - bx\right) dx \tag{A.8}$$

and by completing the square, (A.8) can be written as:

$$\rho(i,j) = \int\limits_{0}^{1} \cos\left[\left(\sqrt{a}x - \frac{b}{2\sqrt{a}}\right)^2 - \left(\frac{b}{2\sqrt{a}}\right)^2\right] dx \qquad (A.9)$$

applying the difference formula for the cosine $\cos(\alpha - \beta) = \cos\alpha\cos\beta + \sin\alpha sin\beta$, (A.9) can be expressed as:

$$\rho(i,j) = \int\limits_{0}^{1} \cos\left[\left(\frac{b}{2\sqrt{a}}\right)^2\right] \cos\left[\left(\sqrt{a}x - \frac{b}{2\sqrt{a}}\right)^2\right] +$$

$$\int\limits_{0}^{1} \sin\left[\left(\frac{b}{2\sqrt{a}}\right)^2\right] \sin\left[\left(\sqrt{a}x - \frac{b}{2\sqrt{a}}\right)^2\right] dx \qquad (A.10)$$

By changing the variable $\sqrt{a}x - \dfrac{b}{2\sqrt{a}}$ in (A.10) into $\sqrt{\dfrac{\pi}{2}}u$ and accordingly changing the limits of the integration, we get:

$$\rho(i,j) = \frac{\cos(\Omega)}{\sqrt{2\gamma w}} \left[\int\limits_{0}^{u_h} \cos(\sqrt{\tfrac{\pi}{2}}u)^2 du - \int\limits_{0}^{u_l} \cos(\sqrt{\tfrac{\pi}{2}}u)^2 du\right]$$

$$+\frac{\sin(\Omega)}{\sqrt{2\gamma w}} \left[\int\limits_{0}^{u_h} \sin(\sqrt{\tfrac{\pi}{2}}u)^2 du - \int\limits_{0}^{u_l} \sin(\sqrt{\tfrac{\pi}{2}}u)^2 du\right] \qquad (A.11)$$

where $\Omega = \dfrac{\pi}{4}|d_i - d_j|\dfrac{(q+w)^2}{w}$ and $\gamma = |d_i - d_j|$. Solving the integral in (A.11) by applying Fresnel integral, the normalized cross correlation can be given as:

$$\rho(i,j) = \left[\frac{\cos(\Omega)}{\sqrt{2\gamma w}}\left(\mathbf{C}[u_h] - \mathbf{C}[u_l]\right) + \frac{\sin(\Omega)}{\sqrt{2\gamma w}}\left(\mathbf{S}[u_h] - \mathbf{S}[u_l]\right)\right] \qquad (A.12)$$

where the function $\mathbf{C}(.)$ and $\mathbf{S}(.)$ are the Fresnel cosine and sine integral which are given by [41]:

$$\mathbf{C}(u) = \int\limits_{0}^{u} \cos(\frac{\pi x^2}{2}) \ dx$$

$$\mathbf{S}(u) = \int\limits_{0}^{u} \sin(\frac{\pi x^2}{2}) \ dx$$

Appendix B
Complex Correlation for M-Level Chirp Signals

In this appendix, we derive an expression for the complex cross correlation between signals $S_i(t)$ and $S_j^*(t)$. The complex correlation can be defined as:

$$\rho_c(i,j) = \frac{1}{2E_s} \int\limits_0^{nT} S_i(t) S_j^*(t) dt \tag{B.1}$$

which is equal to:

$$\rho_c(i,j) = \frac{1}{2E_s} \int\limits_0^{nT} \sqrt{\frac{2E_s}{T}} e^{j\left(w_c t + d_i \pi \left\{ h\left(\frac{t}{T}\right) - w\left(\frac{t}{T}\right)^2 \right\}\right)}$$
$$\times \sqrt{\frac{2E_s}{T}} e^{-j\left(w_c t + d_j \pi \left\{ h\left(\frac{t}{T}\right) - w\left(\frac{t}{T}\right)^2 \right\}\right)} dt \tag{B.2}$$

(B.2) can be rewritten as:

$$\rho_c(i,j) = \frac{1}{T} \int\limits_0^{T} e^{j\left(|d_i - d_j|\pi \left\{ h\left(\frac{t}{T}\right) - w\left(\frac{t}{T}\right)^2 \right\}\right)} \tag{B.3}$$

Applying Euler's formula to (B.3)

$$\rho_c(i,j) = \frac{1}{T} \int\limits_0^{T} \left[\cos(\Theta) + j\sin(\Theta) \right] dt \tag{B.4}$$

where $\Theta = |d_i - d_j|\pi \left\{ h\left(\dfrac{t}{T}\right) - w\left(\dfrac{t}{T}\right)^2 \right\}$ The integral for the cosine and sine in (B.4) can be solved following the same procedure in Appendix A. The correlation is given by:

$$\rho(i,j) = \left[\frac{\cos(\Omega)}{\sqrt{2\gamma w}} \left(\mathbf{C}[u_h] - \mathbf{C}[u_l]\right) + \frac{\sin(\Omega)}{\sqrt{2\gamma w}} \left(\mathbf{S}[u_h] - \mathbf{S}[u_l]\right) \right]$$

$$+ j \left[\frac{\cos(\Omega)}{\sqrt{2\gamma w}} \left(\mathbf{S}[u_h] - \mathbf{S}[u_l]\right) + \frac{\sin(\Omega)}{\sqrt{2\gamma w}} \left(\mathbf{S}[u_h] - \mathbf{S}[u_l]\right) \right] \qquad \text{(B.5)}$$

where $\Omega = \dfrac{\pi}{4}|d_i - d_j|\dfrac{(q+w)^2}{w}$, $\gamma = |d_i - d_j|$ and the function $\mathbf{C}(.)$ and $\mathbf{S}(.)$ are the Fresnel cosine and sine integral which are given by [41]:

$$\mathbf{C}(u) = \int_0^u \cos\left(\frac{\pi x^2}{2}\right) dx$$

$$\mathbf{S}(u) = \int_0^u \sin\left(\frac{\pi x^2}{2}\right) dx$$

Curriculum Vitae

Name:	Alsharef Mohammad
Place of birth:	Taif, Saudi Arabia
Year of birth:	1985
Post-secondary	2016, Ph.D. Engineering Science Faculty of Engineering The University of Western Ontario London, Ontario, Canada
	2011, Master of Engineering Science Faculty of Engineering The University of Western Ontario London, Ontario, Canada
	2007, Bachelor of Electrical Engineering Science Faculty of Engineering King Fahd University of Petroleum and Minerals Dhahran, Saudi Arabia
Honors and Awards	Best Student Paper Award at ICCST 2015 October 21st, 2015
	Best Conference Paper Award at ICCST 2015 October 21st, 2015
	Best Conference Paper Finalist at CCECE 2015 May 3rd, 2015
Employment	Lecturer, Taif University, Saudi Arabia 2014-present

Publications:

[1] Alsharef, M.; Rao, R.K., "Multi-level continuous phase chirp modulation: coherent detection," Submitted to IEEE Transactions on Wireless Communications.

[2] Alsharef, M.; Rao, R.K., "Multi-level continuous phase chirp modulation: non-coherent detection," Submitted to IEEE Transactions on Wireless Communications

[3] Mohammad Alsharef, Abdulbaset M. Hamed, and Raveendra K. Rao, "Error rate performance of digital chirp communication system over fading channels," Lecture Notes in Engineering and Computer Science: Proceedings of The World Congress on Engineering and Computer Science 2015, 21-23 October, 2015, San Francisco, USA, pp727-732 (Adjudged as the best student paper)

[4] Abdulbaset Hamed, Mohammad Alsharef, and Raveendra K. Rao, "MGF based performance analysis of digital wireless system in urban shadowing environment," Lecture Notes in Engineering and Computer Science: Proceedings of The World Congress on Engineering and Computer Science 2015, 21-23 October, 2015, San Francisco, USA, pp679-684 (Adjudged as the best conference paper)

[5] Alsharef, M.; Rao, R.K., "M-ary chirp modulation for coherent and non-coherent data transmission," Electrical and Computer Engineering (CCECE), 2015 IEEE 28th Canadian Conference on , vol., no., pp.213-219, 3-6 May 2015 (Best conference paper, Finalist)

[6] Hamed, A.M.; Alsharef, M.; Rao, R.K., "Bit error probability performance bounds of CPFSK over fading channels," Electrical and Computer Engineering (CCECE), 2015 IEEE 28th Canadian Conference on , vol., no., pp.1329-1334, 3-6 May 2015

[7] Alsharef, M.; Rao, R.K., "Spectral properties of multi-mode CPCM," The International Conference on Communications, Computer Science and Information Technology (ICCCSIT), Dubai, UAE, 12-14 March 2016

[8] Alsharef, M.; Rao, R.K., "Multi-mode multi-level continuous phase chirp modulation: coherent detection," Accepted for Presentation in IEEE CCECE 2016, Vancouver, Canada, 15-18 May 2016

Manuscripts under Preparation:

[1] Alsharef, M.; Rao, R.K., "Multi-level continuous phase chirp modulation."

[2] Alsharef, M.; Rao, R.K., "Multi-mode multi-level continuous phase chirp modulation."

[3] Alsharef, M.; Rao, R.K., "Constant envelope multi-level chirp modulated signals: distance properties."